



Comparison of thermodynamic data files for PHREEQC

Peng Lu^{a,*}, Guanru Zhang^{a,b}, John Apps^c, Chen Zhu^{a,*}

^a Department of Earth and Atmospheric Sciences, Indiana University, Bloomington, IN 47405, USA

^b College of Ecology and Environment, Chengdu University of Technology, Chengdu 610059, China

^c Earth and Environmental Sciences Area, Lawrence Berkeley National Laboratory, Berkeley, CA 94705, USA



ARTICLE INFO

Keywords:

Geochemical modeling
PHREEQC
Thermodynamic data files
Water
Mineral solubility

ABSTRACT

PHREEQC is a geochemical computer code developed by the United States Geological Survey and used to model mineral solubilities, aqueous solutions, and water-rock interactions over a large range of conditions. This easy-to-use and open-source program is widely used in the fields of geochemistry, environmental science and engineering, petroleum industry, mining and chemical engineering and biogeochemistry. However, the quality of the modeling depends on the experience of the modeler, and the quality of thermodynamic data available for the code, which is addressed in this review. The authors of the PHREEQC program clearly stated that the choice of thermodynamic data files (TDFs) is the responsibility of the user. Thirteen, mostly “third party”, TDFs are distributed along with the software release without detailed documentation or critical evaluation. The quality of the TDFs varies with a wide spectrum of the internal consistency of the thermodynamic data, comprehensiveness of the chemical components and species, the temperature-pressure coverage of log K values, activity coefficient models suitable for ionic strength, and traceability of the sources of data.

In this review, we provide some basic documentation, evaluate and compare these TDFs, and attempt to outline the limits of their applicability. We also used the TDFs to model examples of river water, seawater, groundwater, oil-field brine, and selected mineral solubility data for some oxides, oxy-hydroxides, hydroxides, aluminosilicates, carbonates, and sulfates. These comparisons clearly demonstrate that, with the same PHREEQC computer code but a different TDF, significantly different modeling results can be produced. It is imperative that users specify which TDF they used when referring to their modeling results.

1. Introduction

PHREEQC is a widely used geochemical modeling computer program developed by the United States Geological Survey and distributed free to the public (Parkhurst and Appelo, 1999, 2013) in both compiled form and as source code. The program's primary function is to evaluate aspects relating to homogeneous chemical equilibrium within a multi-component aqueous phase, and/or heterogeneous multi-component equilibria between the aqueous phase and multiple solid phases at a given temperature and pressure. It can also be used for reaction path modeling, optionally incorporating chemical kinetics, and one-dimensional coupled reactive mass transport calculations.

The popularity of the PHREEQC computer program and a large user base has also resulted in confusion and misunderstanding about geochemical modeling. It is common, even in top-ranked geochemical journals, to see statements such as “PHREEQC results”, “PHREEQC

shows the speciation of Fe is ...”, and “the PHREEQC model”. This situation is probably worse in the grey literature (e.g., consulting reports). Furthermore, thermodynamic courses are disappearing in earth science curricula in some countries including the United States. Many users do not have the proper training or background. It is the intention of this review to highlight the needed attention to the principles and fundamental data underlying geochemical modeling and help overcome some misconceptions and confusion.

A key issue is the thermodynamic data files (TDFs), which together with the computer code and an input file, are essential for PHREEQC to perform a modeling exercise. TDFs provide equilibrium constants, K , of chemical reactions and activity coefficient parameters for calculating chemical equilibria. Because PHREEQC is capable of addressing a wide range of topics in aqueous solution geochemistry, many TDFs have been independently created to facilitate the study of specific topics in addition to that issued with the program. It is the purpose of this paper to

* Corresponding authors.

E-mail addresses: peng.lu@aramco.com (P. Lu), chenzhu@indiana.edu (C. Zhu).

¹ Present address: EXPEC Advanced Research Center, Saudi Aramco, Dhahran 31311, Saudi Arabia

evaluate the roles that such TDFs play in meeting the needs of modelers, in terms of their suitability, limitations, and potential for improvement, and as a guide in their use for specific applications. Ultimately, however, it is the modeler's responsibility to ensure the quality and applicability of their contained data with respect to the ranges of temperature, pressure, chemical components, salinity, and other constraints for a particular study.

The TDFs for use with the PHREEQC program are described in Section 2 below. They vary to different degrees in the following characteristics, which are indicative of their quality (Zhu and Anderson, 2002):

Internal consistency: The thermodynamic functions, reference states, reference values, and thermodynamic models should be consistently applied to all data within a given TDF. Further details are given below.

Comprehensiveness: The TDF should contain all chemical components and species, the necessary temperature and pressure ranges, and the fluid salinity needed to represent the expected behaviors of the relevant chemical systems.

Traceability: Data in a TDF should be referenced to sources that are available to the public.

T-P range: The database should contain $\log K_s$ in the T-P range of interest. Most TDFs cite $\log K$ only at 25 °C and 1 bar.

Ionic strength range and activity coefficients: Suitable activity coefficient models for the pertinent salinity in the system to be modeled should be prescribed.

Dynamics: TDFs can be updated and improved with time.

1.1. Internal consistency

The importance of internal consistency has been known for decades (e.g., Helgeson et al., 1978; Wagman et al., 1982). Taking thermodynamic data from one source and merging them with data from another source without ensuring that they are internally consistent leads to degraded results. Inconsistencies can arise through failure to recognize the following (see Nordstrom and Munoz, 1994): (a) That data are consistent with thermodynamic relationships (the basic laws and their consequences); (b) That common scales are used for T , energy, atomic mass, and fundamental physical constants; and (c) That an appropriate choice of standard states has been made, and the same standard states have been used consistently for all similar substances.

For example, consistent thermodynamic properties for minerals can be derived from calorimetric measurements and phase equilibrium experiments at high temperatures and pressures (e.g., Holland and Powell, 2011), including water, carbon dioxide, and a limited set of aqueous species, but which omit consideration of corresponding data for some of the same minerals derived independently from solubility experiments incorporating previously unconsidered aqueous species. If such a comparison is made, the calculated results sometimes agree well, but at other times do not, e.g. see Oelkers et al. (2009), Tutolo et al. (2014), and Miron et al. (2016). Combining independent sources therefore cannot be made without first ensuring that internal consistency has been achieved between the thermodynamic properties of all participating species; a task which is commonly not undertaken with the necessary rigor.

Another example of this problem arises from combining a database for surface complexation model parameters with a more recent database for aqueous species if earlier aqueous species data were used in developing the former database. A similar situation exists between equilibrium constant data files and kinetic parameters. In deriving rate laws, saturation states could be calculated from a different set of thermodynamic properties than those used when the rate law is applied.

1.2. Calculations and extrapolations to higher temperatures and pressures

Some modeling applications of environmental and geological problems require calculations of gas-water-mineral interactions at elevated

temperatures and pressures. Geological carbon storage, involving the injection of large amounts of CO₂ into deep geological formations to mitigate the impact of anthropogenic CO₂ on the climate, requires the repository to be at least 800 m deep to ensure injection of CO₂ at supercritical conditions (IPCC, 2005). Clastic and carbonate diagenesis involves chemical reactions between sediments, formation water, and gas during and after burial. The relevant T-P range for CO₂ injection and sediment diagenesis is ~40–200 °C and 50–1000 bars. For nuclear waste disposal, some proposed repository scenarios and designs may lead to repository temperatures upwards of ~200 °C (IAEA, 2009).

Many approaches have been used to account for the variation in the Gibbs free energy of formation, ΔG_f^o , for aqueous species as a function of temperature and pressure. The van't Hoff equation (Atkins and De Paula, 2006) (Eq. 2), which relates the change in the equilibrium constant, K_T , of a chemical reaction to the change in temperature, assumes that the standard state enthalpy of reaction, ΔH_r^o , is constant, and hence the standard molal heat capacity for the reaction is zero. This limits its application in most cases to a narrow temperature range. Log K_T in some PHREEQC TDFs at elevated temperatures is computed with this approach.

$$\Delta_r G^o = -2.303RT\log K_T \quad (1)$$

$$\log K_{T_1} - \log K_{T_2} = \frac{-\Delta_r H^o}{2.303R} \left(\frac{1}{T_1} - \frac{1}{T_2} \right) \quad (2)$$

Some data files (e.g., *phreeqc.dat*, *core10.dat*, *carbfix.dat*, *pitzer.dat*, and *diogenesis.dat*) correct the pressure effect on log K_s with molar volumes of solids and aqueous species (Appelo et al., 2014) with the equation,

$$\log K_{P,T} = \log K_{P=P_{ref},T} - \Delta V_r \frac{P - 1}{2.303RT} \quad (3)$$

where $\log K_{P,T}$ denotes the equilibrium constant at pressure P and temperature T ; $\log K_{P=P_{ref},T}$ is the equilibrium constant at temperature T and reference pressure P_{ref} ($P_{ref} = 1$ bar); ΔV_r is the standard volume of the reaction; R is the universal gas constant.

The revised Helgeson-Kirkham-Flowers (HKF) equation of state (EOS) model was developed to describe the standard Gibbs free energy of an aqueous species at temperatures to 1000 °C and pressures to 5000 bar (Helgeson et al., 1981; Tanger and Helgeson, 1988). A large number of parameters are needed for the HKF EOS model but are not experimentally available in most cases. However, Shock and Helgeson (1988), Shock and Koretsky (1993), Sassani and Shock (1998), and Plyasunov and Shock (2001) found many correlations among the EOS parameters, which allow them to estimate those that are not experimentally measured. These efforts led to the most comprehensive, in relative terms, thermodynamic database for aqueous species available at temperatures above the reference temperature of 25 °C (Shock et al., 1997; Sverjensky et al., 1997). This database is contained in the SUPCRT92 software package (Johnson et al., 1992), and hence is colloquially called the "SUPCRT92" aqueous database. Although the estimation of HKF EOS parameters always requires careful experimental verification, the predictive power of the method is useful for estimating thermodynamic properties at elevated temperatures and pressures. Recently, the Deep Earth Water model has extended the applicability to Earth deep crust and mantle conditions (Sverjensky et al., 2014; Huang and Sverjensky, 2019).

Although this study focuses on the comparison of TDFs prepared for use with PHREEQC (Parkhurst and Appelo, 1999, 2013), the issues identified have broader relevance to analogous files used in other computer programs to evaluate gas-water-rock interaction systems, including those used with ChemEQL (Müller, 2004), CHESS (van der Lee et al., 2002), CHIM-XPT (Reed et al., 2010), CRUNCH (Steefel, 2001), EQ3/6 (Daveler and Wolery, 1992), The Geochemist's Workbench (Bethke and Yeakel, 2014), MINEQL+ (Schecher and McAvoy, 1994),

MINTEQA2 (Allison et al., 1991), REAKTORO (Leal, 2015), TOUGH-REACT (Xu et al., 2004), WATEQ4F (Ball and Nordstrom, 1991), and databases compiled to simulate high-level radioactive waste disposal, e.g., those of the Yucca Mountain Project (USA) (Jove-Colon et al., 2007), Nagra/PSI Chemical Thermodynamic Data Base (Switzerland) (Hummel et al., 2002), ThermoChimie (France) (Duro et al., 2012; Giffaut et al., 2014), MOLDATA (Belgium) (Wang et al., 2011), JAEA Thermodynamic DataBase (Japan) (Yoshida and Shibata, 2004; Kitamura et al., 2012), and HATCHES Thermodynamic Database (UK) (Bond et al., 1997). Proprietary modeling software, coming with their own dedicated TDFs and without restriction to liquid aqueous/solid systems, e.g., FactSage, and HSC Chemistry, are also available.

2. Data files for use with PHREEQC

The latest version of PHREEQC (version 3.7.1., September 1, 2021) provides 13 TDFs along with the software release (see Table 1). Other TDFs for use with PHREEQC are not distributed with the software but are available for download. Table 1 compares the principal characteristics of these TDFs, all of which are discussed in this review. Table 2 lists the limitations of each TDF. Here, we briefly introduce these TDFs.

Fig. 1 summarizes the development and lineages of TDFs in use with PHREEQC. The TDFs can be classified into six categories in terms of their origin and specialties. Category V includes the TDFs using the Pitzer model (Pitzer, 1973) and the sole TDF of Category VI, *sit.dat* uses the specific ion interaction theory (SIT) approach. A brief introduction to these TDFs is given below.

(1) *phreeqc.dat*, the default TDF of PHREEQC, is derived from

PHREEQE (Parkhurst et al., 1980). *phreeqc.dat* is consistent with *wateq4f.dat* but has a smaller set of elements, aqueous species, and minerals. This TDF has been recently augmented. The latest *phreeqc.dat* features (1) parameters needed for the Peng-Robinson equation of state (Peng and Robinson, 1976) to calculate fugacity coefficients of gases in a gas mixture and their solubility in water, (2) molar volumes of solids and aqueous species to calculate the pressure dependence of log *K*_s (applicable up to ~1000 bar and 200 °C) (Eq. 1), and (3) the Redlich-type equation for temperature and pressure dependence of the volume of aqueous species (Appelo et al., 2014; Parkhurst and Appelo, 2013). However, only a small set of aqueous species, minerals, and gases include the parameters available for corrections to ~200 °C. Some reactions lack parameters for calculating log *K*_s above 25 °C. For others, only ΔH_r^0 , the enthalpy of reaction, is available, and the log *K*_s are calculated using the van 't Hoff equation to extrapolate from 25 °C to higher temperatures, assuming that ΔH_r^0 is invariant, which may result in relatively large uncertainties at higher temperatures (Anderson and Crerar, 1993; Neveu et al., 2017; Voigt et al., 2018).

(2) *amm.dat* is a TDF modified from *phreeqc.dat*. The only difference is the definition of ammonia as a component distinct from those of the other components of the nitrogen system, which possess different oxidation states. *amm.dat* also includes the latest features found in *phreeqc.dat*, such as improved fugacity coefficients of gases and temperature and pressure dependence of log *K*_s for some aqueous species and minerals.

(3) *iso.dat* is derived from *phreeqc.dat*, focusing on isotopic calculations (Thorstenson and Parkhurst, 2002, 2004). Minor isotopes are treated as individual thermodynamic components. The equilibrium

Table 1
Comparison of thermodynamic data files discussed in this study.

Database	T-P range	Pressure correction	Corrected P range	Aqueous activity coefficient model	Fugacity coefficients	Number of species	Sources
<i>phreeqc.dat</i>	<200 °C, <1 kb	Appelo et al. (2014)	up to ~1 kb	mixed WATEQ ¹ and Davies equation	Peng-Robinson	~310 ²	Appelo et al. (2014)
<i>amm.dat</i>	<200 °C, <1 kb	Appelo et al. (2014)	up to ~1 kb	mixed WATEQ and Davies equation	Peng-Robinson	~310 ²	Appelo et al. (2014)
<i>iso.dat</i>	0.01–100 °C at 1 bar	N.A.	N.A.	mixed WATEQ and Davies equation	Ideal gas law	~330	Thorstenson and Parkhurst (2002, 2004)
<i>wateq4f.dat</i>	0.01–100 °C at 1 bar	N.A.	N.A.	mixed WATEQ and Davies equation	Ideal gas law	~770	Ball and Nordstrom (1991)
<i>llnl.dat</i>	0.01–100 °C at 1 bar, 100–300 °C along <i>P</i> _{SAT}	SUPCRT92	N.A.	B-dot	Ideal gas law	~2590	Greg M. Anderson; EQ3/6 ³
<i>core10.dat</i>	0.01–100 °C at 1 bar, 100–300 °C along <i>P</i> _{SAT}	Appelo et al. (2014) & <i>P</i> _{sat} log <i>K</i> in SUPCRT92	up to ~1 kb	B-dot	Peng-Robinson	~630	Neveu et al. (2017)
<i>carbfix.dat</i>	0.01–100 °C at 1 bar, 100–300 °C along <i>P</i> _{SAT}	Appelo et al. (2014) & <i>P</i> _{sat} log <i>K</i> in SUPCRT92	up to ~1 kb	B-dot	Peng-Robinson	~660	Voigt et al. (2018)
<i>sit.dat</i>	15–80 °C at 1 bar	N.A.	N.A.	SIT	Ideal gas law	~2300	Amphos 21, BRGM and HydrAsa for ANDRA
<i>minseq.dat</i>	0.01–100 °C at 1 bar	N.A.	N.A.	mixed WATEQ and Davies equation	Ideal gas law	~1610	Allison et al. (1991)
<i>minseq.v4.dat</i>	0.01–100 °C at 1 bar	N.A.	N.A.	Mostly Davies equation	Ideal gas law	~1990	Allison et al. (1991)
<i>pitzer.dat</i>	<200 °C, <1 kb	Appelo et al. (2014)	up to ~1 kb	Pitzer equation	Peng-Robinson	~120	Plummer et al. (1988)
<i>frezchem.dat</i>	−73–25 °C at 1 bar	Appelo et al. (2014)	up to ~1 kb	Pitzer equation	Peng-Robinson	~70	Spencer et al. (1990), Marion and Farren (1999), and Marion (2001)
<i>ColdChem.dat</i>	−73–25 °C at 1 bar	N.A.	N.A.	Pitzer equation	N.A.	~40	Toner and Catling (2017)
<i>geothermal.dat</i>	0.01–100 °C at 1 bar, 100–300 °C along <i>P</i> _{SAT}	SUPCRTBL	N.A.	B-dot	Ideal gas law	~1050	SupPHREEQC (Zhang et al., 2020)
<i>diagenesis.dat</i>	0.01–100 °C at 1 bar, 100–200 °C along <i>P</i> _{SAT}	Appelo et al. (2014) & <i>P</i> _{sat} log <i>K</i> in SUPCRTBL	up to ~1 kb	WATEQ equation	Peng-Robinson	~1050	SupPHREEQC (Zhang et al., 2020)
<i>bl.dat</i>	Up to 1000 °C and 5 kb (variable <i>T</i> isobaric)	SUPCRTBL	up to 5 kb	B-dot	Ideal gas law	~1050	SupPHREEQC (Zhang et al., 2020)

¹ Hückel (1925); Helgeson (1969); Truesdell and Jones (1974).

² The number of species with parameters for calculations at elevated T-P is much smaller. See Appelo et al. (2014).

³ From 'thermo.com' V8.R6.230' prepared by Jim Johnson at Lawrence Livermore National Laboratory in Geochemist's Workbench format. Converted to PHREEQC format by Greg Anderson with assistance from David Parkhurst. The actual number of species with parameters for calculations at elevated T-P is much smaller than the total number of species in the dataset.

Table 2

Limitations of thermodynamic data files discussed in this study.

Database	Limitations						Notes
<i>phreeqc.dat</i>	A						F Only a small part of species is with <i>T-P</i> corrections.
<i>amm.dat</i>	A						F Only a small part of species is with <i>T-P</i> corrections.
<i>iso.dat</i>	A	B	C	D	E	F	
<i>wateq4f.dat</i>		B		D	E	F	
<i>llnl.dat</i>				D	E	F	Pressure along P_{SAT} ; some log K_s extrapolation using the van 't Hoff equation;
<i>core10.dat</i>			C			F	
<i>carbfix.dat</i>			C			F	
<i>sit.dat</i>	B	C	D	E	F		
<i>minTEQ.dat</i>	B	C	D	E	F		
<i>minTEQ.v4.dat</i>	B	C	D	E	F		
<i>pitzer.dat</i>	A						Only a small part of the components is with <i>T-P</i> corrections.
<i>frezchem.dat</i>	A	B					For $T \leq 25^\circ\text{C}$
<i>ColdChem.dat</i>	A	B					For $T \leq 25^\circ\text{C}$; no gases
<i>geothermal.dat</i>			D		F		
<i>diagenesis.dat</i>					F		
<i>bl.dat</i>			D	F			Isobaric

A = Number of species (or components) is relatively small; B = Small *T-P* range; C = log K_s extrapolation using the van 't Hoff equation; D = Ideal gas law for gas fugacity coefficients; E = No pressure correction; F = Ionic strength generally less than one molal.

constants of aqueous and solid species of minor isotopes differ slightly from those of the major isotopes, which account for fractionation processes. The equilibrium constants in *iso.dat* are derived from empirical fractionation factors, from statistical mechanical theory, or where no data are available (in most cases), by assuming no fractionation. It contains fewer aqueous species and minerals than *phreeqc.dat*.

(4) *wateq4f.dat* is a TDF derived from WATEQ4F (Ball and Nordstrom, 1991). It is largely the same as *phreeqc.dat* but contains thermodynamic data for more elements, aqueous species, and minerals. *wateq4f.dat* does not incorporate the high *T-P* improvements found in *phreeqc.dat*.

(5) *llnl.dat* was created by Greg M. Anderson through conversion of the Lawrence Livermore National Lab (LLNL) TDF thermo.com.V8.R6+.dat (Daveler and Wolery, 1992). *llnl.dat* covers a *T-P* range of 0.01–100 °C at 1 bar and 100–300 °C at P_{SAT} (water vapor saturation pressure). However, not all chemical species listed in *llnl.dat* include the parameters necessary for calculations above 25 °C. Furthermore, at higher temperatures and pressures, the ideal gas law is used to estimate the fugacity of gases. The ideal gas law is an approximation to real gas behavior, because it neglects molecular interactions (Appelo et al., 2014).

(6) *core10.dat* was developed by Neveu et al. (2017) for the geochemical modeling of icy moons and dwarf planets at elevated temperatures and pressures up to 1 kb. To model the pressure effects, they adopted the *phreeqc.dat* format along with the activity model of *llnl.dat*. The log K_s in this TDF are taken mainly from *llnl.dat*, but are fewer in number. A few ammonium-bearing and organic species were added, and most phyllosilicate properties were updated, although several mineral species e.g., colemanite, $\text{Ca}_2\text{N}_6\text{O}_{11} \cdot 5\text{H}_2\text{O}$ and $\text{UO}_2\text{SO}_4 \cdot \text{H}_2\text{O}$, were excluded. Many transcription errors in the original *llnl.dat* were corrected through verification with original sources. Polynomial analytical expressions of log K in *core10.dat* cover the *T-P* range of 0.01–100 °C at 1 bar and 100–300 °C along with P_{SAT} . Pressure effects on log K_s away from P_{SAT} were accounted for using a molar volume term, similar to that used in *phreeqc.dat*.

(7) *carbfix.dat* was developed by Voigt et al. (2018) and is based on *core10.dat*. The thermodynamic properties of several minerals and aqueous species were modified to meet the needs for modeling mineral carbonation. Additional minerals include 18 from the zeolite group, ferroactinolite, and ankerite. Additional aqueous species include carbonate species CaHCO_3^+ , NaCO_3^- , NaHCO_3^0 , MgCO_3^0 , and MgHCO_3^+ ; Al-bearing species $\text{AlH}_3\text{SiO}_4^{2+}$, AlSO_4^+ , and NaAl(OH)_4^0 ; iron-bearing species Fe(OH)_2^+ , Fe(OH)_3 , Fe(OH)_4^- , Fe(OH)_2^0 , Fe(OH)_3^- ; Cl-related species HClO^0 and HClO_2^0 ; S-bearing species NaSO_4^- and HS_2O_3^0 ; and KOH^0 . The calculation of log K at elevated *T-P* in *carbfix.dat* is the same as for *core10.dat*.

(8) *sit.dat* was developed by Amphos 21, BRGM (French Bureau of Research for Geology and Mining), and HydrAsa for ANDRA (French Agency for the Management of Nuclear Waste) based on ThermoChimie Version 9b0. This TDF uses specific ion interaction theory (SIT) for calculations in concentrated solutions (Grenthe et al., 1997; Sipos, 2008). It is suitable for use within the range of conditions expected in both near-surface and geological disposal facilities: pH 6–14, ionic strength up to SIT limit, redox potential (Eh) within the stability fields of water, and temperatures from 15 to 80 °C (Grivé et al., 2015).

(9) *minTEQ.dat* is a TDF derived from the databases for the US EPA's program MINTEQA2 (Allison et al., 1991).

(10) *minTEQ.v4.dat* is a TDF derived from MINTEQA2 version 4.

(11) *pitzer.dat* is a TDF for the specific-ion-interaction model of Pitzer (Pitzer, 1973) as implemented in PHRQPITZ (Plummer et al., 1988). It is developed for high salinity waters, with a focus primarily on a limited number of components (B, Ba, Br, C, Ca, Cl, Fe, K, Li, Mg, Mn, Na, S, Si, and Sr).

(12) *frezchem.dat* is based on a comprehensive Pitzer model in the Na-K-Ca-Mg-H-Cl-SO₄-CO₃-HCO₃-OH-H₂O system valid for low temperature, from <200 to 298.15 K, developed by Spencer et al. (1990), Marion and Farren (1999), and Marion (2001).

(13) *ColdChem.dat* is a low-temperature aqueous thermodynamic model for the Na-K-Ca-Mg-Cl-SO₄ system incorporating new experimental heat capacities in Na₂SO₄, K₂SO₄, and MgSO₄ solutions (Toner and Catling, 2017). It also uses Pitzer equations.

(14) *geothermal.dat* is one type of PHREEQC TDF generated by the SUPPHREEQC program, which follows the framework of *llnl.dat* and uses B-dot equation parameters for computing activity coefficients of aqueous species (Zhang et al., 2020). The *T-P* range of *geothermal.dat* is 0.01–100 °C at 1 bar and 100–300 °C at P_{SAT} . The log K_s are calculated by SUPCRTBL (Zimmer et al., 2016). *geothermal.dat* does not include the pressure modification parameters used by PHREEQC. In this TDF, the thermodynamic properties of minerals are mostly from Holland and Powell (2011), but with updated properties for boehmite, gibbsite, and dawsonite (Zimmer et al., 2016). Also, aqueous species have been added, mostly from Sverjensky et al. (1997) and those internally consistent with Sverjensky et al. (1997) from earlier publications by Helgeson and coworkers, as well as Al-bearing aqueous species from Tagirov and Schott (2001). The thermodynamic properties of SiO₂(aq) are from Apps and Spycher (2004) and HSiO₃[−] are from Sverjensky et al. (1997). Improvements in Mg-bearing species, magnesite, siderite, dolomite, calcite, and gypsum are reported in appendices A and B to this study.

(15) *diagenesis.dat* is the second type of PHREEQC TDF automatically generated by the SupPhreeqc program. *Diagenesis.dat* follows the framework of *phreeqc.dat* and includes (a) the analytic formula for the log K_s of aqueous, mineral, and gas reactions covering the *T-P* range of 0.01–100 °C at 1 bar and 100–200 °C at P_{SAT} ; (b) molar volume parameters for solids and aqueous species for estimating the effect of the pressure change on log K (suitable up to ~1000 bar and 200 °C (Appelo et al., 2014); and (c) Peng-Robinson equation parameters, critical temperature, pressure, and acentric factor (Parkhurst and Appelo, 2013) for calculating the gas fugacity. The log K_s are calculated by SUPCRTBL (Zimmer et al., 2016). In this TDF, the thermodynamic properties of minerals are taken mostly from Holland and Powell (2011), but the

Family Tree of TDFs

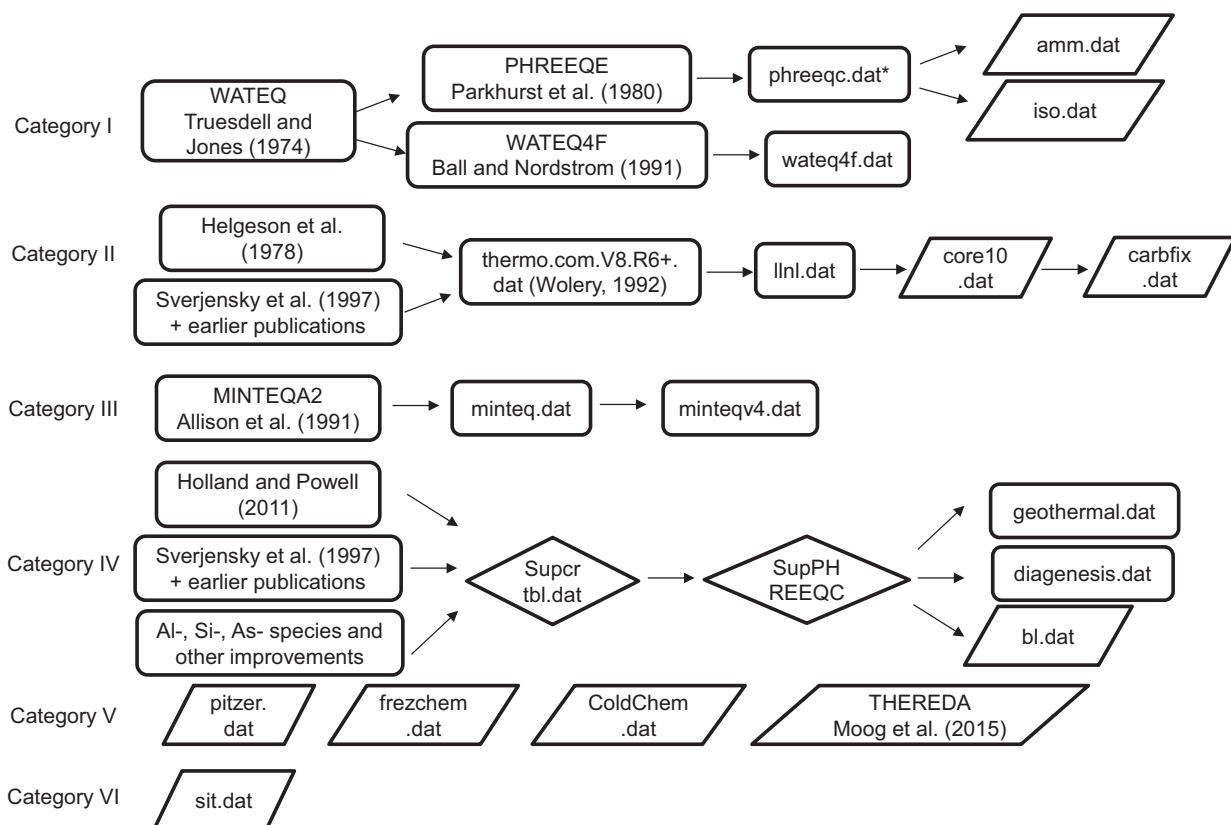


Fig. 1. Development and lineages of thermodynamic data files in use with PHREEQC. Rectangles represent general-purpose TDFs (e.g., *llnl.dat*, *phreeqc.dat*, *minteq.dat*, *geothermal.dat*) and parallelograms represent special-purpose TDFs (e.g., *amm.dat*, *iso.dat*, *core10.dat*, *carbfix.dat*). *Currently, *phreeqc.dat* is a subset of *wateq4f.dat*, but was updated with parameters for improved gas fugacity coefficients and temperature and pressure dependence of log Ks for some aqueous species and minerals (Appelo et al., 2014). Diamonds represent the pathway to create the three data files in Category IV.

properties for boehmite, gibbsite, and dawsonite are updated (Zimmer et al., 2016). Aqueous species are mostly taken from Sverjensky et al. (1997) and those internally consistent to Sverjensky et al. (1997) from earlier publications by Helgeson and coworkers, together with Al-bearing aqueous species from Tagirov and Schott (2001). As for *geothermal.dat*, the thermodynamic properties of $\text{SiO}_2\text{(aq)}$ are from Apps and Spycher (2004) and HSiO_3^- are from Sverjensky et al. (1997), together with improvements in Mg-bearing species, magnesite, siderite, dolomite, calcite, and gypsum, reported in appendices to this study. We also added the parameters for the “-gamma” keywords to use the WATEQ equation for activity coefficient calculations for aqueous species.

(16) *bl.dat* is the third type of PHREEQC TDF automatically generated by SupPhreeqc program (Zhang et al., 2020), following the *llnl.dat* dataset structure which uses B-dot equation parameters for computing activity coefficients of aqueous species. The temperature polynomial for the log K of aqueous species, minerals, and gaseous reactions covers the *T-P* range up to 1000 °C and 5000 bars, respectively. *bl.dat* datasets do not include the pressure modification parameters used by the *phreeqc.dat* framework; instead, the log Ks are calculated by SUPCRTBL (Zimmer et al., 2016) to variable temperatures at a isobaric pressures to 5000 bars. Currently, for applications over a wide range of pressures, multiple files are required (each at a specific pressure). In this TDF, the thermodynamic properties of minerals are taken mostly from Holland and Powell (2011), but the properties for boehmite, gibbsite, and dawsonite are updated (Zimmer et al., 2016), aqueous species are mostly from

Sverjensky et al. (1997) and those internally consistent with Sverjensky et al. (1997) from earlier publications by Helgeson and coworkers, together with Al-bearing aqueous species from Tagirov and Schott (2001), and $\text{SiO}_2^0\text{(aq)}$ and HSiO_3^- from Miron et al. (2016). The improvements in Mg-bearing species, magnesite, siderite, dolomite, and calcite, reported in appendices to this study, are also included.

geothermal.dat, *diagenesis.dat* and four examples of *bl.dat* at 0.5, 1, 2, and 5 kb can be downloaded at <https://models.earth.indiana.edu/phreeqc.php>.

cemdata18, a TDF recently developed for use with PHREEQC for investigating the behavior of hydrated Portland cements and alkali-activated materials (Lothenbach et al., 2019) was not evaluated in this study, but promises to be a valuable adjunct in the investigation of anthropogenic and naturally occurring cementitious materials.

3. Modeling concentrated solutions

PHREEQC is capable of using either an ion-association (Davies, WATEQ, or B-dot equation) or an ion interaction (Pitzer or Specific Ion Interaction Theory, SIT) equation to account for the nonideality of aqueous solutions (Parkhurst and Appelo, 2013). *minteq.v4.dat* uses mostly the Davies equation. *phreeqc.dat*, *minteq.dat*, *diagenesis.dat* and *wateq4f.dat* use mixed WATEQ (Truesdell and Jones, 1974) and Davies equations (mostly WATEQ). *llnl.dat*, *carbfix.dat*, *core10.dat* and *geothermal.dat* use the B-dot equation (Helgeson, 1969; Daveler and Wolery, 1992). *pitzer.dat*, *frezchem.dat* and *coldchem.dat* use the Pitzer

equation (Pitzer, 1973; Plummer et al., 1988). *sit.dat* uses the SIT equation (Grenthe et al., 1997).

For the ion-association methods, the activity coefficient of the species of interest must be calculated to account for the differences between the real state of Gibbs free energy of this species in the solution and its standard state.

For a neutral species (e.g., NaCl⁰), PHREEQC uses the *Setchénov* equation to calculate their activity coefficients:

$$\log\gamma_i = K_s \times I \quad (4)$$

where the K_s is a fit coefficient, and I is the ionic strength. The default value of K_s for Davies and WATEQ models is 0.1, which may be redefined with the “-gamma” keyword for a species. However, for the B-dot model, the coefficient is 0, unless the “-CO2_llnl_gamma” keyword is defined for a neutral species. In this case, the value of the B-dot is defined by the “LLNL_AQUEOUS_MODEL_PARAMETERS” data block.

For charged species, the default ion-association model is the Davies equation, should neither the “LLNL_AQUEOUS_MODEL_PARAMETERS” data block nor the “-gamma” keyword be defined in a TDF. In PHREEQC, 0.3 is used for the empirical parameter of the last term of the Davies equation:

$$\log\gamma = -Az^2 \left(\frac{\sqrt{I}}{1 + \sqrt{I}} - 0.3I \right) \quad (5)$$

In this equation, γ is the activity coefficient, I is the ionic strength, and A is a constant which varies slightly with temperature.

If the “-gamma” keyword is entered, the equation from WATEQ (Truesdell and Jones, 1974) is used for activity coefficient calculations:

$$\log\gamma = \frac{-Az^2\sqrt{I}}{1 + B\sqrt{I}} + bI \quad (6)$$

where B is a constant which varies slightly with temperature; \dot{a} is the ion-size parameter; b is a Debye-Hückel parameter.

If the “LLNL_AQUEOUS_MODEL_PARAMETERS” and “llnl_gamma” data blocks are defined in a data file, then the Lawrence Livermore National Laboratory type of B-dot equation will be used (Daveler and Wolery, 1992):

$$\log\gamma_i = \frac{-A_\gamma z_i^2 \sqrt{I}}{1 + \dot{a}_i B_\gamma \sqrt{I}} + \dot{B}I \quad (7)$$

where A_γ is the Debye-Hückel A parameter, B_γ is the Debye-Hückel parameter, \dot{B} is the Debye-Hückel B -dot parameter, and \dot{a}_i is the hard-core diameter, which is specific to each aqueous species.

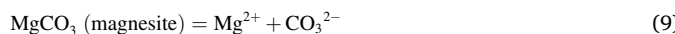
In the LLNL-type model, the activity coefficient of aqueous carbon dioxide CO_{2(aq)}⁰ is defined as a function of temperature and ionic strength (Drummond, 1981; Parkhurst and Appelo, 2013):

$$\log\gamma_{CO_2} = \left(C + FT + \frac{G}{T} \right) I - (E + HT) \left(\frac{I}{I + 1} \right) \quad (8)$$

where T is the temperature (K); I is the ionic strength; C , F , G , E , and H are species-dependent parameters.

4. Temperature-dependent mineral solubility product constant (Log K) calculations in PHREEQC

In PHREEQC, the mineral solubility product constant (log K) can be calculated by the law of mass action. If we take magnesite as an example, its dissolution reaction can be written as:



The magnesite solubility product (K) can be calculated from the relationship:

$$\log K = \log a_{Mg^{2+}} + \log a_{CO_3^{2-}} \quad (10)$$

The activities $a_{Mg^{2+}}$ and $a_{CO_3^{2-}}$ are calculated from speciation modeling with experimentally measured pH, Mg, and C concentrations in the solutions as well as their T -dependence.

$\log K$ is calculated from the Gibbs free energy of the reaction:

$$\Delta_r G^\circ = \Delta G_{f,Mg^{2+}}^\circ + \Delta G_{f,CO_3^{2-}}^\circ - \Delta G_{f,MgCO_3}^\circ \quad (11)$$

where $\Delta G_{f,Mg^{2+}}^\circ$, $\Delta G_{f,CO_3^{2-}}^\circ$, $\Delta G_{f,MgCO_3}^\circ$ are the Gibbs free energy of Mg²⁺, CO₃²⁻, and magnesite, respectively, and ΔG_r° can be used to calculate the relevant $\log K$ value (Eq. 1). Both SUPCRT92 and SUPCRTBL can be used to facilitate the calculation of ΔG_r° at elevated temperatures.

If $\log K$ is obtained from experimentally determined solubility measurements, its quality depends on the quality of the thermodynamic properties of the relevant species, their activity coefficients, and the solubility product constant of the magnesite dissolution reaction in the TDF used. Commonly, this is conducted with a limited set of aqueous components. For example, when the experimentally derived magnesite solubility data are compared with PHREEQC modeling results using the *diagenesis.dat* TDF, as described below, the Mg-bearing aqueous species Mg²⁺, MgCO₃⁰, MgOH⁺, MgHCO₃⁻ are included in the calculation. The temperature dependence of magnesite and aqueous species, as well as the activity coefficient model, are included in this comparison.

In this study, a comparison of experimental data with speciation-solubility modeling results affiliated with a particulate TDF was conducted. This type of comparison provides us with opportunities to evaluate the fidelity of mineral solubility calculations by PHREEQC with a particular database, in the context of how these solubility data would be used together in the geochemical models.

Such comparisons also serve to evaluate the internal consistency between phase-equilibrium derived mineral properties and those based on aqueous solution-based solubility data, for example, whether the $\Delta G_{f,MgCO_3}^\circ$ derived from regression of magnesite phase-equilibrium relationships at high P - T in Holland and Powell (2011) can reproduce solubility data of Bénédith et al. (2011). In this example, independently derived mineral and aqueous datasets are inconsistent, which has also been observed elsewhere (Holland and Powell, 2011; Tutolo et al., 2014; Miron et al., 2016, 2017).

5. Test cases

To explore the capabilities of different PHREEQC TDFs for calculating chemical equilibrium under different conditions, we selected several test cases covering a wide range of environmental and geological systems. These systems include those for river water, seawater, groundwater, organic-rich oil field brine, very high salinity water (e.g., Dead Sea brine), stream flow contaminated with hazardous metals, geothermal water (to represent the role of geothermometry), and high T - P water. The chemical compositions of samples selected as representative of each aqueous phase category are given in the supplementary material (Tables C1). A test case on the solubility of common minerals was also conducted. As *amm.dat* and *iso.dat* are specialized subsets of *phreeqc.dat*, they were not used for analysis and comparison. Also, because *bl.dat* is a specialized TDF designed for high T - P applications, it was only discussed in a high T - P water case. *pitzer.dat*, *frezchem.dat* and *coldchem.dat* focus on applications for high ionic strength aqueous solutions; they are only tested in the high salinity water case. Such TDFs omit significant numbers of elements and species, which limits coverage of the ion interaction approach for activity coefficient calculations.

Special precautions must be taken for the calculation of SiO_{2(aq)}⁰. *minseq.dat* uses H₄SiO_{4(aq)}⁰ as the basis and needs a multiplier factor of 1.6 in the input file if the analytical data is reported as mg/L. For the water chemistry analysis, some samples were reported as Si (e.g., river water), but others were reported as SiO₂ (e.g., seawater) (Table C1).

It is well known that under natural conditions the aqueous phase does not achieve equilibrium among redox couples (e.g., see Lindberg

and Runnels, 1984; Stumm and Morgan, 1996; Zhu and Anderson, 2002). This condition is aggravated when there is an imposed radiation flux, as is the case with seawater, river waters, meromictic lakes, and groundwaters in granitic terrains. Many situations involving anthropogenic interference or corrosion also fall under this category. For modeling purposes, it is therefore, necessary to establish on a case-by-case basis how the redox state should be defined in calculating the distribution of species. PHREEQC allows several options to input the redox state, i.e., as dissolved oxygen (DO), pe, or Eh. Any redox pair that has been analyzed can also be used in specifying an Eh value for a given pH, or the redox chemistry can be fixed by any specified Eh at a given pH. However, redox equilibrium can also be disabled, which permits redox pairs with different redox states to co-exist without interaction. Finally, alternative master or basis species can be specified to allow partial redox equilibrium.

In this evaluation, redox related modeling is not reviewed. Where necessary, we calculated the distribution of redox components, either by setting the O(–2)/O(0) redox couple, when the DO concentration is provided in the chemical analysis (the river water and seawater cases), or by specifying the *pe* value using the provided Eh value, e.g., in the case involving a stream flow contaminated with hazardous metals.

For this review, we also categorized the solute composition in terms of major and minor species. Following Hem (1992), we assume major species are those components having a concentration > 1 mg/L, while minor species are those with <1 mg/L. This definition applies to the river water, seawater, and groundwater cases. However, the concentrations of Ba, Fe, Sr, and some organic species are high in the studied oil field brine and Al, Zn, Mn, Cu are high in the contaminated stream flow. In these two cases, we assign the above mentioned species as the minor species to follow the convention of environmental practices.

5.1. River water

We used the river water test case from Nordstrom et al. (1979) to evaluate the ability and uncertainty of different PHREEQC databases in speciation-solubility calculations for this class of water. The chemical composition of the river water is listed in Table C1.

5.1.1. Major species

Table D1 and Fig. D1 compare the concentrations (expressed as log molalities) of selected major and minor species computed for the river water test case. The results from the calculations using different TDFs show remarkable consistency and agreement in terms of the concentrations of major species. The ability of the aquatic chemistry community to perform speciation calculations has improved compared to the time when Nordstrom et al. (1979) compared geochemical modeling codes and their associated thermodynamic datasets. The discrepancies between computed major species concentrations in this study are generally incrementally less than those reported by Nordstrom et al. (1979), as would be expected from subsequent refinements of the thermodynamic data. Table 3 lists the performance of different TDFs on speciation calculations for the river water.

5.1.2. Minor species

Table 3 lists the minor species lacking in specific TDFs. Generally, the computed concentrations of such species display larger variations than those for major species (cf. Figs. D1 and D2). The detailed comparison for the computed minor species concentrations from each TDF for this case is shown in Appendix D.

5.2. Seawater

We adopted the modern seawater case from Nordstrom et al. (1979) for evaluation. The chemical composition is listed in Table C1. Disagreements are expected to be greater than those for river water, because the higher ionic strength results in potentially greater ionic

complexation and less consistent activity coefficients.

5.2.1. Major species

Overall, the calculated species concentrations for major constituents between TDFs are quite consistent (Fig. E1; Table E1), with the differences being usually less than ±0.5 log unit (Fig. E1). Because the concentrations of Cl, Na, Ca, and Mg are elevated, CaCl^+ , MgCl^+ , and NaCl^\ominus are important species. However, in *phreeqc.dat*, *minteq.dat*, *minteq.v4.dat*, *wateq4f.dat* and *sit.dat*, they are omitted. For databases incorporating those species, the log molal differences for CaCl^+ are less than 0.5, for MgCl^+ are less than 0.4 and for NaCl^\ominus are less than 0.1 units (Figs. E1a, E1b, E1c). Although Sr^{2+} is an important species in seawater, it is omitted from *core10.dat* and *carfix.dat* (Fig. E1h).

5.2.2. Minor species

The modeled concentrations of selected minor species in the seawater test case using different TDFs are shown in Fig. E2 and Table E1. The findings are largely consistent with the river water case. However, the discrepancies between different TDFs are greater. For seawater, minor constituents such as Li^+ , Rb^+ , Cs^+ , Ba^{2+} and Cl-bearing complexes such as MnCl^+ , NiCl_2^\ominus , AgCl_4^{3-} , CdCl^+ , CdCl_2^\ominus , HgCl_3^- , PbCl_2^\ominus are important. Other species, e.g., S(–2) become insignificant. Table 3 lists minor species omitted in different TDFs. Li^+ , Rb^+ , Cs^+ and Ba^{2+} concentrations calculated from different TDFs are quite consistent, generally within 0.1 log unit (Fig. E2a). For Cl-bearing complexes, values from *minteq.v4.dat* usually display greater differences than those from other databases (Figs. E2b, E2d, E2f, E2h, E2i, and E2k).

5.2.3. Activity coefficients

With an ionic strength of ~0.65 M for seawater, the activity coefficients of species calculated using different PHREEQC TDFs are expected to show some differences. Table E2 compares the log activity coefficients of selected major species in the test case. Generally, the differences are within 0.1 log unit. Neutral species also show some differences (0.068 vs. 0 in logarithmic scale), as explained in Section 3.

5.3. Groundwater

We tested a groundwater example from Langmuir (1997). The chemical composition is listed in Table C1. Table F1 and Figs. F1 and F2 compare the aqueous concentrations of selected major and minor constituents, calculated using different PHREEQC TDFs.

5.3.1. Major species

Similar conclusions as those from the river water and seawater test cases can be reached for major constituents. However, the groundwater was analyzed for many more minor components. Table 3 lists the major and minor species omissions in different TDFs.

5.3.2. Minor species

Where included, fairly consistent results can be obtained for such minor species as Li^+ , Rb^+ , Cs^+ , Ba^{2+} , Zn^{2+} , ZnHCO_3^+ , Cd^{2+} , Cs^+ , Al^{3+} , Al(OH)_3^\ominus , Al(OH)_4^- , Pb^{2+} , PbCl^+ , PbCO_3^\ominus , HSeO_3^- , La^{3+} , LaCO_3^\ominus , HVO_4^{2-} , H_2VO_4^- , WO_4^{2-} , PO_4^{3-} , HPO_4^{2-} , H_2PO_4^- , and I^- (Table F1; Fig. F2); the differences are generally less than 0.5 between TDFs. The detailed comparison for other minor species concentrations from each TDF for this case is shown in Appendix F.

5.4. Organic-rich oil field brine

We used an oil field brine sample 83-TX-10 taken from Well A-14B at High Island Field, offshore Texas (Kharaka et al., 1986) to evaluate the capabilities of different TDFs for organic-rich oil field brine applications. With an ionic strength close to double that of seawater, similar issues also arise regarding ionic complexation, and the computation of ion activity coefficients. The chemical composition of the brine is listed in

Table 3

Performance of different data files with the test cases.

	<i>phreeqc.dat</i>	<i>wateq4f.dat</i>	<i>llnl.dat</i> & <i>core10.dat</i>	<i>carbfix.dat</i>	<i>sit.dat</i>	<i>miniteq.dat</i>	<i>miniteq.v4.dat</i>	<i>geothermal.dat</i> & <i>diagenesis.dat</i>	<i>pitzer.dat</i> , <i>frezchem.dat</i> & <i>ColdChem.dat</i>
River water major species	Most comprehensive	Most comprehensive	<i>llnl.dat</i> is most comprehensive; <i>Core10.dat</i> lacking F ⁻ , Br ⁻ , CaHCO ₃ ⁺ , MgHCO ₃ ⁺ , and KSO ₄ ⁻ .	Most comprehensive	Lacking NaSO ₄ ⁻ and KSO ₄ ⁻	Most comprehensive	Most comprehensive	Most comprehensive	N.E.
River water minor species	Lacking Ag, As, Co, Cr, Hg, I, Mo and Ni bearing species; Cd ²⁺ and CdOH ⁺ ~ 2–3 units lower	Lacking Cr and Hg bearing species; Ni ²⁺ and NiCO ₃ ^o about one unit lower; Cd ²⁺ and CdOH ⁺ ~ 2–3 units lower	<i>llnl.dat</i> lacking NiCO ₃ ^o , Cu(OH) ₂ ^o , AgHS ^o , Zn(HS) ^o and CdHS ⁺ ; <i>Core10.dat</i> N.R. Lacking additionally MnOH ⁺ , Fe(OH) ₄ ⁻ , Ag, Cd, Hg, Pb, As-bearing species, ZnCO ₃ ^o , I ⁻	N.R.; lacking NiCO ₃ ^o , Cu(OH) ₂ ^o , Zn(HS) ^o , CdHS ⁺ , MnOH ⁺ , Ag, Cd, Hg, Pb, As-bearing species, ZnCO ₃ ^o , I ⁻	AgHS ^o and CdHS ⁺ exceptionally low	Ni ²⁺ and NiCO ₃ ^o about one unit lower	Cu(OH) ₂ ^o , Zn(HS) ₂ ^o , Cd ²⁺ and CdOH ⁺ ~ 2–3 units lower	Lacking AgHS ^o , ZnCO ₃ ^o , Zn(HS) ₂ ^o , CdHS ⁺ , and PbCO ₃ ^o	N.E.
Seawater major species	Lacking CaCl ⁺ , MgCl ⁺ , NaCl ^o ,	Lacking CaCl ⁺ , MgCl ⁺ , NaCl ^o ,	<i>llnl.dat</i> is most comprehensive; <i>Core10.dat</i> lacking CaHCO ₃ ⁺ , MgHCO ₃ ⁺ , NaSO ₄ ⁻ , Br ⁻ , F ⁻ , MgF ⁺ , Sr ²⁺	Lacking Br ⁻ , MgF ⁺ , Sr ²⁺	Lacking CaCl ⁺ , NaSO ₄ ⁻ , NaCl ^o , KSO ₄ ⁻	Lacking CaCl ⁺ , MgCl ⁺ , NaCl ^o ,	Lacking CaCl ⁺ , MgCl ⁺ , NaCl ^o ,	Lacking NaHCO ₃ ^o	N.E.
Seawater minor species	Lacking Rb ⁺ , Cs ⁺ , Cr ³⁺ , Ni ²⁺ , NiCl ₂ ^o , NiCO ₃ ^o , Ag ⁺ , AgCl ₄ ³⁻ , Hg ²⁺ , HgCl ₃ ⁻ , AsO ₄ ³⁻ , HAsO ₄ ²⁻ , I ⁻	Lacking Cr ³⁺ , Ag ⁺ , Hg ²⁺ , HgCl ₃ ⁻ ,	Lacking NiCl ₂ ^o , NiCO ₃ ^o , Cu(OH) ₂ ^o , HgCl ₃ ⁻ ; <i>Core10.dat</i> lacking additionally Rb ⁺ , Cs ⁺ , Ba ²⁺ , Fe(OH) ₃ ^o , Fe(OH) ₄ ⁻ , CuCO ₃ ^o , Ag, Cd, Hg, Pb, As-bearing species, ZnCO ₃ ^o , I ⁻	Lacking Rb ⁺ , Cs ⁺ , Ba ²⁺ , NiCO ₃ ^o , Cu(OH) ₂ ^o , CuCO ₃ ^o , Ag, Cd, Hg, Pb, As-bearing species, ZnCO ₃ ^o , HgCl ₃ ⁻	Lacking NiCl ₂ ^o , Cu(OH) ₂ ^o , CuCO ₃ ^o , ZnCO ₃ ^o , HgCl ₃ ⁻	Lacking Cr ³⁺	Lacking Rb ⁺ , Cs ⁺	Lacking NiCl ₂ ^o , NiCO ₃ ^o , CuCO ₃ ^o , ZnCO ₃ ^o , PbCO ₃ ^o	N.E.
Ground water major species	CaCl ⁺ and MgCl ⁺ not included, as not considered relevant	CaCl ⁺ , MgCl ⁺ , KSO ₄ ⁻ not included, as not considered relevant	<i>Core10.dat</i> lacking CaHCO ₃ ⁺ , MgHCO ₃ ⁺ , NaSO ₄ ⁻ , Br ⁻ , F ⁻ , MgF ⁺ , Sr ²⁺	Lacking Br ⁻ , MgF ⁺ , Sr ²⁺	CaCl ⁺ , NaSO ₄ ⁻ , KSO ₄ ⁻ not included, as not considered relevant	CaCl ⁺ and MgCl ⁺ not included, as not considered relevant	CaCl ⁺ and MgCl ⁺ not included, as not considered relevant	Lacking NaHCO ₃ ^o	N.E.
Ground water minor species	Lacking Ag-, As-, Au-, Co-, Cs-, Cr-, Hg-, I-, La-, Ni-, Rb-, Sb-, Se-, Sn-, Th-, Ti-, U-, V-, W-bearing species and AsO ₃ F ²⁻	Lacking Au-, Co-, Cr-, Hg-, La-, Sb-, Sn-, Th-, Ti-, V-, W-bearing species and AsO ₃ F ²⁻	<i>Core10.dat</i> lacking Ag-, As-, Au-, Ba-, Cd-, Cs-, Hg-, I-, La-, Rb-, Sb-, Se-, Sn-, U-, V-, W-bearing species	Lacking Ag-, As-, Au-, Ba-, Cd-, Cs-, Hg-, I-, La-, Rb-, Sb-, Se-, Sn-, U-, V-, W-bearing species	Lacking Au-, La-, Sn-, Ti-, V-, W-bearing species	Lacking Au-, Co-, Cs-, La-, Sn-, Th-, Ti-, W-bearing species	Lacking Au-, Cs-, La-, Rb-, Sn-, Th-, Ti-, W-bearing species	Lacking Sn-, Th-, Ti-, U- bearing species	N.E.
Oil field brine major species	Lacking CaCl ⁺ , MgCl ⁺ , NaCl ^o , KCl ^o , CaF ⁺	Lacking CaCl ⁺ , MgCl ⁺ , NaCl ^o , KCl ^o	<i>llnl.dat</i> is most comprehensive; <i>Core10.dat</i> lacking CaHCO ₃ ⁺ , MgHCO ₃ ⁺ , NaSO ₄ ⁻ , Br ⁻ , Sr ⁺ , F ⁻ bearing species	Lacking Sr-, F-bearing species	Lacking CaCl ⁺ , MgCl ⁺ , NaCl ^o , KCl ^o , KSO ₄ ⁻	Lacking CaCl ⁺ , MgCl ⁺ , NaCl ^o , KCl ^o , Sr-complexes	Lacking CaCl ⁺ , MgCl ⁺ , NaCl ^o , KCl ^o	Lacking NaHCO ₃ ^o	N.E.
Oil field brine minor species	Lacking I ⁻ , S ₂ ²⁻ and all organic species	Lacking all organic species	Lacking BaHCO ₃ ⁺ , and Butyrate-, Propionate- and Valerate- species; <i>core10.dat</i> lacking I ⁻ , Ba-bearing species and all organic-species	Lacking I ⁻ , Ba-bearing species and all organic-species	Lacking Butyrate-, Propionate- and Valerate- species and some Acetate-bearing species	Lacking some Ba-bearing species	Species are most comprehensive	Lacking Butyrate-, Propionate- and Valerate- species and some Acetate-bearing species	N.E.
	~ 1	~ 3		~ 0.4	~ 0.4	~ 2.4	~ 0.4	~ 0.4	Up to 6 (continued on next page)

Table 3 (continued) *phreeqc.dat*

	<i>wateq4f.dat</i>	<i>llnl.dat</i> & <i>core10.dat</i>	<i>carbfix.dat</i>	<i>sit.dat</i>	<i>minteq.dat</i>	<i>minteq.v4.dat</i>	<i>geothermal.dat</i> & <i>diagenesis.dat</i>	<i>pitzer.dat</i> , <i>frezchem.dat</i> & <i>ColdChem.dat</i>
Application salinity range for NaCl solution	~ 1	~ 1	~ 0.3	~ 0.3	~ 1	~ 0.1	~ 0.1	Up to 3; ~1.2 for <i>frezchem.dat</i>
Application salinity range for CaCl ₂ solution	< 0.2	< 0.2	< 0.3	< 0.3	< 0.3	< 0.1	< 0.1	Up to 3
Application salinity range for MgSO ₄ solution	< 0.2	< 0.2	< 0.4	< 0.4	~ 0.2	< 0.4	< 0.1	Up to 4
Application salinity range for Na ₂ SO ₄ solution	Lacking CaCl ⁺ , MgCl ⁺ , NaCl ⁰ , and some Al-complexes	Lacking CaCl ⁺ , MgCl ⁺ , NaCl ⁰ , and some Al-complexes	<i>llnl.dat</i> is most comprehensive; <i>Core10.dat</i> lacking NaSO ₄ ⁻ , Br ⁻ , F-bearing species, some Al-complexes	Lacking Br ⁻ , F-bearing complexes, some Al-complexes	Lacking CaCl ⁺ , NaSO ₄ ⁻ , NaCl ⁰ , KSO ₄ ⁻ , HF ⁰ , and some Al-complexes	Lacking CaCl ⁺ , MgCl ⁺ , NaCl ⁰ , and some Al-complexes	Lacking CaCl ⁺ , MgCl ⁺ , NaCl ⁰ , and some Al-complexes	Lacking some Al-complexes N.E.
Stream flow contaminated with hazardous metals major species	Lacking Ag-bearing species	Species are most comprehensive	<i>llnl.dat</i> is most comprehensive; <i>Core10.dat</i> lacking Ag-, Cd-, and Pb-bearing species, some Cu-bearing complexes	Lacking Ag-, Cd-, and Pb-bearing species, some Cu-bearing complexes	Lacking some Cu- and Zn-bearing complexes	Lacking FeCl ⁺	Lacking FeCl ⁺	Lacking some SO ₄ -bearing complexes N.E.
Stream flow contaminated with hazardous metals minor species								

N.E. = Not evaluated. N.R. = Not recommended.

Table C1. Table G1 compares the concentration of selected species in this test case.

5.4.1. Major species

Cl-bearing and F-bearing ion complexes (CaCl^+ , MgCl^+ , NaCl^\ominus , KCl^\ominus , MgF^+ , NaF^+ and CaF^+) cannot be ignored, due to the relatively high Cl^- (37,700 mg/L) and F^- (13.1 mg/L) concentrations. We evaluated the capability of different TDFs for calculating these species (Fig. G1). *phreeqc.dat*, *minteq.dat*, *minteq.v4.dat* and *wateq4f.dat* do not include Cl-bearing complexes and *sit.dat* includes only MgCl^+ (Fig. G1). Generally, concentrations calculated for MgCl^+ and NaCl^\ominus are consistent between TDFs containing these species. For CaCl^+ , the concentrations calculated from *llnl.dat*, *core10.dat* and *carfix.dat* are consistent, whereas from *geothermal.dat* it is ~ 0.5 log unit higher and from *diagenesis.dat* it is ~ 0.7 log unit higher. Voigt et al. (2018) also noticed that the $\log K$ of CaCl^+ in *llnl.dat*, *core10.dat* and *carfix.dat* in the unfinished version (1994) of Sverjensky et al. (1997) differs by 0.3 log K at 0 °C, 1.2 log K at 300 °C in the later (1997) version. For KCl^\ominus , values from *llnl.dat*, *core10.dat* and *carfix.dat* are consistent, but from *geothermal.dat* and *diagenesis.dat*, it is ~ 0.8 units higher. The thermodynamic data of KCl^\ominus used for *llnl.dat*, *core10.dat* and *carfix.dat* are also from the 1994 version of Sverjensky et al. (1997), whereas those for *geothermal.dat* and *diagenesis.dat* are from the latter.

core10.dat and *carfix.dat* omit MgF^+ , NaF^+ , and CaF^+ and *phreeqc.dat* omits CaF^+ (Fig. G1b). For MgF^+ , values from *phreeqc.dat* and *wateq4f.dat* are respectively -3.6 to -3.7 log units; those from *llnl.dat* and *geothermal.dat* are 0.4–0.5 log units lower, from *minteq.dat* and *minteq.v4.dat*; 0.3 log unit higher, from *sit.dat*; 0.2 log unit lower, and from *diagenesis.dat*; ~ 1 log unit lower. NaF^+ values from *phreeqc.dat* and *wateq4f.dat* are all about -4.1 log units; those from *llnl.dat*, *sit.dat*, *geothermal.dat* and *diagenesis.dat* are ~ 0.2 log unit lower, from *minteq.dat*; about 0.6 log unit lower, and from *minteq.v4.dat*; about 0.3 log unit higher. For CaF^+ , log molalities calculated from *minteq.dat*, *minteq.v4.dat*, *wateq4f.dat* and *sit.dat* are all -4.3 to -4.2 log units, and from *llnl.dat*, *geothermal.dat* and *diagenesis.dat* are ~ 0.2 to 0.3 log units lower.

5.4.2. Minor species

Some oil field brines contain relatively high concentrations of short-chain aliphatic acid anions; for the test case, the concentrations of acetate, propionate, butyrate, and valerate are 221.9, 34.6, 11.3, and

11.1 mg/L, respectively. Here, we focus on the comparison of these organic species. *Minteq.dat* and *minteq.v4.dat* include all the cited organic species (Table G1). However, only $\log K$ values at 25 °C were provided for these species. *llnl.dat* has all acetate-bearing species, *sit.dat* has Acetate $^-$ and $\text{Ca}(\text{Acetate})^+$, and *geothermal.dat* and *diagenesis.dat* have Acetate $^-$. All other databases omit organic species. The detailed comparison for minor species concentrations from each TDF for this case is shown in Appendix G.

5.5. Very high salinity water

We evaluated the capability of different TDFs in handling speciation-solubility modeling for concentrated saline solutions as exemplified by a Dead Sea brine analysis from Jones and Deocampo (2003). As discussed in Section 3, *pitzer.dat*, *frezchem.dat* and *coldchem.dat* use the Pitzer equation (Pitzer, 1973). All other TDFs use ion-association (Davies, WATEQ, or B-dot equation) or SIT (Specific ion Interaction Theory) equations to account for the nonideality of aqueous solutions (Parkhurst and Appelo, 2013). We introduce the subject by first testing the performance of different TDFs with various pure electrolytes up to high concentrations (Figs. 2; H1-H3).

NaCl is commonly the dominant electrolyte in high salinity water. The mean ion-activity coefficient of NaCl as a function of NaCl concentration (up to 6 M) using different TDFs is calculated and compared in Fig. 2. For a solute A_xB_y that fully dissociates.

$$\text{A}_x\text{B}_y \rightarrow x\text{A}_+ + y\text{B}_- \quad (12)$$

the mean ion-activity coefficient is:

$$\gamma_{\pm} = (\gamma_A^x \gamma_B^y)^{\frac{1}{x+y}} \quad (13)$$

However, for an electrolyte that is incompletely dissociated, i.e., containing ion pairs or ionic complexes, the individual concentrations and activities of ions are effectively reduced and therefore a correction to the mean ion-activity coefficient must be made (Nordstrom and Munoz, 1994). A correction factor a can be introduced, which denotes the fraction of free ions with respect to the total concentration of this ion coefficient (Nordstrom and Munoz, 1994). The mean ion-activity coefficient becomes:

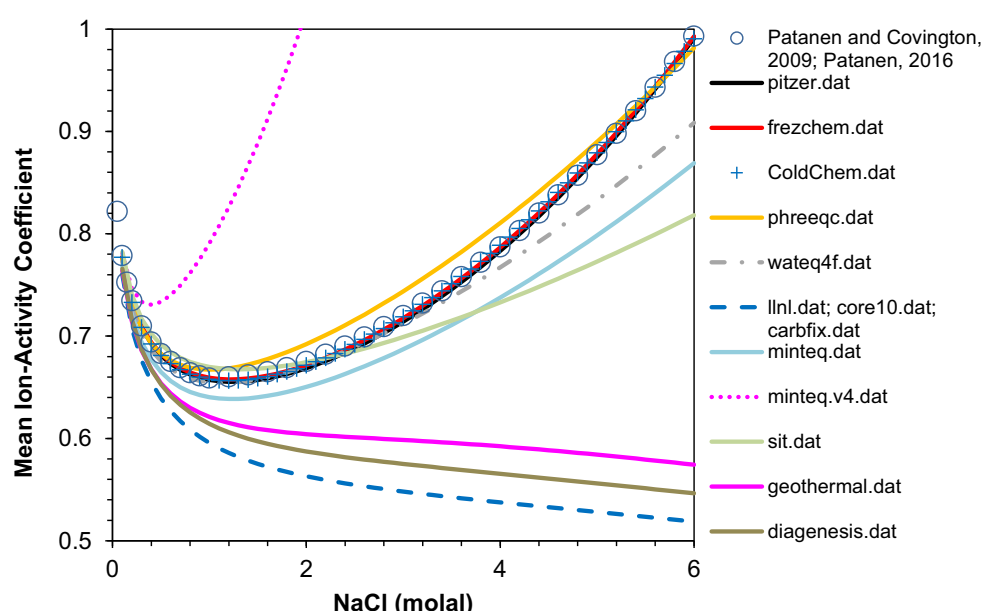


Fig. 2. The mean ion-activity coefficient of NaCl at 25 °C and 1 bar as a function of NaCl concentration derived using different PHREEQC TDFs. The experimental data are from Partanen and Covington (2009) and Partanen (2016).

$$\gamma_{\pm} = ((a_A \gamma_A)^x (a_B \gamma_B)^y)^{\frac{1}{x+y}} \quad (14)$$

The data files that use the ion association model (e.g., *phreeqc.dat*, *miniteq.dat*, *miniteq.v4.dat*, *wateq4f.dat*, *llnl.dat*, *carbfix.dat*, *core10.dat*, *geothermal.dat* and *diagenesis.dat*) require Eq. 13 to calculate the mean ion-activity coefficient. Otherwise, there would be large uncertainties if the mean ion-activity coefficients were not corrected for ion pairing.

The calculated values using TDFs with Pitzer equations (*frezchem.dat*, *ColdChem.dat* and *pitzer.dat*) have errors $< \pm 0.01$. Generally, TDFs using the WATEQ equation (*phreeqc.dat*, *miniteq.dat*, *diagenesis.dat* and *wateq4f.dat*) and SIT equation (*sit.dat*) fit the experimental results better than those using the Davies equation (*miniteq.v4.dat*) or B-dot equation (*llnl.dat*, *carbfix.dat*, *core10.dat* and *geothermal.dat*). The predicted values from *geothermal.dat* match the experimental data better than those of *llnl.dat*, *carbfix.dat* and *core10.dat*, because of the B-dot parameters from Oelkers and Helgeson (1990) used in *geothermal.dat*.

In addition to NaCl, we evaluated the performance of different TDFs in modeling concentrated CaCl₂, MgSO₄, and Na₂SO₄ solutions. The results are detailed in Appendix H.

To test the effectiveness of different TDFs in modeling mineral solubilities in high salinity water, we compared their calculated gypsum (CaSO₄•2H₂O) solubilities as a function of NaCl concentration with corresponding experimental data from Marshall and Slusher (1966) (Fig. 3). The TDFs using Pitzer equations (*pitzer.dat*, *frezchem.dat* and *ColdChem.dat*) fit the experimental data very well (errors $< 0.005 M$), even for the NaCl concentrations of 6 M or higher. Using *carbfix.dat* and *geothermal.dat*, the prediction errors of gypsum solubility are $< \pm 0.002 M$ up to NaCl concentration of $\sim 1 M$; the prediction errors of *diagenesis.dat* are $< \pm 0.002 M$ for up to $\sim 0.5 M$. Beyond that concentration, the gypsum solubility is overpredicted. *Miniteq.v4.dat* seriously under-predicts the gypsum solubility for NaCl concentrations between 0 and 7 M (errors up to $\pm 0.03 M$). Other databases using ion association models generally under-predict the solubility when NaCl concentration is $< 3 M$ and overpredict it when NaCl concentration is $> 3 M$.

Using an analysis of the Dead Sea brine from Jones and Deocampo (2003), its chemical composition being listed in Table C1, we evaluated the saturation index (SI) of minerals calculated with different TDFs (Table 4), where SI is defined as

$$SI = \log(IAP/K_{sp}) \quad (15)$$

where *IAP* is ion activity product and *K_{sp}* is equilibrium solubility product. Highly soluble salts can precipitate from high-salinity waters, and therefore a more comprehensive mineral set must be considered than for low salinity waters. *ColdChem.dat* is the only TDF of the three using Pitzer equations (*pitzer.dat*, *frezchem.dat* and *ColdChem.dat*), that does not include carbonate minerals, as the C component is lacking. SIs of minerals from *pitzer.dat* and *frezchem.dat* largely agree with each other, with the differences of 0.1–0.2 units, except for carbonate minerals, which display the differences up to 2 units. The large uncertainties of carbonate mineral SIs in high salinity water call for further study.

Of the TDFs using non-Pitzer methods, *llnl.dat* includes almost all the relevant minerals (lacking one), followed by *sit.dat* (lacking two), *wateq4f.dat*, *core10.dat* and *carbfix.dat* (lacking six), *miniteq.dat* and *miniteq.v4.dat* (lacking seven), *phreeqc.dat*, *diagenesis.dat* and *geothermal.dat* (lacking 11) (Table 4).

The SIs of minerals using these TDFs are largely underestimated when compared to those using Pitzer methods. If the SI values from *pitzer.dat* are used for reference, values from non-Pitzer methods are ~ 2.5 –3 units lower for calcite, ~ 2 –2.5 units lower for aragonite and magnesite, ~ 3 –5 units lower for dolomite, ~ 0.5 –1.8 units lower for nahcolite, ~ 2 –3 units lower for nesquehonite, and ~ 8.5 –12 units lower for huntite.

5.6. Stream flow contaminated with hazardous metals

To evaluate the ability of the different PHREEQC TDFs for environmental applications, we selected a groundwater sample contaminated with heavy metals from the Penn Mine in Calaveras County, California (Hamlin and Alpers, 1995). The sample was collected from well GS-6 on April 15, 1992. The water is moderately acidic (pH 4.1), and contains highly elevated concentrations of toxic metals (including Zn 170 mg/L, Cd 0.69 mg/L, Pb 0.004 mg/L, and Cu 13 mg/L; Table C1). Table 3 lists omissions of major and minor species in the different TDFs.

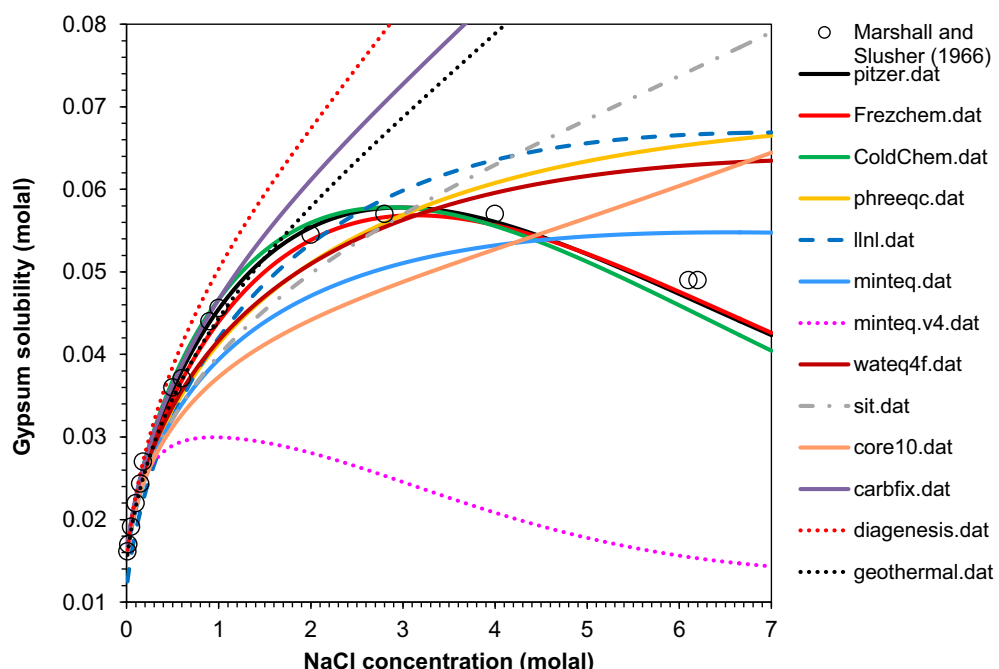


Fig. 3. The solubility of gypsum at 25 °C and 1 bar as a function of NaCl concentration (molality) calculated using different PHREEQC TDFs. Circles are experimental data from Marshall and Slusher (1966).

Table 4
Saturation indices for selected minerals in the Dead Sea brine test case.

Formula	pitzer.dat	freezechem.dat	GoldChem.dat	phreeqc.dat	lml.dat	minetq.dat	minetq.v4.dat	sit.dat	water4f.dat	core10.dat	Carbfix.dat	Geothermal.dat	Diagenesis.dat
Ionic strength	11.96	11.97	11.96	11.91	6.833	11.91	10.71	11.91	7.211	6.834	6.832	5.184	5.087
Calcite	CaCO ₃	2.12	0.82	-	-0.50	-0.13	-0.48	0.06	-0.50	0.36	0.27	-0.10	0.26
Aragonite	CaCO ₃	1.83	0.68	-	-0.64	-0.28	-0.62	-0.12	-0.64	0.19	0.12	-0.25	0.22
Dolomite	CaMg(CO ₃) ₂	5.39	2.90	-	0.21	1.69	0.14	0.67	0.21	0.30	0.49	1.08	0.95
Magnesite	MgCO ₃	2.52	1.51	-	-	0.20	0.13	-0.54	0.12	0.21	0.60	0.22	-0.15
Natrolite	NaHCO ₃	-2.04	-2.54	-	-	-2.85	-	-	-3.85	-2.67	-2.45	-2.82	-
Nesquehonite	MgCO ₃ •3H ₂ O	-0.88	-1.95	-	-	-3.10	-2.65	-3.70	-2.66	-3.92	-2.70	-3.07	-
Huntite	CaMg ₃ (CO ₃) ₄	8.80	-	-	-1.12	-2.69	-2.45	-2.45	-2.72	-0.49	-1.00	-	-
Gypsum	CaSO ₄ •2H ₂ O	0.66	0.80	1.03	0.06	-0.90	0.22	-0.42	0.07	-0.03	-0.87	-0.89	-0.21
Anhydrite	CaSO ₄	0.80	0.95	1.38	0.01	-0.89	0.50	-0.42	0.10	0.02	-0.86	-0.89	-0.26
Epsomite	MgSO ₄ •7H ₂ O	-2.24	-2.02	-1.92	-	-3.16	-1.82	-3.11	-1.92	-3.88	-	-	-
Hexahydrite	MgSO ₄ •6H ₂ O	-2.28	-2.02	-1.96	-	-3.30	-	-	-	-4.01	-	-	-
Thenardite	Na ₂ SO ₄	-2.32	-2.17	-1.95	-	-3.43	-2.89	-6.60	-2.86	-3.04	-3.40	-3.43	-
Glauberite	Na ₂ Ca ₂ (SO ₄) ₂	-0.72	-	-0.07	-	-3.57	-	-	-	-9.80	-	-	-
Goergeyite	K ₂ Ca ₅ (SO ₄) ₆ H ₂ O	5.91	-	-	-	-	-	-	-	-	-	-	-
Halite	NaCl	0.47	0.51	0.50	0.30	-0.78	0.12	2.24	0.16	-0.56	-0.78	-0.75	-0.83
Sylvite	KCl	-0.52	-0.52	-0.51	-0.89	-0.93	-	-	-	-1.04	-0.93	-0.92	-1.33
Bischoffite	MgCl ₂ •6H ₂ O	-1.71	-1.65	-1.63	-	-4.06	-	-	-	-4.64	-	-	-
Carnallite	KMgCl ₃ •6H ₂ O	-1.16	-0.92	-0.98	-	-4.04	-	-	-	-4.68	-	-	-

5.6.1. Major species

For major species, the focus is on F-bearing species, because the sample contains a relatively high concentration of F (3.2 mg/L) (Table 11). *core10.dat* omits F-bearing species and *carbfix.dat* omits F-bearing ionic complexes. For TDFs that include F-bearing species, the calculated species concentrations are generally consistent (Fig. 11a). The differences are less than 0.3 log units for F⁻, except for *minetq.v4.dat* (up to 0.5 log units) and *carbfix.dat* (where the dominant species is F⁻, instead of AlF²⁺). Correspondingly, they are less than 0.02 for AlF²⁺, 0.5 for AlF₂⁺, 0.7 for MgF⁺ (except for *minetq.v4.dat*, which is 1.2) and 0.3 for HF⁰ (except for *minetq.v4.dat*, which is 0.6).

5.6.2. Minor species

For minor species, we focus on Al-, Zn-, Mn- and Cu-bearing species, because of their relatively high concentrations in the sample. For Al-bearing species, *core10.dat* omits AlSO₄⁺. Al(SO₄)₂⁻ is lacking in *core10.dat*, *carbfix.dat*, *geothermal.dat* and *diagenesis.dat*. Only *llnl.dat* contains Al₂(OH)₂⁴⁺. AlH₃SiO₄²⁺ is found only in *sit.dat*, *carbfix.dat*, *geothermal.dat* and *diagenesis.dat*. The differences in computed concentrations are less than 0.2 log unit for AlSO₄⁺, 0.4 for Al(SO₄)₂⁻, 1.0 for Al₂(OH)₂⁴⁺ and 0.5 for AlH₃SiO₄²⁺ (Fig. 11b).

The calculated concentrations of Zn-bearing species using different TDFs are generally consistent with each other (Fig. 11c). For Mn-bearing species, the differences in calculated MnCl⁺ concentrations are relatively large (up to one log unit) (Fig. 11d). For Cu-bearing species, the differences in calculated concentrations are generally within 0.5 log units (Fig. 11e), but CuSO₄⁰ is lacking in *sit.dat*, *core10.dat*, *carbfix.dat*, *geothermal.dat* and *diagenesis.dat*, and CuCl⁺ is lacking in *sit.dat*, *core10.dat* and *carbfix.dat*.

5.7. Solubilities of common minerals

The focus of this section is to compare the calculated equilibrium solubility product constants or solubilities of selected common minerals from different TDFs and compare them with those based on experimental measurements. The selection criteria are that: (1) they are common rock-forming minerals of both detrital and authigenic origin, (2) they are stable under natural surficial and near-surface conditions, and, most importantly, (3) reliable experimental data are available covering a considerable range of 0–300 °C at P_{sat}. Although important, some clay minerals, e.g., illite, smectite, and chlorite, are not compared, because (1) log K for many low-temperature clay minerals are not given in several of the TDFs under discussion, (2) if given, the data quality is questionable, (3) retrieving accurate thermodynamic properties from solubility data is difficult, because of complexities associated with solid solutions, structural disorder, poor crystallinity, and secondary phase formation, (4) the chemical formulas for a given clay in both TDFs and experiments are commonly inconsistent, and (5) attainment of reversible equilibrium in solution is not achievable in practice unless the temperature is sufficiently elevated (e.g., Guggenbach, 1985; May et al., 1986; Aja et al., 1991; Vieillard, 2000; Prieto, 2009; Oelkers et al., 2009).

Modeling of aqueous-solid systems follows two paths: (1) the Gibbs free energy minimization approach (White et al., 1958; Kulik et al., 2013, 2) the mass-action/mass balance approach (Brinkley Jr, 1947). Zeleznik and Gordon (1960, 1968) and Smith and Brinkley (1960) proved that both methods are thermodynamically equivalent. However, the latter favors the direct application of experimental solubility measurements when applied to minerals and other solid phases. For this review, we compare the different TDFs using mineral equilibrium solubility product constants as examples, which benefit from the mass action approach.

The mineral solubility data are either presented as log K or as dissolved concentrations. In this section, we use log K to compare the solubilities for most minerals, but use dissolved concentrations for quartz, gypsum, anhydrite and gibbsite to allow direct comparison with

the experimental data.

Tutolo et al. (2014) and Miron et al. (2016, 2017) derived internally consistent thermodynamic data for the aluminum system and some aqueous species, respectively. However, their work focused mainly on high T - P applications (e.g., > 400 °C, 1 kb), while this study focuses on lower temperatures (0–300 °C). Only a few cases with overlapping T - P ranges allow direct comparison.

For kaolinite solubility product constants, the results from *geothermal.dat* and *diagenesis.dat* are similar to those of the trend line for Holland and Powell (2011) in Fig. 2 of Tutolo et al. (2014). Tutolo et al. (2014)'s model weighted the experimental data from Devidal et al. (1996) more than *geothermal.dat* and *diagenesis.dat*. When using the G_f^0 , H_f^0 , S^0 of kaolinite from Robie and Hemingway (1995), a similar log K curve to that calculated by Tutolo et al. (2014) can be generated. We decided, however, to retain the thermodynamic properties given by Holland and Powell (2011) rather than using those from Robie and Hemingway (1995), because the experimental data are poorly constrained at the temperature interval of 100–190 °C in Devidal et al. (1996).

For quartz solubility, Miron et al. (2016) (their Fig. 5A) used a log scale to illustrate Si concentrations at saturated water vapor pressure; we believe our refinement (using thermodynamic properties of $\text{SiO}_2 \cdot (\text{aq})$ from Apps and Spycher (2004) and HSiO_3^- from Sverjensky et al. (1997) at 0–50 °C under the same conditions are more precise. For boehmite and gibbsite, Miron et al. (2017) focused on comparing experimental data at higher ionic strengths, and for calcite, they focused on high-pressure data. Miron et al. (loc. cit.) also modeled magnesite, brucite, and dolomite solubility. This study produced similar results when adopting the thermodynamic properties of their Mg-bearing species (e.g., in *geothermal.dat* and *diagenesis.dat*).

5.7.1. Oxides, oxy-hydroxides, and hydroxides

Brucite. Brucite often forms as a byproduct of periclase in dolomite, or as a vein mineral due to low-temperature hydrothermal alteration or metamorphism of carbonate rocks, or during the serpentinization of dunites (Anthony, 1990). It can be used as a basis for calibrating the thermodynamic values of Mg^{2+} (e.g., Miron et al., 2017).

For brucite solubility product constant, *sit.dat* results match the experimental data within ± 0.1 unit in its applicable T range (15–80 °C) (Fig. 4). *minteq.dat*, *minteq.v4.dat* and *wateq4f.dat* slightly under-predict

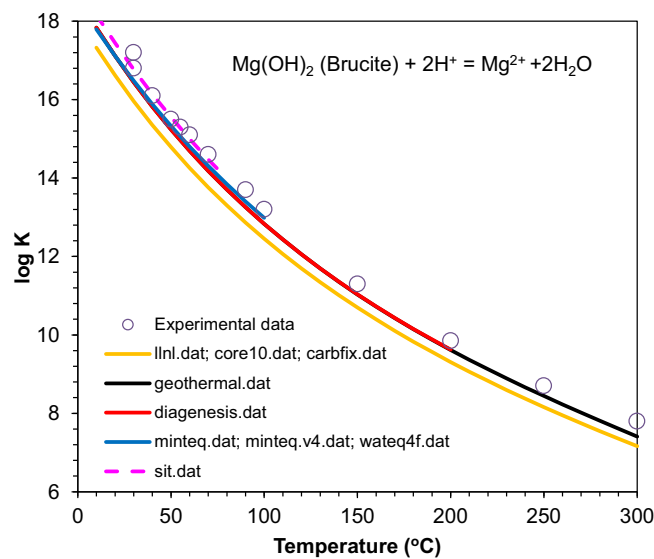


Fig. 4. Brucite solubility product constants as a function of temperature. Experimental data are from Brown et al. (1996) and McGee and Hostetler (1977). (For interpretation of the references to color in this figure legend, the reader is referred to the web version of this article.)

the log K values by 0.2 unit at $T < 100$ °C. The predictions from *llnl.dat*, *core10.dat* and *carbfix.dat* are systematically low by ~ 0.8 units. The prediction errors from *geothermal.dat*, *diagenesis.dat* are within ± 0.2 unit.

The differences in calculated log K values from different TDFs are mainly because of the different sources of thermodynamic properties of brucite and Mg^{2+} . The ΔG_f^0 of brucite in Holland and Powell (2011) is ~ 2.6 kJ lower than Blanc (2008), but ΔG_f^0 of Mg^{2+} in Miron et al. (2017) is ~ 0.6 kJ lower than Blanc (2008) (Table K1). Summing up, the difference for brucite dissolution reaction is ~ 2 kJ/mol between *sit.dat* and *geothermal.dat*/*diagenesis.dat*. The ΔG_f^0 of brucite in Helgeson et al. (1978) is ~ 3.3 kJ/mol lower and ΔG_f^0 of Mg^{2+} in Shock and Helgeson (1988) is ~ 1.4 kJ/mol higher. Thus, for the brucite dissolution reaction, the difference is ~ 4.7 kJ/mol between *sit.dat* and *llnl.dat*/*core10.dat*/*carbfix.dat*.

Gibbsite, boehmite, and diasporite. Gibbsite, boehmite, and diasporite are important controls in calibrating the thermodynamic properties of Al-bearing species in the solution (e.g., Tagirov and Schott, 2001). Three other naturally occurring polymorphs of gibbsite are known, bayerite, doyleite, and nordstrandite, but their thermodynamic properties have not been well characterized. Unstable amorphous or microcrystalline forms of Al(OH)_3 are not considered as their thermodynamic properties in terms of crystallinity or particle size are not provided for in the TDFs under review.

Palmer and Wesolowski (1992) conducted gibbsite solubility studies and collected the experimental data from the literature. For gibbsite solubility product constants in acidic solutions, the errors of log K values calculated using *geothermal.dat*, *diagenesis.dat*, *sit.dat*, *llnl.dat*, *core10.dat* and *carbfix.dat* are within ± 0.1 unit compared to the experimental data at 10–80 °C (Fig. 5). Calculations from *phreeqc.dat*, *wateq4f.dat*, *minteq.v4.dat* and *minteq.dat* over-predict the log K values for ~ 0.4 –1.4 unit and the differences increase with the increasing T .

For gibbsite solubility product constants in basic solutions, log K values calculated using *geothermal.dat* and *diagenesis.dat* generally match the experimental data within ± 0.1 unit between 10 and 170 °C (Fig. 6). *sit.dat* predicts the gibbsite solubility within ± 0.1 unit in its applicable temperature range (< 80 °C). The differences between the predictions from *llnl.dat*, *core10.dat* and *carbfix.dat*, and the experimental data, are $< \pm 0.1$ for $T < \sim 70$ °C; above that temperature they

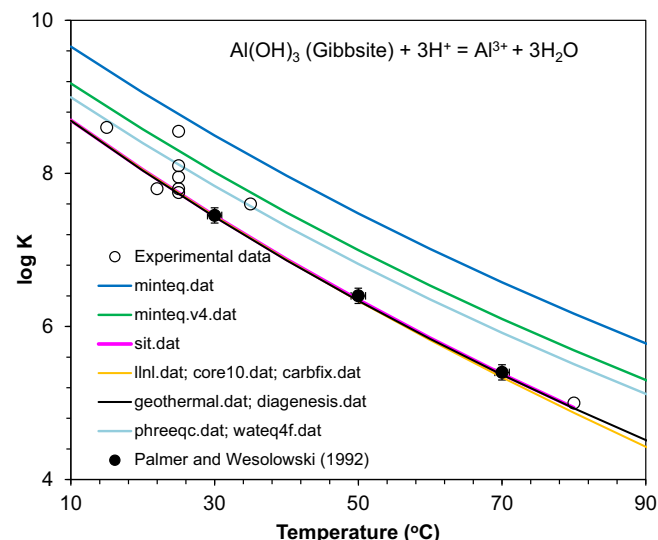


Fig. 5. Gibbsite solubility product constants as a function of temperature in acidic solutions. Symbols represent experimental data. The experimental data are from Frink and Peech (1962), Kittrick (1966), Singh (1974), May et al. (1979), Bloom and Weaver (1982), Peryea and Kittrick (1988), Nagy and Lasaga (1992) and Palmer and Wesolowski (1992). The experimental error of Palmer and Wesolowski (1992) is ± 0.084 –0.113 log unit.

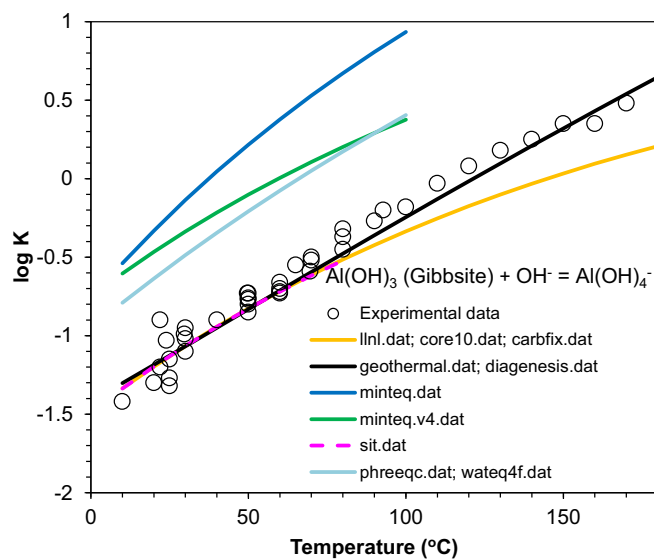


Fig. 6. Gibbsite solubility product constants as a function of temperature in basic solutions. Symbols represent experimental data for comparison. The experimental data are from Russell et al. (1955), Kittrick (1966), Apps (1970), Berecz and Szita (1970), Packer (1979), Verdes et al. (1992) and Wesolowski (1992).

underpredict the log K values for up to 0.35 unit at 170 °C. Other TDFs over-predict the log K values for 0.5–1.1 units compared to the experimental data.

Tagirov and Schott (2001) collected and selected experimental data for boehmite solubility product constants. The data presented in Figs. J1 and J2 follow their selections. Boehmite solubility product constant measurements are more reliable for temperatures between 100 and 250 °C (Apps et al., 1989). Below 100 °C solubility product constant measurements are difficult, because the equilibration rate for boehmite saturation is slow (Apps et al., 1989).

For log K values for boehmite saturation in acidic solutions, the differences between the values calculated using *geothermal.dat* and *diagenesis.dat*, and the experimental data, are generally within ± 0.1 unit for $T > 100$ °C (Fig. J1). *llnl.dat*, *core10.dat* and *carbfix.dat* match within ± 0.1 unit with the experimental data between 100 and 260 °C. For T up to 80 °C, calculations from *sit.dat* have only ± 0.02 unit differences from *diagenesis.dat*, *geothermal.dat*, *llnl.dat*, *core10.dat* and *carbfix.dat*. The log K values calculated using *minteq.dat*, *minteq.v4.dat* and *wateq4f.dat* are systematically 0.8 units higher than those from all other TDFs for T range of 10–100 °C. *phreeqc.dat* does not include boehmite. ΔG_f^0 for boehmite in Robie and Waldbaum (1968) is ~ 8 kJ/mol higher than given by Robie and Hemingway (1995), Hemingway et al. (1991) and Helgeson et al. (1978) (Table K1).

Log K values for boehmite saturation in basic solution, calculated using *geothermal.dat*, are $\sim \pm 0.2$ unit different from the experimental data between 60 and 250 °C (*diagenesis.dat* for 60–200 °C) (Fig. J2). Predictions from *llnl.dat*, *core10.dat* and *carbfix.dat* are $\sim \pm 0.2$ units different from the experimental data up to 200 °C, whereas above 200 °C, the predicted log K values trend lower than the experimental data up to 0.35 unit at 300 °C. For T up to 80 °C, the differences between the calculations from *sit.dat* and the experimental data are $\sim \pm 0.2$ unit. *Minteq.dat*, *minteq.v4.dat* and *wateq4f.dat* over-predict the log K values for ~ 0.6 – 0.8 log unit for $T < 100$ °C compared to the experimental data, and the gap increases with temperature.

Diaspore solubility product constant experimental data in basic solution were compiled by Apps et al. (1989) and Verdes et al. (1992). The experimental data below 150 °C are problematic, which is likely due to the lack of diaspore equilibration and insufficient run time. The experimental data are quite scattered between 150 and 300 °C. Log K values

calculated using *geothermal.dat*, *llnl.dat*, *core10.dat* and *carbfix.dat* fall within ± 0.2 unit differences from the experimental data at 150–300 °C (*diagenesis.dat* 150–200 °C) (Fig. J3). Calculations using *wateq4f.dat* are consistent with *diagenesis.dat*, *geothermal.dat*, *llnl.dat*, *core10.dat* and *carbfix.dat* at 50–100 °C, but are ~ 0.1 unit lower when $T < 50$ °C. Log K values predicted using other TDFs are up to 0.5 units lower than that calculated using *geothermal.dat* for $T < 100$ °C. *phreeqc.dat* does not include diaspore.

Hematite. Hematite (α -Fe₂O₃) is widespread in rocks and soils (Cornell and Schwertmann, 2003). It is chosen for the evaluation of solubility product constant calculations in this study because it is thermodynamically stable up to 670 °C (Hemingway, 1990) and is used to obtain thermodynamic data of the Fe³⁺ species and its first hydroxide complex (Diakonov et al., 1999).

For hematite log K calculations under acidic conditions, the differences between the calculated values using *llnl.dat*, *core10.dat* and *carbfix.dat* and the experimental data are within ± 0.2 unit (Fig. 7). Those from *geothermal.dat* and *diagenesis.dat* slightly overpredict log K values for ~ 0.2 – 0.6 units. All other TDFs underpredict log K for up to 4 units. The difference between *geothermal.dat*/*diagenesis.dat* and *llnl.dat*/*core10.dat*/*carbfix.dat* is mainly due to ΔG_f^0 of hematite (~ 1.7 kJ/mol) (Table K1). The difference between *sit.dat* and *llnl.dat*/*core10.dat*/*carbfix.dat* is ~ 3.2 kJ/mol, i.e., ~ 1.2 kJ from the difference in ΔG_f^0 hematite and ~ 2 kJ from the difference in $2 \times \Delta G_f^0$ Fe³⁺.

For hematite log K calculations under alkaline conditions, the values calculated using *carbfix.dat* are within $\sim \pm 0.2$ unit difference to the experimental data (Fig. 8). The calculations from *geothermal.dat* and *diagenesis.dat* are within $\sim \pm 0.2$ unit difference to the experimental data below 60 °C, but overpredict the log K values by ~ 0.2 – 0.6 unit between 110 and 280 °C. The divergence increases with temperature. Note that the model does not converge for $T > 280$ °C using *geothermal.dat*. The reason for the calculated differences is due to the source of the thermodynamic properties of hematite (Table K1). Note that *core10.dat* does not include the Fe(OH)₄⁻ species and is therefore not evaluated. The predictions from all other TDFs differ substantially.

Quartz. Accurately predicting quartz solubility is important, because SiO₂ is the most abundant oxide on Earth and quartz solubility controls silica transport in most hydrothermal and geothermal fluids (Fournier, 1985). Rimstidt (1997) reviewed quartz solubility experiments in the literature, and his compilation is used in this study for comparison with modeling results for $T < 300$ °C, because the quartz solubility values from his results are in good agreement with dissolved silica concentrations found in ancient groundwaters. The solubilities of quartz at low temperatures by Fournier and Potter (1982) and Walther and Helgeson (1977) are recognized as being too low (Rimstidt, 1997). It should be noted, however, that below about 100 °C, groundwaters generally do not achieve equilibrium with respect to quartz, but instead tend to equilibrate metastably with respect to chalcedony or cristobalite. The lower solubility of quartz at $T < 90$ °C from Fournier and Potter (1982) and Walther and Helgeson (1977) arose, because of their choice of experimental data from Morey et al. (1962). Rimstidt (1997) indicated that the 25–84 °C solubility data from Morey et al. (1962) are problematic.

The calculated quartz log K values using *llnl.dat*, *core10.dat*, *carbfix.dat* are ~ 0.1 log unit lower than those from *geothermal.dat* and *diagenesis.dat* (Fig. 9a). The log K s from *wateq4f.dat* and *phreeqc.dat* are ~ 0.1 log unit lower than those from *geothermal.dat* and *diagenesis.dat* at 20–100 °C and 20–150 °C, respectively. The predicted values from *minteq.v4.dat* are up to 0.25 log units lower than those from *geothermal.dat* and *diagenesis.dat* and the differences increase with the increasing T . The predicted values from *sit.dat* are up to 0.3 log units higher than those from *geothermal.dat* and *diagenesis.dat* at $T < 50$ °C and the differences decrease with the increasing T .

For quartz solubility at the temperature and pressure range of 25–300 °C and 1 bar to P_{sat} (Fig. 9b), values calculated from *geothermal.dat* and *diagenesis.dat* match the experimental data within ± 0.02 mM.

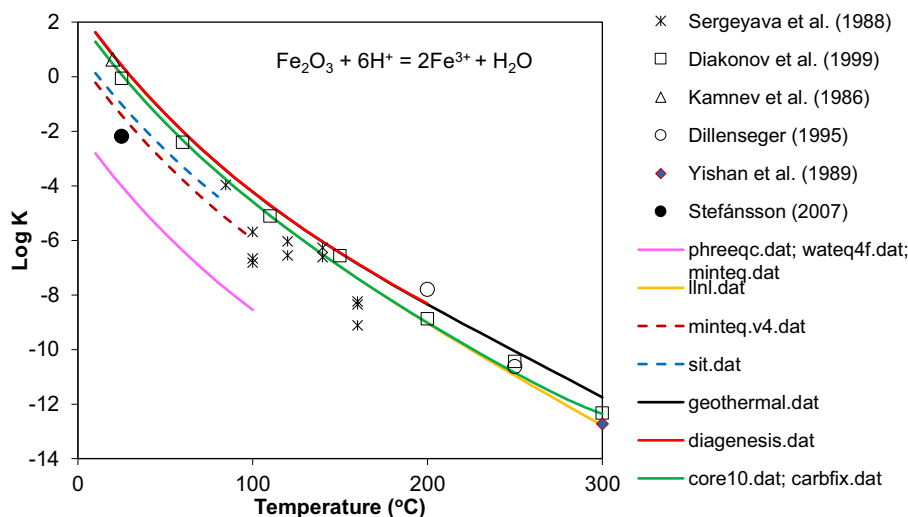


Fig. 7. Hematite solubility product constants as a function of temperature under acidic conditions. The experimental data are from Yishan et al. (1989), Kamnev et al. (1986), Suleimenov (1988), Dillenseger (1995), and Diakonov et al. (1999) and Stefánsson (2007).

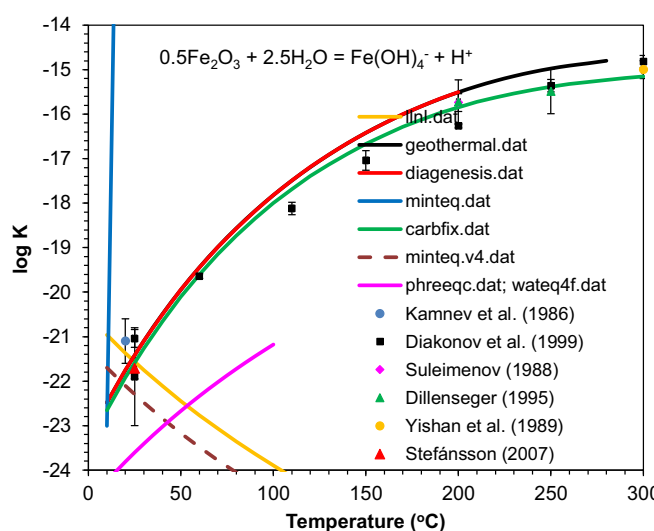


Fig. 8. Hematite solubility product constants as a function of temperature under alkaline conditions. The experimental data are from Yishan et al. (1989), Kamnev et al. (1986), Suleimenov (1988), Dillenseger (1995), and Diakonov et al. (1999), and Stefánsson (2007). The error of Kamnev et al. (1986) is ± 0.5 log unit at 20 °C; the errors of Diakonov et al. (1999) are ± 1.1 at 25 °C, ± 0.06 at 60 °C, ± 0.12 at 110 °C, ± 0.22 at 150 °C, ± 0.04 at 200 °C, ± 0.14 at 250 °C, and ± 0.14 at 300 °C; the error of Suleimenov (1988) is ± 0.2 at 200 °C; the errors of Dillenseger (1995) are ± 0.5 at 200 °C and 250 °C; the error of Yishan et al. (1989) is ± 0.2 at 300 °C.

Values from *sit.dat* also within ± 0.02 mM compared to the experimental data at temperatures < 80 °C. The predictions from *minteq.v4.dat*, *llnl.dat*, *core10.dat*, *carbfix.dat*, *phreeqc.dat*, *wateq4f.dat* and *minteq.dat* at $T < 90$ °C are substantially lower than the experimental data for up to 0.1 mM. This arises because the source of the thermodynamic data for quartz in *phreeqc.dat* and *wateq4f.dat* is from Nordstrom et al. (1990), who accepted the values from Fournier and Potter (1982); whereas the data source in *llnl.dat*, *core10.dat* and *carbfix.dat* is from Helgeson et al. (1978) and Shock and Helgeson (1988), which originated in Walther and Helgeson (1977). The ΔG_f° SiO_{2,aq} in Shock and Helgeson (1988) is ~ 1.4 kJ/mol higher than that in Apps and Spycher (2004) (Table K1), which can explain the difference between the calculated log *K* values from *llnl.dat*/*core10.dat*/*carbfix.dat* and *geothermal.dat*/*diagenesis.dat*.

5.7.2. Aluminosilicates

Kaolinite. Previous researchers recognized that the solubilities of Al-bearing minerals are likely to show systematic uncertainties from their actual values (Hemingway et al., 1982; Tutolo et al., 2014). We selected kaolinite to evaluate the extent of agreement between calculations from specific TDFs with experimental observations because kaolinite was used as an anchor mineral for the Al₂O₃ component in Helgeson et al. (1978) (Wolery and Sutton, 2013; Tutolo et al., 2014).

Fig. 10 demonstrates the kaolinite solubility product constant calculated using different PHREEQC TDFs compared with experimental data. Log *K* values calculated from *geothermal.dat* and *diagenesis.dat* match the experimental data within ± 0.4 unit. Curves from *minteq.dat* (~ 0.8 unit), and *phreeqc.dat* and *wateq4f.dat* (~ 2.8 units) systematically over-predict the log *K* values. Other TDFs also over-predict log *K* values for up to 1 unit.

Feldspars. The feldspars comprise the most abundant group of minerals in the Earth's crust (Dietrich, 2018), commonly occurring as rock-forming minerals in igneous, metamorphic, and sedimentary rocks. It is difficult to measure the solubility of feldspars, especially at low temperatures where rates of equilibration are slow. Phase equilibrium studies involving feldspars have been performed at temperatures higher than 300 °C, e.g., Hemley (1959), Davis (1972), Montoya and Hemley (1975), Sverjensky et al. (1991), Haselton et al. (1995), Hauzenberger et al. (2001) and Pak et al. (2003).

Because the applicable temperature range of most PHREEQC TDFs is < 300 °C, we used field data from Stefánsson and Arnórsson (2000) to assess the capabilities of the TDFs in calculating solubility product constants of these two feldspars. Stefánsson and Arnórsson (loc. cit.) investigated the saturation state of feldspar minerals in geothermal waters. Although unverified, they concluded that equilibrium is closely approached between the aqueous phase and both low albite and potash feldspar (microcline) under field conditions.

Fig. 11 shows the calculated low albite solubility product constant using different TDFs compared with those evaluated from geothermal waters at 0–300 °C. The results indicate that the log *K* of albite dissolution reaction calculated using *geothermal.dat*, *llnl.dat*, *core10.dat* and *carbfix.dat* correspond well with the data from geothermal waters at 0–300 °C, given the large measure of associated uncertainty (up to 2 units). Results from *diagenesis.dat* agree well for 0–200 °C and *sit.dat* are good between 15 and 80 °C (within ± 0.2) with *geothermal.dat*, *llnl.dat*, *core10.dat* and *carbfix.dat*. The predicted values using *minteq.dat* are about 0.4 units higher than those from *llnl.dat*, *core10.dat* and *carbfix.dat*. However, the log *K* values calculated using *phreeqc.dat* and *wateq4f.dat*

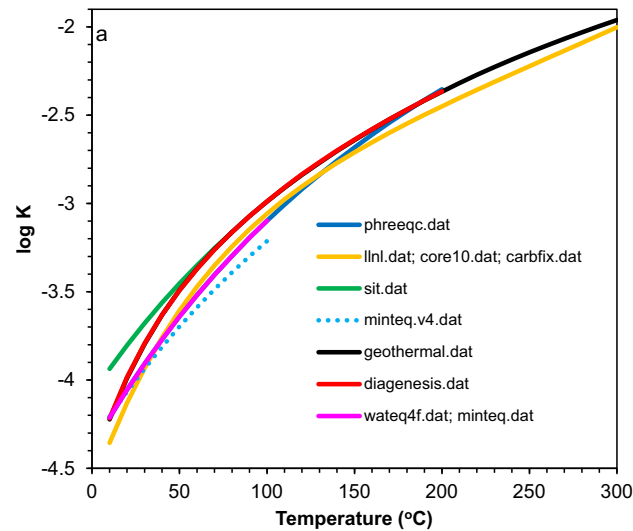


Fig. 9. Calculated quartz solubility product constants (a) and solubility (b) using different PHREEQC TDFs compared with the experimental data. Symbols are from Kennedy (1950), Fournier (1960), Kitahara (1960), van Lier et al. (1960), Morey et al. (1962), Siever (1962), Crerar and Anderson (1971), Mackenzie and Gees (1971), Hemley et al. (1980) and Rimstidt (1997).

dat are about two units higher than those from all other TDFs and the values from geothermal waters.

ΔG_f° albite from Robie and Waldbaum (1968) is ~ 14.4 kJ/mol higher than that from Holland and Powell (2011) (Table K1), which can explain the large difference between the calculated log *K* from *wateq4f.dat/phreeqc.dat* and *geothermal.dat/diagenesis.dat*.

The results for K-feldspar (microcline) dissolution equilibrium solubility product constants are comparable to those for low albite in that *geothermal.dat*, *llnl.dat*, *core10.dat*, *carbfix.dat*, *diagenesis.dat* and *sit.dat* all agree well within the limits of the uncertainty of the field data at their applicable temperature ranges (up to 3 units at $T < 50$ °C) (Fig. J4). Results from *minEQ.dat* are about 0.4 units higher and from *phreeqc.dat* and *wateq4f.dat* are about two units higher than those from all other TDFs and the values from geothermal waters.

ΔG_f° K-feldspar from Robie and Waldbaum (1968) is ~ 13.45 kJ/mol higher than from Holland and Powell (2011) (Table K1), which can explain the large difference between the calculated log *K* from *wateq4f.dat/phreeqc.dat* and *geothermal.dat/diagenesis.dat*.

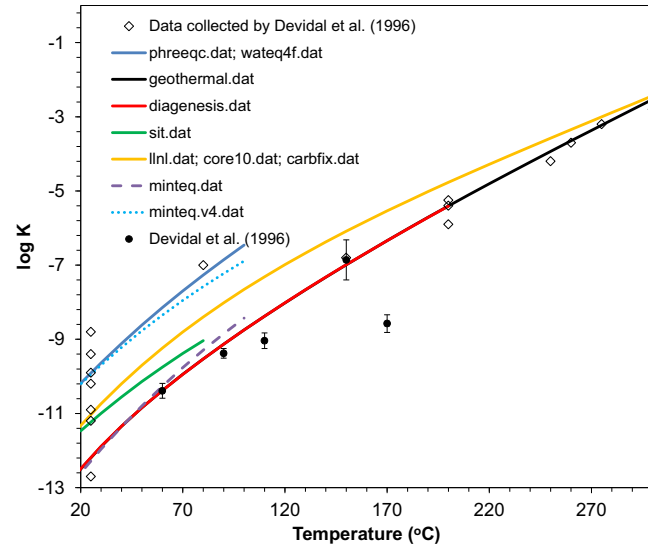


Fig. 10. Kaolinite solubility product constant calculated using different PHREEQC TDFs compared with experimental data. The experimental data are from Devidal et al. (1996) and those collected by them from the literature. The errors of Devidal et al. (1996) are ± 0.11 at 60 °C, ± 0.06 at 90 °C, ± 0.11 at 110 °C, ± 0.48 at 150 °C, and ± 0.24 at 170 °C.

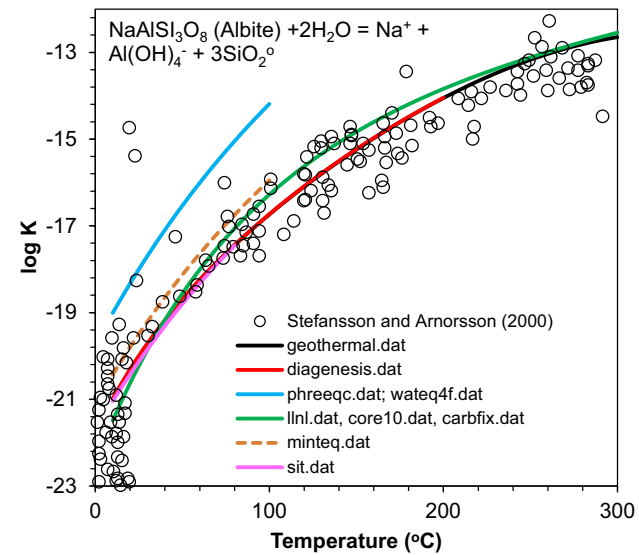


Fig. 11. Low albite solubility product constants as a function of temperature. Symbols are the saturation state of the natural waters with respect to albite collected and calculated by Stefánsson and Arnórsson (2000).

dat/phreeqc.dat and *geothermal.dat/diagenesis.dat*.

5.7.3. Carbonates

The thermodynamic properties of carbonate minerals have gained attention over the last decade or so, because of their relevance to geological carbon sequestration studies. Indeed, the trapping of injected CO₂ in the subsurface as carbonate minerals is considered the most secure means of carbon storage. The solubilities of carbonates are determined in part by the fugacity of CO₂, which in turn depends on the experimental conditions. These may be closed or open, the latter having an externally imposed CO₂ partial pressure, as occurs when equilibration takes place while exposed to the atmosphere at temperatures below the boiling point of the aqueous phase, or at externally controlled values above that temperature. But their importance in relation to petrology

and sedimentology goes far beyond the recent focus on carbon sequestration. Numerous experiments have recently been conducted to measure solubilities of carbonate minerals at elevated temperatures by the CNRS/IRD/Université Toulouse group, which has significantly improved our knowledge of the solubilities of these minerals at 0–300 °C.

For calcite solubility, expressed as the solubility product, $\log K$, *geothermal.dat* and *diagenesis.dat* are within ± 0.05 unit from the experimental data (Fig. 12). Results from *wateq4f.dat* are within ± 0.05 unit from the experimental data at 0–100 °C. For *phreeqc.dat*, the prediction is within ± 0.05 unit from the experimental data at 0–100 °C, but slightly overpredicts the $\log K$ values by 0.1–0.2 unit at 100–200 °C. The discrepancy increases with the increasing temperature. Values from *llnl.dat*, *core10.dat* and *carbfix.dat* are within ± 0.1 unit from the experimental data up to 100 °C. Above 100 °C, they overpredict by 0.1–0.6 unit, and the differences increase with temperature. *Sit.dat*, *minteq.dat* and *minteq.v4.dat* are within ± 0.1 unit from the experimental data well up to 50 °C; > 50 °C, *sit.dat* and *minteq.v4.dat* overpredict the calcite solubility by up to 0.4 unit, whereas it is slightly underpredicted by *minteq.dat* by up to 0.1 unit.

The differences in ΔG_f° values of calcite, Ca^{2+} , and CO_3^{2-} at 25 °C and 1 bar are small (only up to 0.5 kJ/mol; Table K1). Therefore, the differences in calculated $\log K$ values mainly arise in the high T extrapolation of $\log K$. Modeling results using the thermodynamic properties for calcite from Holland and Powell (2011) and the properties for aqueous species in the SUPCRTBL database (Zimmer et al., 2016) show reasonable agreement with experimental data below ~100 °C, but over-estimate calcite solubility above 100 °C (Fig. B5). In this study, a provisional polynomial analytic expression was regressed and implemented into *geothermal.dat* and *diagenesis.dat* (Appendix B) to achieve a better fit to the recent experimental data from Bénédéth et al. (2013) and Bychkov et al. (2020).

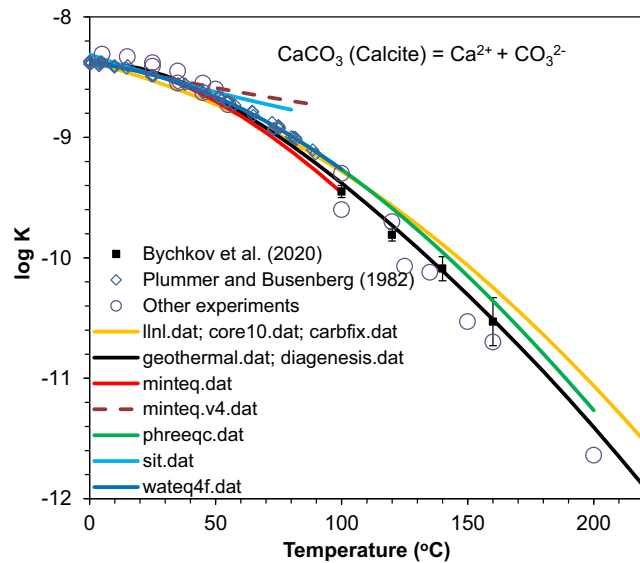


Fig. 12. Calcite solubility product constants as a function of temperature. The experimental data are taken from Ellis (1963), Jacobson and Langmuir (1974), Berner (1976), Plummer and Busenber (1982), Sass et al. (1983), Gledhill and Morse (2006), Bénédéth et al. (2013) and Bychkov et al. (2020). The errors of Bychkov et al. (2020) are ± 0.05 at 100 °C, ± 0.03 at 120 °C, ± 0.1 at 140 °C, and ± 0.2 at 160 °C. The models represent a system closed to atmosphere without the presence of CO_2 gas phase. For experiments conducted at $T < 100$ °C, the system is open to atmosphere with a total pressure of 1 bar and $p\text{CO}_2$ concentration in the atmosphere at the time the experiments were performed (e.g., $p\text{CO}_2 = -3.47$ for Plummer and Busenber, 1982). For Ellis (1963), the $p\text{CO}_2$ is up to 65 bars at 200 °C and for Bychkov et al. (2020) it is up to 50 bars at 160 °C.

Measured dolomite solubility product constants at 25 °C (Fig. 13) show large discrepancies. The “experimental data” below 25 °C are solubility products by Bénédéth et al. (2018), which were calculated using an equation provided by Langmuir (1971) and are in good agreement with their experimental results for T at 50–250 °C. Modeling results using the thermodynamic properties for dolomite from Holland and Powell (2011) and the properties for aqueous species in the SUPCRTBL database (Zimmer et al., 2016) and Mg^{2+} from Miron et al. (2017) show good agreement with experimental data collected in Bénédéth et al. (2018) below ~100 °C, but they over-estimate dolomite solubility above 100 °C (Fig. B3). In this study, a provisional polynomial analytic expression was regressed and implemented into *geothermal.dat* and *diagenesis.dat* (Appendix B) to achieve a better fit to the recent experimental data from Bénédéth et al. (2018).

diagenesis.dat and *geothermal.dat* fit the data within the experimental uncertainty (± 0.3 unit). *phreeqc.dat*, *wateq4f.dat*, *minteq.v4.dat*, *sit.dat* and *minteq.dat* match the within ± 0.2 unit for 10–25 °C, but overpredict the solubility products for $T > 25$ °C for up to 1.8 unit. *llnl.dat* and *core10.dat* are within one-unit difference from the experimental data for the T range of 100–225 °C. *carbfix.dat* appears to be the best among the available PHREEQC TDFs, as its prediction is within the experimental uncertainty (± 0.3 unit) for 50–250 °C.

The value of ΔG_f° of dolomite from Helgeson et al. (1978) is ~3 kJ/mol lower than that from Holland and Powell (2011) (Table K1), which accounts for the differences in calculated $\log K$ values between *llnl.dat*/ *core10.dat* and *geothermal.dat*/*diagenesis.dat* at 25 °C.

For magnesite, modeling results using the thermodynamic properties for magnesite from Holland and Powell (2011) and the properties for aqueous species in the SUPCRTBL database (Zimmer et al., 2016) and Mg^{2+} from Miron et al. (2007) do not match the experimental data. The thermodynamic properties for magnesite from Robie and Hemingway (1995) and the same properties for aqueous species do, however,

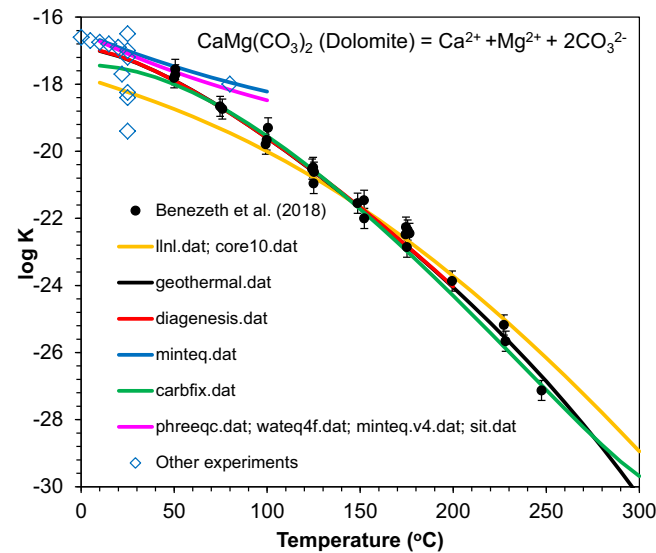


Fig. 13. Dolomite solubility product constants as a function of temperature. The experimental data are from the compilation of Bénédéth et al. (2018). The data below 25 °C are dolomite solubility products calculated by Bénédéth et al. (2018) using the equation provided by Langmuir (1971). The errors of Bénédéth et al. (2018) are ± 0.3 . The models represent a system closed to atmosphere without the presence of CO_2 gas phase. For most experiments conducted at $T < 100$ °C, the system is open to atmosphere with a total pressure of 1 bar and $p\text{CO}_2$ concentration in the atmosphere at the time the experiments were performed. Yanat'eva (1952) and Garrels et al. (1960) performed dissolution experiments with dolomite in pure water at 25 °C and 1 atm $p\text{CO}_2$ and Halla and Van Tassel (1965) at 22 °C and 1 bar $p\text{CO}_2$. Bénédéth et al. (2018)'s experiments were at 4 bars $p\text{CO}_2$.

achieve a good match (Fig. B1).

Fig. J5 compares the predictions from different PHREEQC TDFs with the experimental data for magnesite solubility product constants from Bénédéth et al. (2011). *lml.dat*, *core10.dat*, *carbfix.dat*, *diagenesis.dat* and *geothermal.dat* predictions are consistent with measurements within experimental error (up to ± 0.35) for the T range of 50–200 °C. *wateq4f.dat* and *minseq.dat* overpredict the solubility for $T > 75$ °C for up to 0.6 units. The predictions from *minseq.v4.dat* and *sit.dat* deviate substantially from those of other TDFs. Future work is needed to improve the thermodynamic TDFs for magnesite solubility, especially for $T < 100$ °C.

ΔG_f^0 of magnesite from Helgeson et al. (1978) differs from that by Robie and Hemingway (1995) by ~ 1.67 kJ/mol but is offset by a difference in Mg^{2+} (~ 1.4 kJ/mol) (Table K1). Therefore, the overall difference of ΔG_f^0 for the magnesite dissolution reaction is ~ 0.27 kJ/mol between *lml.dat*/*core10.dat*/*carbfix.dat* and *geothermal.dat*/*diagenesis.dat*. For the difference between *sit.dat* and *geothermal.dat*/*diagenesis.dat*, it is ~ 5.1 kJ/mol (~ 4.5 kJ/mol from ΔG_f^0 of magnesite and ~ 0.6 kJ/mol from ΔG_f^0 of Mg^{2+}).

Only *lml.dat*, *core10.dat*, *carbfix.dat*, *wateq4f.dat*, *minseq.dat* and *minseq.v4.dat* include thermodynamic data for hydromagnesite, and the experimental data cover only 25–75 °C (Berninger et al., 2014) (Fig. J6). The predictions from *wateq4f.dat* and *minseq.dat* are within \sim one unit different from the experimental data. *Minseq.v4.dat* under-predicts hydromagnesite $\log K$ for $T > 50$ °C for \sim one unit. *lml.dat*, *core10.dat* and *carbfix.dat* under-predict hydromagnesite $\log K$ by 1.7–4 units at T range of 25–75 °C, the differences increasing with temperature. Future work is needed to improve the thermodynamic data for hydromagnesite solubility and extend predictions for $T > 100$ °C.

Bénédéth et al. (2007) provide experimental data for dawsonite solubility product constants at the T range of 50–200 °C (Fig. J7). The prediction from *sit.dat* differs by $\sim \pm 0.15$ unit from the experimental data for its applicable T range (15–80 °C). *lml.dat*, *core10.dat* and *carbfix.dat* largely match the experimental data within $\sim \pm 0.1$ unit at T range of 50–100 °C, but their predictions are up to one unit higher at the $T > 100$ °C, and the difference increases with temperature. The predictions from *diagenesis.dat* and *geothermal.dat* fit within $\sim \pm 0.1$ unit for $T < 150$ °C; above 150 °C, the predictions are within ~ 0.2 unit higher than the experimental data. *Diagenesis.dat* and *geothermal.dat* are superior TDFs for dawsonite solubility calculations. Improvements are nevertheless needed to fit the experimental data better.

For siderite, modeling results using the thermodynamic properties from Holland and Powell (2011) and the properties for aqueous species in the SUPCRTBL database (Zimmer et al., 2016) do not match the experimental data. The thermodynamic properties for siderite from Robie and Hemingway (1995) and the same properties for aqueous species do, however, achieve a good match (Fig. B2).

Fig. 14 compares the calculated $\log K$ values from different PHREEQC TDFs with experimental data of siderite solubility product constants from Bénédéth et al. (2009). *carbfix.dat* closely matches the data within $\sim \pm 0.1$ units between 25 and 75 °C, but underpredicts $\log K$ values by 0.4–0.6 units above 150 °C. *lml.dat* and *core10.dat* match experimental data within $\sim \pm 0.1$ unit at T of 200–250 °C, but overpredict the $\log K$ values by 0.4–0.6 units between 0 and 150 °C. *geothermal.dat* and *diagenesis.dat* fit the data within $\sim \pm 0.05$ unit above 50 °C and slightly underpredict $\log K$ for ~ 0.1 unit below 50 °C, but within experimental errors. *Phreeqc.dat*, *wateq4f.dat* and *sit.dat* match the data within $\sim \pm 0.05$ unit between 25 and 50 °C, but overpredict the $\log K$ values by 0.4–0.8 unit between 50 and 100 °C. Both *minseq.dat* and *minseq.v4.dat* overpredict the $\log K$ values for up to one unit.

The difference in ΔG_f^0 of siderite is ~ 3.8 kJ/mol between Robie and Hemingway (1995) and Chivot (2004) but offset by ~ 1 kJ/mol from ΔG_f^0 of Fe^{2+} (Table K1). Therefore, the overall difference in ΔG_f^0 of siderite dissolution reaction is ~ 2.8 kJ/mol between *sit.dat* and *geothermal.dat*/*diagenesis.dat*. There is ~ 3.3 kJ/mol difference from ΔG_f^0 siderite between *lml.dat*/*core10.dat* and *geothermal.dat*/*diagenesis.dat*.

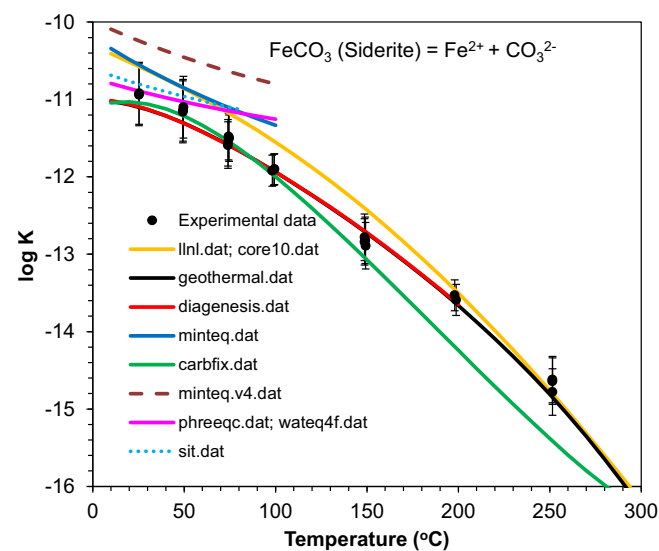


Fig. 14. Siderite solubility product constants as a function of temperature. The experimental data are from Bénédéth et al. (2009). The errors of Bénédéth et al. (2009) are ± 0.4 at 25 °C and 50 °C, ± 0.3 at 75 °C, ± 0.2 at 100 °C, ± 0.3 at 150 °C, ± 0.2 at 200 °C and ± 0.3 at 250 °C. The models represent a system closed to atmosphere without the presence of CO_2 gas phase. Bénédéth et al. (2009)'s experiments were at 4 bars pCO_2 .

5.7.4. Sulfates

Gypsum and anhydrite. Gypsum and anhydrite are the common sulfate minerals and precipitate during the evaporation of seawater. As a consequence, thick and extensive evaporite beds of gypsum and anhydrite have formed in association with sedimentary rocks throughout geological history (Deer et al., 1966). These evaporites may form effective seals for hydrocarbon reservoirs (Warren, 2006). With increasing temperature, gypsum gradually dehydrates and transforms to anhydrite during burial diagenesis. The transition from gypsum to anhydrite occurs at about 40 °C at 1 bar (Azimi and Papangelakis, 2010). However, gypsum can persist metastably at T up to 110 °C for an extended period (Dutrizac, 2002).

The thermodynamic properties for gypsum are not given by Holland and Powell (2011). We adopted those from Matschei et al. (2007). However, the calculated solubility of gypsum based on these thermodynamic properties and aqueous species in the SUPCRTBL database matches poorly with the experimental data from the literature. We therefore regressed the experimental data and provided provisional parameters for the analytical expressions of $\log K$ as a function of temperature (Appendix B).

Fig. 15a compares the calculated gypsum solubility product constants from different TDFs. The predicted $\log K$ values using *phreeqc.dat* and *wateq4f.dat* are close to each other. Those using *geothermal.dat* and *diagenesis.dat* are up to 0.4 log units higher than those using *phreeqc.dat* at $T < 60$ °C. The $\log K$ curve calculated using *lml.dat*, *core10.dat* and *carbfix.dat* does not catch the feature that the $\log K$ values reach a maximum at $T \sim 30$ °C; the $\log K$ values are also up to 1.2 units higher than those using *phreeqc.dat*. The extrapolation of the $\log K$ values of *minseq.v4.dat*, *minseq.dat* and *sit.dat* to relatively higher temperature is problematic because the ΔH values for gypsum are discrepant (the ΔH value in *lml.dat* is -1.66746 kJ/mol, but it is -1.050 kJ/mol in *sit.dat* and 1 kJ/mol in *minseq.v4.dat* and *minseq.dat*).

For gypsum solubility, *phreeqc.dat* gives the best fit to the experimental data (within ± 0.4 mM) (Fig. 15b), although *geothermal.dat* and *diagenesis.dat* fit the experimental data reasonably well (within ± 0.8 mM). *lml.dat*, *core10.dat* and *carbfix.dat* match the experimental data within ± 0.8 mM between 60 and 110 °C, but overpredict gypsum solubility below 60 °C by up to two log units although the divergence

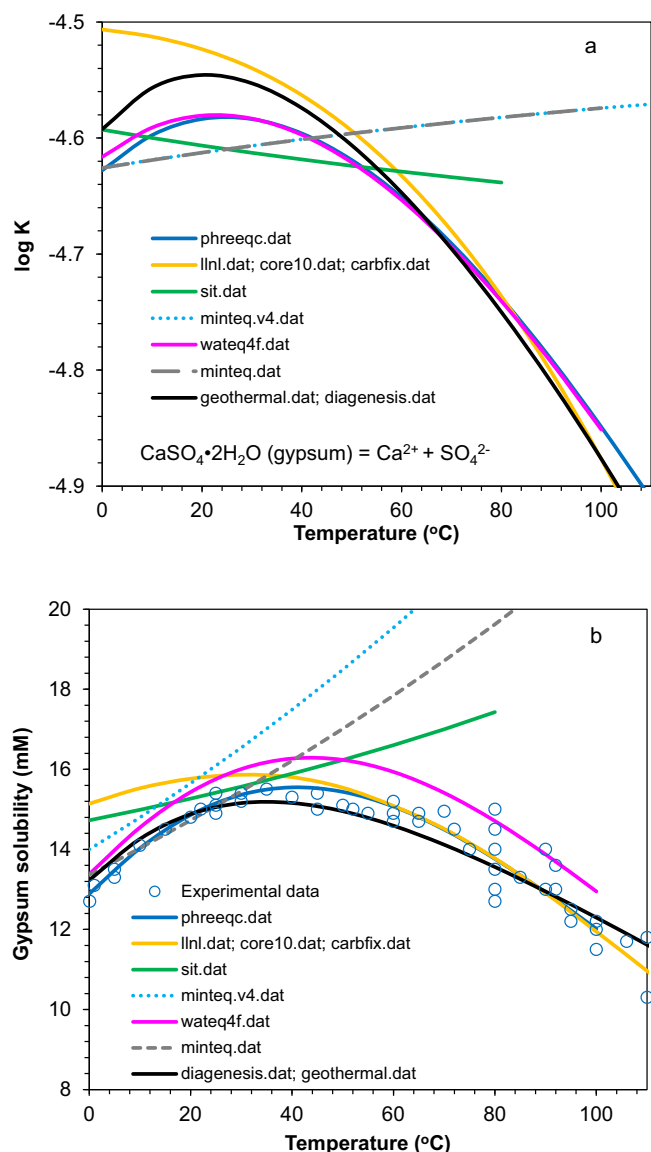


Fig. 15. Calculated gypsum solubility product constants (a) and solubility (mM) (b) as a function of temperature ($P = 1$ bar). The experimental data are from Azimi and Papangelakis (2010) and the literature data they collected.

decreases with the increasing temperature. *wateq4f.dat* overpredicts the solubility for 0.3–0.6 mM and the gap increases with the increasing temperature. The values from *minteq.dat* within ± 0.4 mM at the T range of 10–30 °C; beyond this range, the predictions are poor. The predictions from *minteq.v4.dat* and *sit.dat* are very poor.

Fig. J8a compares the calculated anhydrite solubility product constants with different TDFs. The differences among the calculated $\log K$ values using *geothermal.dat*, *diagenesis.dat*, *sit.dat*, *wateq4f.dat*, *llnl.dat*, *core10.dat* and *carbfix.dat* are generally within 0.2 log unit. As with gypsum, the temperature extrapolation of anhydrite $\log K$ s using *minteq.dat* and *minteq.v4.dat* are problematic, which results in up to 0.4 log unit differences with *geothermal.dat* for *minteq.v4.dat* and 0.8 log unit differences for *minteq.dat*. The differences between *phreeqc.dat* and *geothermal.dat* increase with the increasing temperature, reaching ~0.6 log units at 200 °C.

For anhydrite solubility, the predictions using *geothermal.dat*, *diagenesis.dat*, *llnl.dat*, *core10.dat* and *carbfix.dat* are within $\sim \pm 0.5$ mM (Fig. J8). *sit.dat* predicts anhydrite solubility within $\sim \pm 0.5$ mM below 50 °C, but overpredicts the solubility up to 2.5 mM between 50 and

80 °C, the difference increasing with the increasing temperature. *Phreeqc.dat* and *wateq4f.dat* overpredict anhydrite solubility by up to 5 mM. The predictions from *minteq.dat* and *minteq.v4.dat* are poor.

5.8. High T - P applications

Quartz solubility in the T - P range up to 800 °C and 5 kb can be used to evaluate the capability of different PHREEQC TDFs in handling calculations in elevated T - P systems. The calculated results are compared with the experimental data from Kennedy (1950) for 0.5 kb, from Morey et al. (1962), Walther and Orville (1983), Weill and Fye (1964) and Hemley et al. (1980) for 1 kb, from Walther and Orville (1983), Hemley et al. (1980) and Weill and Fye (1964) for 2 kb, and from Manning (1994) for 5 kb. *bl.dat* is applicable in the temperature range from 0.01–1000 °C at constant pressure (up to 5 kb). Rimstidt (1997) and Miron et al. (2016) indicated that the experimental values for quartz solubility at temperatures below 130 °C from Morey et al. (1962) are problematic because equilibrium was not attained. Therefore, only the data >130 °C from Morey et al. (1962) are used for comparison. *bl.dat* is a TDF covering a range of temperatures (up to 1000 °C) at constant pressure (up to 5000 bars). It is suitable for thermodynamic calculations in high T - P systems. Quartz solubility calculated using *bl.dat* fits all four sets of the experimental data (0.5, 1, 2, and 5 kb) within ± 0.04 mol/kgw (Fig. 16).

phreeqc.dat, *core10.dat*, *carbfix.dat* and *diagenesis.dat* allow quartz solubility calculations in the T - P range of <200 °C and <1 kb, respectively. As the experimental data for 0.5 kb is above 300 °C (Kennedy, 1950), we compared the calculations using these TDFs using only the 1 kb experimental data. In Fig. 16, the line calculated using *diagenesis.dat* matches the experimental data within ± 1 mM up to 200 °C, indicating the effectiveness of the pressure correction function implemented in PHREEQC by Appelo et al. (2014). The predicted quartz solubilities from *core10.dat* and *carbfix.dat* are up to 2 mM lower, and those from *phreeqc.dat* diverge somewhat. These deviations relate to sources of the thermodynamic data of quartz used in these TDFs (Fournier and Potter, 1982; Walther and Helgeson, 1977). Predictions using TDFs without pressure corrections generally have large uncertainties. We therefore selected *llnl.dat* and *geothermal.dat* for comparison. As shown in Fig. 17, the quartz solubility calculated with *llnl.dat* (at P_{SAT}) (up to 4 mM lower) and *geothermal.dat* (up to 3 mM lower) did not match the experimental data very well at 1 kb.

5.9. Geothermometry

Geothermometry is a technique using chemical equilibrium between fluids and their coexisting mineral assemblages to estimate the subsurface temperatures at which the fluids and minerals are sampled. Geothermometrical modeling uses reaction path calculations to calculate the saturation states of minerals with a co-existing fluid and to estimate the temperature at which most of the minerals are at equilibrium (Bethke, 2008; Palandri and Reed, 2001; Blasco et al., 2017). In this approach, the entire chemical analysis (rather than just a portion of it) and compensation for escaping gas and/or mineral precipitation (when bringing the sample from the reservoir to the surface) is required to minimize errors (Bethke, 2008).

In this study, we selected the formation water from well Bernard #6 Frio Formation zone “A,” Brazoria County, Texas, from Kharaka et al. (1977) for geothermometrical modeling (Table G1). The Oligocene Frio Formation is a deltaic, alternating sand-and-shale sequence (Freed, 1982; Kharaka et al., 1977). This formation contains albite, calcite, kaolinite, potassium-feldspar, quartz, and interlayered illite-smectite (ibid.). Following Palandri and Reed (2001), we used albite, K-feldspar, muscovite, paragonite, kaolinite, quartz or chalcedony, dolomite and calcite to estimate the temperature of the formation water.

Fig. 18 shows the temperature estimated from the chemical equilibrium of different minerals co-existing with the water using different

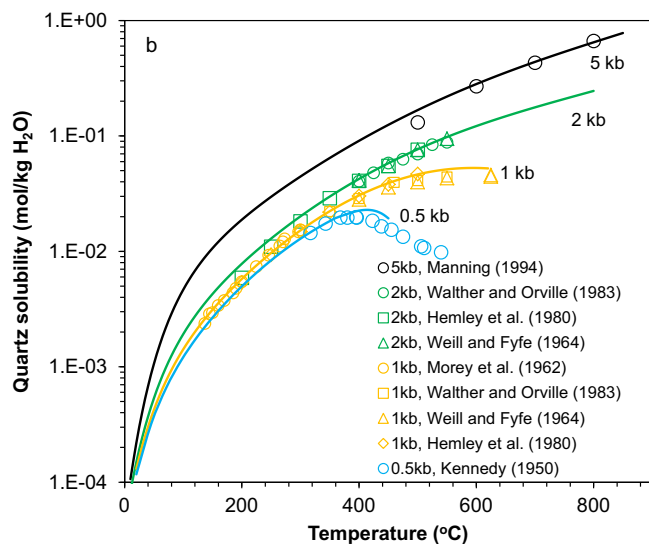
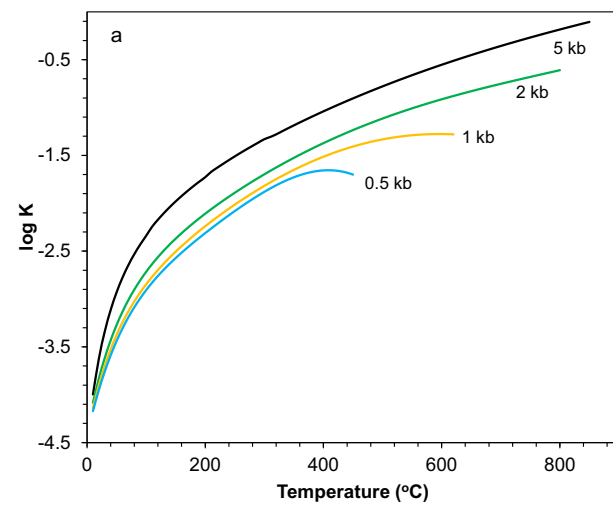


Fig. 16. Calculated quartz solubility product constants (a) and solubility (mol/kg H₂O) (b) in pure water at the pressures of 0.5, 1, 2, and 5 kb. Symbols denote the experimental data. Solid lines are calculated with *bl.dat* at fixed pressures of 0.5, 1, 2 and 5 kb, respectively.

PHREEQC TDFs. Figs. 19 and L1 illustrated the calculated mineral saturation indices with increasing temperatures using different PHREEQC TDFs.

The estimated equilibrium temperature is ~95 °C with *llnl.dat* and *geothermal.dat*, ~90 °C with *core10.dat*, ~85 °C with *carbfix.dat*, ~97 °C with *diagenesis.dat* (Figs. 18, 19, and L1). For comparison, Palandri and Reed (2001) estimated the temperature of this water to be 94 °C (the dotted line in Fig. 18). However, as 94 °C was also an estimated value, predictions from *llnl.dat* and *geothermal.dat* closer to this value do not necessarily mean the two TDFs are better than others in this case.

The convergence of different minerals towards equilibrium simultaneously at the estimated temperature for a TDF can be an indicator for the performance of this TDF in geothermometrical modeling (Bethke, 2008; Palandri and Reed, 2001; Blasco et al., 2017), that is assuming that thermodynamic equilibrium has been achieved between minerals and brine in the sampled formation. We used the range of estimated temperatures for all involved minerals at equilibrium (saturation indices to be zero) in Figs. 19 and L1 to evaluate the performance of different TDFs. The list of TDFs from the best to the worst in terms of geothermometrical modeling performance is *diagenesis.dat* (~ 12 °C),

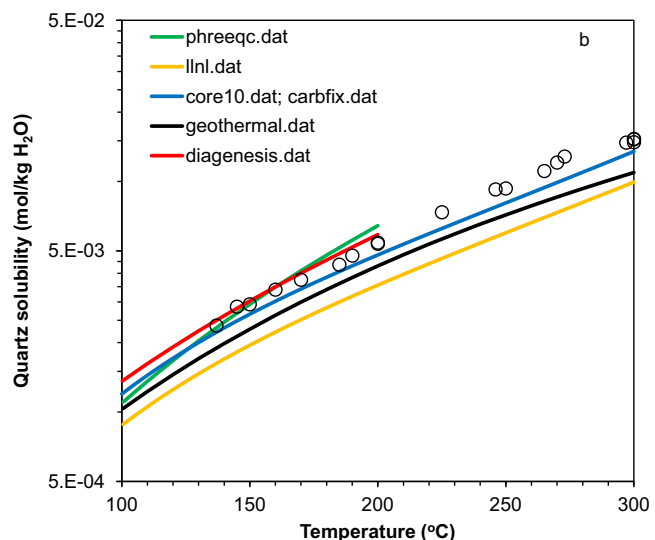
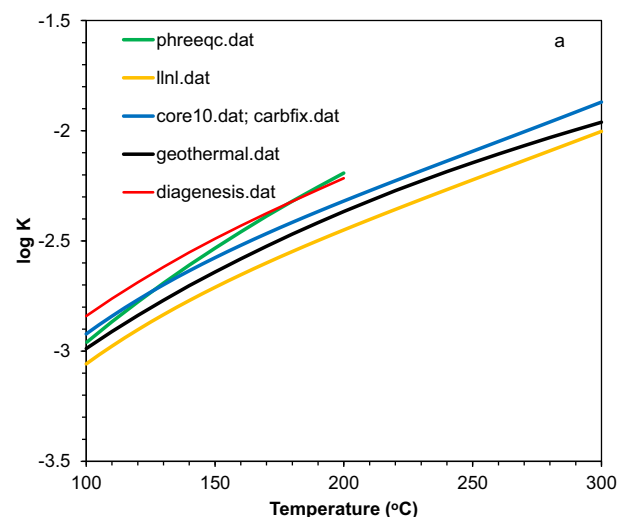


Fig. 17. Calculated quartz solubility product constants (a) and solubility (mol/kg H₂O) (b) in pure water at the pressure of 1 kb. Lines represent quartz solubility calculated with PHREEQC using different datasets. Symbols denote the experimental data from Morey et al. (1962) and Hemley et al. (1980).

geothermal.dat (~ 17 °C), *carbfix.dat* (~ 32 °C), *core10.dat* (~ 40 °C), *llnl.dat* (~ 48 °C), *miniteq.dat* (~ 34 °C; equilibrium not reached for one mineral), *sit.dat* (~ 65 °C; calculated equilibrium not attained for one mineral), *phreeqc.dat* (~ 80 °C; calculated equilibrium not attained for one mineral), and *miniteq.v4.dat* (~ 50 °C; calculated equilibrium not attained for one mineral and 5 other minerals not taken into account).

6. Summary and recommendations

Tables 3 and 5 summarize the applicability and performance of different PHREEQC TDFs in each test case.

6.1. Dilute waters (e.g., river, lake, and shallow ground water) at ambient temperatures

In general, for the calculation of the aqueous species distribution and activities of major components in dilute waters, the major general purpose TDFs in all four categories shown in Fig. 1 (e.g., *phreeqc.dat*, *miniteq.dat*, *geothermal.dat* series) are suitable, although all have minor issues.

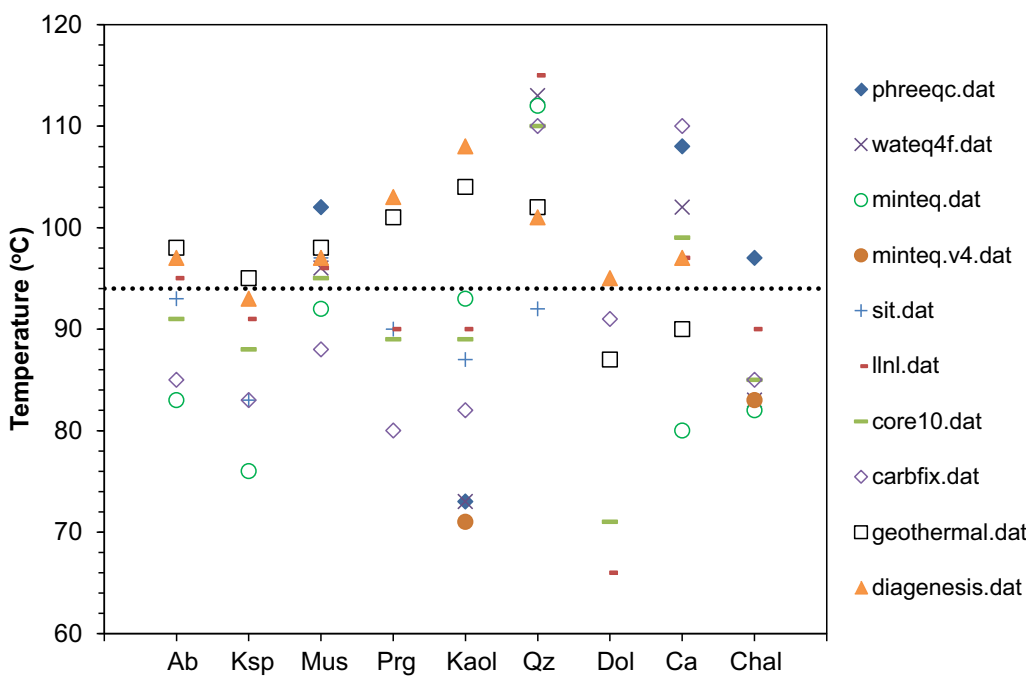


Fig. 18. Temperatures estimated from the chemical equilibrium of different minerals using different PHREEQC TDFs. The formation water composition of well Bernard #6 is from Kharaka et al. (1977).

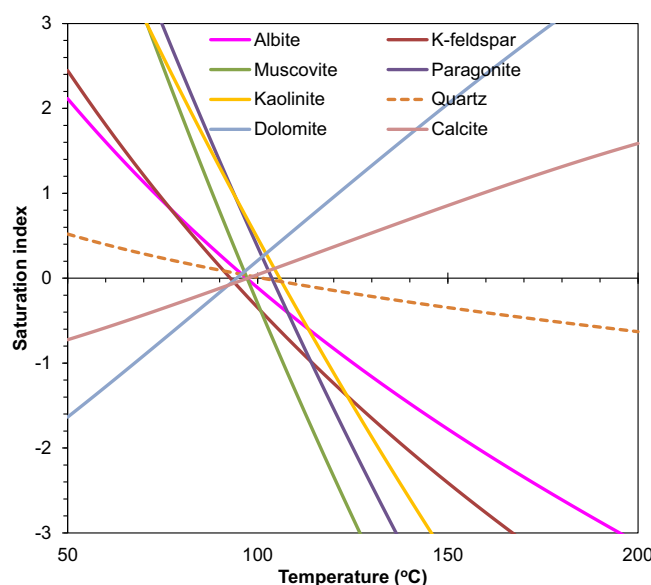


Fig. 19. Mineral saturation indices as a function of temperature over the course of simulating the reheating of formation water calculated with *diagenesis.dat*. Formation water composition is from well Bernard #6, Frio Formation zone “A,” Brazoria County, Texas from Kharaka et al. (1977).

However, the special purpose TDFs (e.g., *core10.dat* and *sit.dat*) generally do not include sufficient important components and species (Table 3). *phreeqc.dat* series TDFs reproduce carbonate mineral solubility experimental data well but not Al-oxyhydroxides or aluminosilicate mineral saturation indices. For the calculation of the saturation indices and mineral solubilities, we recommend the *geothermal.dat* series.

For modeling the distribution and activities of the minor constituents in surficial waters, it is even more important to use the chemically comprehensive general-purpose databases (e.g., *phreeqc.dat*, *minteq.dat*,

geothermal.dat series) and avoid special-purpose TDFs such as *core10.dat* and *carbfix.dat* because many (>10) minor components are omitted in these TDFs.

6.2. Moderately saline water (e.g., seawater)

We recommend *llnl.dat*, *geothermal.dat* and *diagenesis.dat* for modeling the distribution and activity of major aqueous species. *Phreeqc.dat*, *minteq.dat*, *minteq.v4.dat*, *wateq4f.dat* and *sit.dat* lack most Cl-bearing complexes (Table 3). *core10.dat* and *carbfix.dat* do not include Br^- , MgF^+ , and Sr^{2+} (Table 3). For the distribution and activities of minor species, all TDFs lack some species (Table 3). Users must exercise due diligence to ensure the minor components and species of interest are available and reliable in the TDF.

6.3. Water reporting abundant minor and trace constituents (e.g., groundwater, streams contaminated with hazardous metals)

llnl.dat contains the most comprehensive set of minor constituents, followed by *geothermal.dat* and *diagenesis.dat* and then *sit.dat*, *minteq.dat* and *minteq.v4.dat*. Many (> 20) minor constituents are omitted in *core10.dat*, *carbfix.dat* and *phreeqc.dat*, which make them unsuitable for application to this type of water.

6.4. Organic-rich oil field brine

llnl.dat has many acetate-bearing species. Although *minteq.dat* and *minteq.v4.dat* contain a long list of organic species, they are mainly applicable to environmental problems at ambient temperature and are unsuitable for calculations at elevated temperatures such as basinal or oil-field brine, primarily because both use the van't Hoff equation, which has limited applicability in extrapolating log K_s to higher temperatures. Furthermore, in most cases, $\Delta_f H$ values for the van't Hoff equation are unavailable in either file.

Table 5

Performance and application ranges of different data files on tested mineral solubility.

Mineral solubility	<i>phreeqc.dat</i>	<i>wateq4f.dat</i>	<i>llnl.dat</i> & <i>core10.dat</i>	<i>carbfix.dat</i>	<i>sit.dat</i>	<i>miniteq.dat</i>	<i>miniteqv4.dat</i>	<i>geothermal.dat</i> & <i>diagenesis.dat</i>
Brucite	N.A.	0.2 log unit lower at $T < 100^\circ\text{C}$	0.8 log unit lower	0.4 log unit lower	Best for $15\text{--}80^\circ\text{C}$ (K_{sp} within ± 0.1 unit)	0.2 log unit lower at $T < 100^\circ\text{C}$	0.2 log unit lower at $T < 100^\circ\text{C}$	K_{sp} within ± 0.2 unit for $0\text{--}300^\circ\text{C}$ ($0\text{--}200^\circ\text{C}$ for <i>diagenesis.dat</i>)
Gibbsite	N.R.	N.R.	K_{sp} within ± 0.1 unit for $10\text{--}80^\circ\text{C}$	K_{sp} within ± 0.1 for $10\text{--}80^\circ\text{C}$	K_{sp} within ± 0.1 for $15\text{--}80^\circ\text{C}$	N.R.	N.R.	K_{sp} within ± 0.1 for $10\text{--}170^\circ\text{C}$
Boehmite	N.A.	~ 0.8 unit higher	K_{sp} within ± 0.1 unit for $100\text{--}260^\circ\text{C}$	K_{sp} within ± 0.1 unit for $100\text{--}260^\circ\text{C}$	K_{sp} within ± 0.1 unit for $15\text{--}80^\circ\text{C}$	~ 0.8 unit higher	~ 0.8 unit higher	K_{sp} within ± 0.1 unit for $100\text{--}260^\circ\text{C}$ ($100\text{--}200^\circ\text{C}$ for <i>diagenesis.dat</i>)
Diaspore	N.A.	N.R.	K_{sp} within ± 0.2 unit for $150\text{--}300^\circ\text{C}$	K_{sp} within ± 0.2 unit for $150\text{--}300^\circ\text{C}$	N.R.	N.R.	N.R.	K_{sp} within ± 0.2 unit for $150\text{--}300^\circ\text{C}$ ($150\text{--}200^\circ\text{C}$ for <i>diagenesis.dat</i>)
Hematite	N.R.	N.R.	N.A.	K_{sp} within ± 0.2 unit for $0\text{--}300^\circ\text{C}$	N.A.	N.R.	N.R.	Overpredict log $K \sim 0.2\text{--}0.6$ unit for $0\text{--}200^\circ\text{C}$
Quartz	up to 0.1 mM lower	up to 0.1 mM lower	up to 0.1 mM lower	up to 0.1 mM lower	K_{sp} within $\pm 0.02\text{ mM}$ for $15\text{--}80^\circ\text{C}$	up to 0.1 mM lower	0.1 mM lower	K_{sp} within $\pm 0.02\text{ mM}$ for $10\text{--}300^\circ\text{C}$ ($10\text{--}200^\circ\text{C}$ for <i>diagenesis.dat</i>)
Kaolinite	N.R.	N.R.	N.R.; $\sim 1\text{--}2$ units higher	N.R.; $\sim 1\text{--}2$ units higher	$\sim 0.8\text{--}1.0$ log units higher	~ 0.8 log units higher	N.R.	K_{sp} within ± 0.4 unit for $20\text{--}300^\circ\text{C}$ ($20\text{--}200^\circ\text{C}$ for <i>diagenesis.dat</i>)
Albite	N.R.	N.R.	Good for $0\text{--}300^\circ\text{C}$	Good for $0\text{--}300^\circ\text{C}$	Good for $15\text{--}80^\circ\text{C}$	0.4 log unit higher	N.A.	Best for $0\text{--}300^\circ\text{C}$ ($0\text{--}200^\circ\text{C}$ for <i>diagenesis.dat</i>)
K-feldspar	N.R.	N.R.	Good for $0\text{--}300^\circ\text{C}$	Good for $0\text{--}300^\circ\text{C}$	Good for $15\text{--}80^\circ\text{C}$	0.4 log unit higher	N.A.	Best for $0\text{--}300^\circ\text{C}$ ($0\text{--}200^\circ\text{C}$ for <i>diagenesis.dat</i>)
Calcite	K_{sp} within ± 0.05 unit for $0\text{--}100^\circ\text{C}$, $0\text{--}100^\circ\text{C}$,	K_{sp} within ± 0.05 for $0\text{--}100^\circ\text{C}$	K_{sp} within ± 0.1 unit for $0\text{--}100^\circ\text{C}$	K_{sp} within ± 0.1 unit for $0\text{--}100^\circ\text{C}$	K_{sp} within ± 0.1 for $15\text{--}50^\circ\text{C}$	K_{sp} within ± 0.1 unit for $0\text{--}50^\circ\text{C}$	K_{sp} within ± 0.1 unit for $0\text{--}50^\circ\text{C}$	K_{sp} within ± 0.05 unit
Dolomite	K_{sp} within ± 0.2 unit for $10\text{--}25^\circ\text{C}$	K_{sp} within ± 0.2 unit for $10\text{--}25^\circ\text{C}$	K_{sp} within ± 1 unit for $100\text{--}225^\circ\text{C}$	K_{sp} within ± 0.2 unit for $50\text{--}250^\circ\text{C}$	K_{sp} within ± 0.2 unit for $10\text{--}25^\circ\text{C}$	K_{sp} within ± 0.2 unit for $10\text{--}25^\circ\text{C}$	K_{sp} within ± 0.2 unit for $10\text{--}25^\circ\text{C}$	K_{sp} within ± 0.3 unit for $0\text{--}250^\circ\text{C}$
Magnesite	N.A.	N.R.	K_{sp} within ± 0.35 unit for $100\text{--}200^\circ\text{C}$	K_{sp} within ± 0.35 unit for $100\text{--}200^\circ\text{C}$	N.R.	N.R.	N.R.	K_{sp} within ± 0.35 unit for $100\text{--}200^\circ\text{C}$
Hydromagnesite	N.A.	K_{sp} within ± 1 unit for $25\text{--}75^\circ\text{C}$	N.R.	N.R.	N.A.	K_{sp} within ± 1 unit for $25\text{--}75^\circ\text{C}$	1 unit lower for $50\text{--}75^\circ\text{C}$	N.A.
Dawsonite	N.A.	N.A.	K_{sp} within ± 0.1 for $50\text{--}100^\circ\text{C}$	K_{sp} within ± 0.1 for $50\text{--}100^\circ\text{C}$	K_{sp} within ± 0.15 unit for $15\text{--}80^\circ\text{C}$	N.A.	N.A.	K_{sp} within ± 0.1 for $T < 150^\circ\text{C}$; overpredicted ~ 0.2 unit for $150\text{--}200^\circ\text{C}$
Siderite	N.R.	N.R.	Overpredicted by $0.4\text{--}0.6$ units for $T < 150^\circ\text{C}$; K_{sp} underpredicted by $0.4\text{--}0.6$ units for $200\text{--}250^\circ\text{C}$	K_{sp} within ± 0.1 for $25\text{--}75^\circ\text{C}$; underpredicted by $0.4\text{--}0.6$ units for $T > 150^\circ\text{C}$	N.R.	N.R.	N.R.	K_{sp} within ± 0.05 for $T > 50^\circ\text{C}$; underpredicted by 0.1 unit for $T < 50^\circ\text{C}$
Gypsum	Within $\pm 0.4\text{ mM}$ for $0\text{--}100^\circ\text{C}$	$0.3\text{--}0.6\text{ mM}$ higher at $0\text{--}100^\circ\text{C}$	Within $\pm 0.8\text{ mM}$ for $60\text{--}110^\circ\text{C}$	Within $\pm 0.8\text{ mM}$ for $60\text{--}110^\circ\text{C}$	N.R.	Within $\pm 0.4\text{ mM}$ for $10\text{--}30^\circ\text{C}$	N.R.	Within $\pm 0.8\text{ mM}$ for $0\text{--}100^\circ\text{C}$
Anhydrite	N.R.	N.R.	Within $\pm 0.5\text{ mM}$ for $20\text{--}300^\circ\text{C}$	Within $\pm 0.5\text{ mM}$ for $20\text{--}300^\circ\text{C}$	Within $\pm 0.5\text{ mM}$ for $15\text{--}50^\circ\text{C}$	N.R.	N.R.	Within $\pm 0.5\text{ mM}$ for $20\text{--}300^\circ\text{C}$ ($20\text{--}200^\circ\text{C}$ for <i>diagenesis.dat</i>)

N.A. = Not Applicable. N.R. = Not recommended.

6.5. High-salinity water

TDFs using the Pitzer equation (*pitzer.dat*, *frezchem.dat* and *coldchem.dat*) perform well even at very high electrolyte concentrations, but with a restricted number of components. *frezchem.dat* and *coldchem.dat* are intended for low temperature systems, but *pitzer.dat* can be used at relatively high temperatures. Most TDFs using non-Pitzer methods are unsuitable for salinities higher than $\sim 0.5\text{ M}$ for NaCl, $\sim 1\text{ M}$ for CaCl₂, \sim

0.2 M for MgSO₄, or $\sim 0.3\text{ M}$ for Na₂SO₄ (Table 3). TDFs using the Pitzer equation generate large uncertainties with respect to the calculated solubility of carbonate minerals. TDFs using non-Pitzer methods generally under-predict the SIs of high-solubility salts.

6.6. Sediment pore waters

Sediment pore waters are characterized by elevated temperatures

and pressures, and are usually dominated by NaCl. *phreeqc.dat*, *minseq.dat*, *minseq.v4.dat* and *wateq4f.dat* do not incorporate Cl-bearing complexes and *sit.dat* includes only MgCl⁺. These TDFs also do not have log Ks available at elevated temperatures for all species in the databases. *Diagenesis.dat* is recommended for speciation-solubility calculations for these waters, as the correction to geopressure is taken into account.

6.7. Geothermal waters

Geothermal.dat is the best for modeling speciation-solubility at temperatures above 25 °C up to 300 °C and P_{sat} , in comparison with *core10.dat*, *carbfix.dat*, *llnl.dat* and *diagenesis.dat*, which are good to only fair. All other TDFs either do not provide for log K at $T > 25$ °C for many species, or are deficient due to the use of the van't Hoff equation for extrapolating log K values from 25 °C to higher temperatures.

6.8. High T-P water

TDFs without pressure corrections are unsuitable for applications to this type of solution. *bl.dat* is suitable for high T-P waters up to 1000 °C and 5000 bars.

6.9. Geothermometry

In terms of convergence for all minerals at equilibrium, *diagenesis.dat* and *geothermal.dat* are good and *carbfix.dat*, *core10.dat* and *llnl.dat* are fair. Other TDFs are poor.

6.10. Mineral solubility

The performance and application ranges of different TDFs on tested

mineral solubilities are listed in Table 5. Generally, the *geothermal.dat* series TDFs are the best for most minerals evaluated in this review; *llnl.dat* series are good for most minerals, except for brucite, quartz kaolinite, gypsum, and some carbonate minerals; *carbfix.dat* improved the thermodynamic properties of dolomite and siderite; *phreeqc.dat* is good for gypsum and calcite.

A unified comprehensive database that is internally consistent, and with wide range of applicable T , P and salinity ranges, and suitable for evaluating most natural and experimental conditions, is highly desirable. However, accomplishing this task is a very substantial undertaking, requiring perhaps decades of additional research and testing; a worthy but presently unattainable goal.

Declaration of Competing Interest

The authors declare that they have no known competing financial interests or personal relationships that could have appeared to influence the work reported in this paper.

Acknowledgment

CZ acknowledges the partial support by the U.S. NSF grant EAR-1926734, the Faculty Research Support Program through the office of Vice Provost for Research at Indiana University, and the Haydn Murray chair endowment. Editing the manuscript by Kevin Tu is greatly appreciated. The paper greatly benefited from comments and suggestions made by Kirk Nordstrom, Dave Sherman and two other anonymous reviewers.

Appendix A. Updates on the thermodynamic properties of Mg-bearing species

John Apps (unpublished work) reviewed the thermodynamic properties of Mg²⁺ and found that the thermodynamic properties of Mg²⁺ from Shock and Helgeson (1988) should be updated. The ΔG_f^0 of Mg²⁺ is ~3 kJ/mol lower than that of Shock and Helgeson (1988) (Table A1). Coincidentally, the ΔG_f^0 of Mg²⁺ from Miron et al. (2017) is comparable with that from John Apps, considering the standard deviations. We therefore adopted the thermodynamic properties of Mg²⁺ from Miron et al. (2017) for the *diagenesis.dat* and *geothermal.dat* data files, because Miron et al. (2017) also provided the corresponding parameters for the Cp function (Fig. A1).

Table A1

Thermodynamic properties of Mg²⁺.

Species	ΔG_f^0 kJ/mol	ΔH_f^0 kJ/mol	S_{298}^0 J/mol/K	Reference
Mg ²⁺	-453.985	-465.960	138.072	Shock and Helgeson (1988) Apps (unpublished work) Miron et al. (2017)
	-456.8 ± 1.0	-467.0 ± 0.6	-132.3 ± 3.9	
	-456.005 ± 0.5	-467.997	-138.07	

Mg+2	Mg+2
Mg+2	Mg(1)+(2)
SH98	97.11.06
-453.985	-465.960 -138.072
-3.4380	-35.9782 35.1038 -9.9998
87.0272	-24.6521 6.4316 2.
Mg+2	Mg+2
Mg+2	Mg(1)+(2)
MWKL17	20.10.12
-456.005	-467.997 -138.072
-3.4380	-35.9782 35.1038 -9.9998
87.0272	-24.6521 6.4316 2.

Fig. A1. Comparison of thermodynamic properties of Mg²⁺ from Shock and Helgeson (1988) (upper entry) and Miron et al. (2017) with modified S⁰ (lower entry) in the SUPCRTBL database.

Miron et al. (2017) also provided the thermodynamic properties of MgOH⁺, MgCl⁺, MgCl₂⁰, MgHCO₃⁺, MgCO₃⁺, MgSiO₃⁰, MgHSiO₃⁺. We

adopted them in the SUPCRTBL database to calculate the relevant log K_s for reactions of Mg-bearing species and minerals. The thermodynamic properties of these species are listed in Table A2.

Table A2

Thermodynamic properties of Mg-bearing species from Miron et al. (2017).

Species	$\Delta G_f, 298^0$ (kJ/mol)	$\Delta H_f, 298^0$ (kJ/mol)	S_{298}^0 (J/mol/K)	a1*10 (J/mol/bar)	a2*10 ⁻² (J/mol/bar)	a3 (J/mol/bar)	a4*10 ⁻⁴ (J/mol/bar)	c1 (J/mol/bar)	c2*10 ⁻⁴ (J/mol/bar)	$\omega 2*10^{-5}$ (J/mol/bar)
Mg ²⁺	-456.005	-467.997	-138.07	-3.438	-35.9782	35.1038	-9.9998	87.0272	-24.6521	6.4316
MgOH ⁺	-626.503	-686.926	-67.36	9.5968	-9.1249	27.6445	-11.2499	131.9696	13.5537	3.3263
MgCl ⁺	-592.204	-639.418	-79.5	9.5433	-9.8680	27.9366	-11.2194	119.4411	8.6103	3.5100
MgCl ₂ ⁰	-696.566	-776.233	-11.57	23.4994	24.8207	14.3026	-12.6533	124.4301	22.0932	-0.1590
MgHCO ₃ ⁺	-1048.857	-1157.71	-19.11	13.8072	0.6728	23.7936	-11.6629	198.8254	39.1304	2.5958
MgCO ₃ ⁰	-1000.992	-1134.72	-102.57	-3.0773	-40.0597	39.7739	-9.9709	-41.3856	-36.0493	0
MgHSiO ₃ ⁺	-1479.708	-1616.42	-99.5	2.6313	-26.1199	34.2950	-10.5474	153.9218	19.5401	3.8397
MgSiO ₃	-1418.355	-1555.84	-102	3.5254	-46.3127	221.5860	-9.7136	287.5220	-225.9280	-0.1862

MgCO ₃ ,aq	MgCO ₃
MgCO ₃ ,aq	Mg(1)C(1)O(3)+(0)
MWKL17	20.12.16
	-1000.992 -1134.72 -102.57
	-3.0773 -40.0597 39.7739 -9.9709
	-41.3856 -36.0493 0.0000 0.
Mg(HCO ₃) ⁺	Mg(HCO ₃) ⁺
Mg(HCO ₃) ⁺	Mg(1)H(1)C(1)O(3)+(1)
MWKL17	20.12.16
	-1048.857 -1157.71 -19.110
	13.8072 0.6728 23.7936 -11.6629
	198.8254 39.1304 2.5958 1.
Mg+2	Mg+2
Mg+2	Mg(1)+(2)
MWKL17	20.12.16
	-456.005 -467.997 -138.072
	-3.4380 -35.9782 35.1038 -9.9998
	87.0272 -24.6521 6.4316 2.
MgCl ⁺	MgCl ⁺
MgCl ⁺	Mg(1)Cl(1)+(1)
MWKL17	20.10.12
	-592.204 -639.418 -79.500
	9.5433 -9.8680 27.9366 -11.2194
	119.4411 8.6103 3.5100 1.
MgOH ⁺	MgOH ⁺
MgOH ⁺	Mg(1)O(1)H(1)+(1)
MWKL17	20.12.16
	-626.503 -686.926 -67.360
	9.5968 -9.1249 27.6445 -11.2499
	131.9696 13.5537 3.3263 1.
MgCl ₂ ,aq	MgCl ₂
MgCl ₂ ,aq	Mg(1)Cl(2)+(0)
MWKL17	20.12.16
	-696.566 -776.233 -11.570
	23.4994 24.8207 14.3026 -12.6533
	124.4301 22.0932 -0.1590 0.
Mg(HSiO ₃) ⁺	Mg(HSiO ₃) ⁺
Mg(HSiO ₃) ⁺	Mg(1)H(1)Si(1)O(3)+(1)
MWKL17	20.12.16
	-1479.708 -1616.42 -99.5
	2.6313 -26.1199 34.2950 -10.5474
	153.9218 19.5401 3.8397 1.
MgSiO ₃ ,aq	MgSiO ₃
MgSiO ₃ ,aq	Mg(1)Si(1)O(3)+(0)
MWKL17	20.12.16
	-1418.355 -1555.84 -102.00
	3.5254 -46.3127 221.5860 -9.7136
	287.5220 -225.9280 -0.1862 0.

Appendix B. Comparison of the thermodynamic properties of magnesite, siderite, dolomite, calcite, and gypsum with experimental solubility data

It is beyond the scope of this paper to re-evaluate the thermodynamic properties of these carbonate and sulfate minerals. Here, we compare the modeling results using different sources of thermodynamic data and with experimental solubility data. All standard state thermodynamic properties and HKF parameters for aqueous species and complexes are from Shock and Helgeson (1988) and Sverjensky et al. (1997) unless otherwise indicated. These species are included in the SUPCRTBL database by Zimmer et al. (2016). In the following discussion, the thermodynamic properties and HKF parameters for Mg-bearing aqueous species are modified according to Miron et al. (2017). See Appendix A.

Magnesite

When comparing $\log K$ values based on the experimental solubility data of magnesite from Bénédézeth et al. (2011), with those based on ΔG_f° value for magnesite from Robie and Hemingway (1995) and Holland and Powell (2011), respectively, the former, which is 2.24 kJ/mol lower, is in closer agreement (Fig. B1).

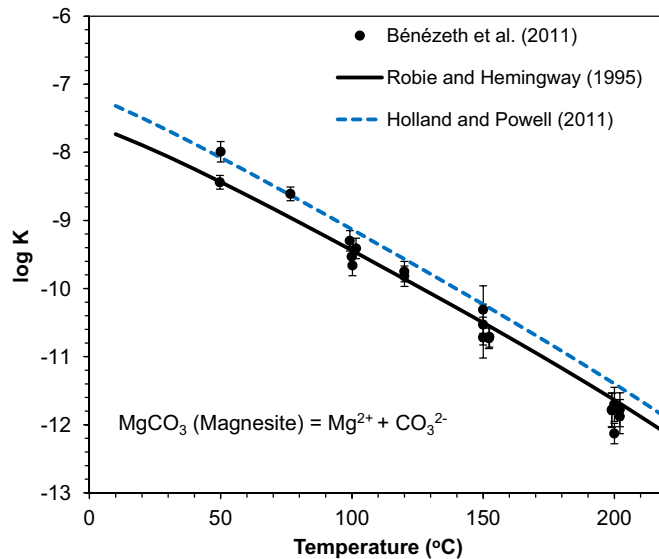


Fig. B1. Comparison of model-predicted solubility product constants of magnesite with the experimental data. The experimental data are from Bénédézeth et al. (2011). The errors of Bénédézeth et al. (2011) are ± 0.1 and ± 0.15 at 50°C , ± 0.1 at 75°C , ± 0.15 at 100°C and 120°C , $\pm 0.2\text{--}0.35$ at 150°C , and $\pm 0.15\text{--}0.25$ at 200°C . The models represent a system closed to atmosphere without the presence of CO_2 gas phase. Bénédézeth et al. (2011)'s experiments were at 4–30 bars $p\text{CO}_2$.

Calcite

The modeling results using the thermodynamic properties for calcite from Holland and Powell (2011) and the properties for aqueous species in the SUPCRTBL database (Zimmer et al., 2016) show reasonable agreement with experimental data below $\sim 100^{\circ}\text{C}$ (Fig. B2). However, the model results over-estimate the experimentally-based calcite solubility product constants above 100°C (Fig. B2).

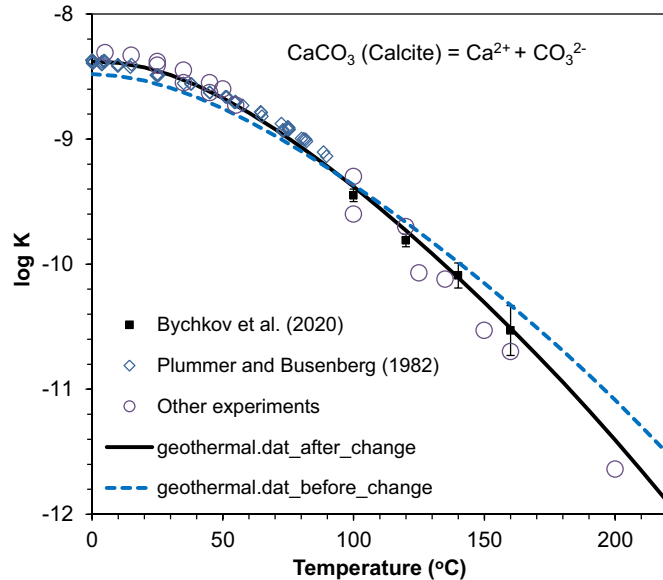


Fig. B2. Comparison of model-predicted solubility product constants of calcite with the experimental data collected by [Bychkov et al. \(2020\)](#). The experimental data are taken from [Ellis \(1963\)](#), [Jacobson and Langmuir \(1974\)](#), [Berner \(1976\)](#), [Plummer and Busenberg \(1982\)](#), [Sass et al. \(1983\)](#), [Gledhill and Morse \(2006\)](#), [Bénézeth et al. \(2013\)](#) and [Bychkov et al. \(2020\)](#). The errors of [Bychkov et al. \(2020\)](#) are ± 0.05 at 100°C , ± 0.03 at 120°C , ± 0.1 at 140°C , and ± 0.2 at 160°C . The models represent a system closed to the atmosphere without the presence of CO_2 gas phase. For experiments conducted at $T < 100^{\circ}\text{C}$, the system is open to atmosphere with a total pressure of 1 bar and $p\text{CO}_2$ concentration in the atmosphere at the time the experiments were performed (e.g., $p\text{CO}_2 = -3.47$ for [Plummer and Busenberg, 1982](#)). For [Ellis \(1963\)](#), the $p\text{CO}_2$ is up to 65 bars at 200°C and for [Bychkov et al. \(2020\)](#) it is up to 50 bars at 160°C .

Extensive reviews of calcite solubility data and comparison with theoretical prediction have been conducted ([Facq et al., 2014](#); [Bychkov et al., 2020](#)). The adoption of updated standard state thermodynamic properties and HKF parameters from these references in the modeling may improve the match with experimental data, but it is beyond the scope of this review.

As an interim measure, the solubility product constant equation in the PHREEQC data files can be matched with the experimental solubility determinations using the following polynomial analytical expression for the temperature dependence of $\log K$ ([Parkhurst and Appelo, 2013](#))

$$\log_{10}K = A_1 + A_2 T + \frac{A_3}{T} + A_4 \log_{10}T + \frac{A_5}{T^2} + A_6 T^2 \quad (\text{B1})$$

Provisional analytical expressions for the experimentally-determined solubility product constants of calcite as a function of temperature, as used in PHREEQC (Fig. B6), is given below. These functions were regressed from the experimental data collected by [Bychkov et al. \(2020\)](#).

Modified:

-analytic 2.153723e+03 7.023428e-01 -8.290205e+04 -8.481322e+02 3.433311e+06 -2.606353e-04 (for *geothermal.dat*)
-analytic -9.791472e+02 -2.522644e-01 4.655034e+04 3.727113e+02 -2.427653e+06 5.815874e-05 (for *diagenesis.dat*)

Dolomite

Direct applications of the modeling results using the thermodynamic properties for dolomite from [Holland and Powell \(2011\)](#) and the properties for aqueous species in the SUPCRTBL database ([Zimmer et al., 2016](#)) and Mg^{2+} from [Miron et al. \(2017\)](#) show good agreement with experimental data collected in [Bénézeth et al. \(2018\)](#) below $\sim 100^{\circ}\text{C}$ (Fig. B3). However, the model results over-estimate dolomite solubility above 100°C (Fig. B3).

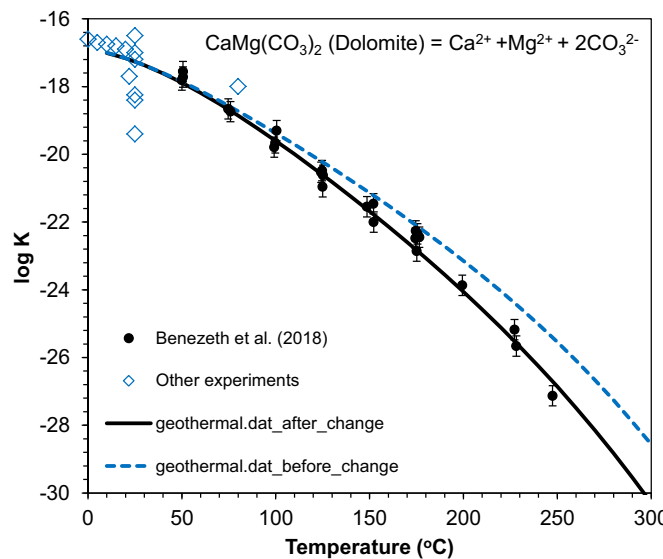


Fig. B3. Comparison of model-predicted solubility product constants of dolomite with those based on experimental data. The experimental data are from the compilation in Bénézeth et al. (2018). The data below 25 °C are dolomite solubility products calculated by Bénézeth et al. (2018) using the equation provided by Langmuir (1971). The errors of Bénézeth et al. (2018) are ± 0.3 . The models represent a system closed to atmosphere without the presence of CO_2 gas phase. For most experiments conducted at $T < 100$ °C, the system is open to atmosphere with a total pressure of 1 bar and $p\text{CO}_2$ concentration in the atmosphere at the time the experiments were performed. Yanat'eva (1952) and Garrels et al. (1960) performed dissolution experiments with dolomite in pure water at 25 °C and 1 atm $p\text{CO}_2$ and Halla and Van Tassel (1965) at 22 °C and 1 bar $p\text{CO}_2$. Bénézeth et al. (2018)'s experiments were at 4 bars $p\text{CO}_2$.

Provisionally, the following polynomial parameters fit the experimentally determined $\log K$ values for dolomite.

Modified:

-analytic 3.895978e+03 1.301346e+00 -1.460980e+05 -1.540963e+03 5.889268e+06 -4.926876e-04 (for *geothermal.dat*)
-analytic -1.567563e+03 -3.620509e-01 7.970411e+04 5.879337e+02 -4.332688e+06 6.212195e-05 (for *diagenesis.dat*)

The resulting solubility product constant equation is designated as “*geothermal.dat_after_change*” in Fig. B3. It must be emphasized, however, that this empirical correlation fails to address the underlying issue that model predictions using thermodynamic data do not correspond with laboratory measurements of dolomite solubility.

Siderite

We show that the application of ΔG_f° for siderite from Robie and Hemingway (1995) provides a better match with the experimental data from Bénézeth et al. (2009) (Fig. B4) than the corresponding ΔG_f° for siderite of Holland and Powell (2011), which is 5.64 kJ/mol lower.

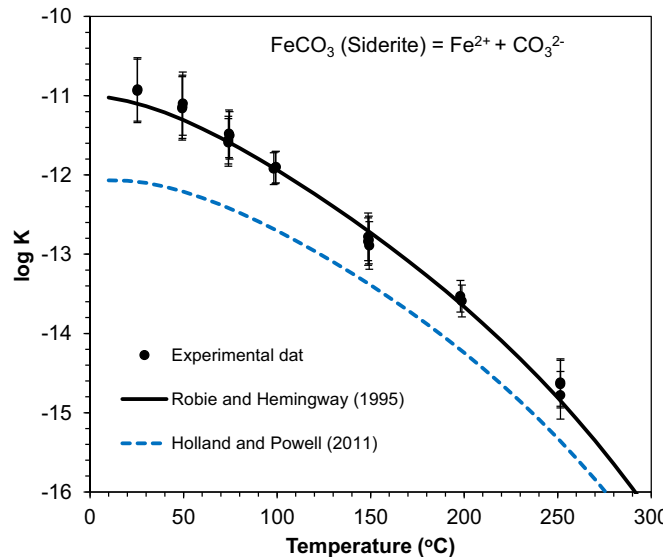


Fig. B4. Comparison of model-predicted solubility product constants of siderite with the experimental data. The experimental data are from Bénézeth et al. (2009). The errors of Bénézeth et al. (2009) are ± 0.4 at 25 °C and 50 °C, ± 0.3 at 75 °C, ± 0.2 at 100 °C, ± 0.3 at 150 °C, ± 0.2 at 200 °C and ± 0.3 at 250 °C. The models represent a system closed to atmosphere without the presence of CO_2 gas phase. Bénézeth et al. (2009)'s experiments were at 4 bars $p\text{CO}_2$.

Gypsum

Thermodynamic properties for gypsum are not given by Holland and Powell (2011). We adopted those from Matschei et al. (2007). However, the combination of these thermodynamic properties for gypsum and aqueous species in the SUPCRTBL database is inconsistent with the experimental data of gypsum solubility from the literature. For modeling with PHREEQC, provisional parameters for the analytical expressions of the solubility product constants as a function of temperature are given below. With these functions, the resulting solubility product constant equation is designated as “geothermal.dat_after_change” in Fig. B8 matches the experimental solubility data reasonably well. The interim nature of this equation is as noted above for an analogous situation arising with respect to dolomite solubility.

Modified:

-analytic 3.600026e+03 1.226125e+00 -1.365718e+05 -1.427393e+03 5.414952e+06 -4.613276e-04 (for *geothermal.dat*)
-analytic -1.926627e+03 -4.527455e-01 9.222760e+04 7.253784e+02 -4.964878e+06 9.767804e-05 (for *diagenesis.dat*)

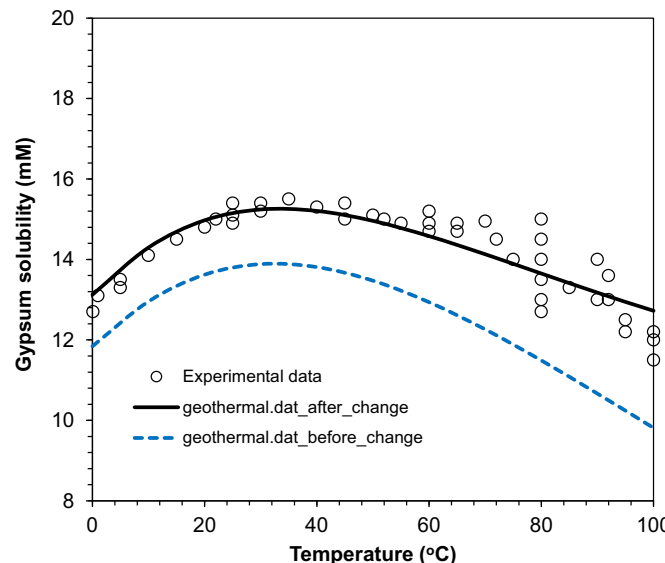


Fig. B5. Comparison of model-predicted gypsum solubility (mM) with the experimental data. The experimental data are from Azimi and Papangelakis (2010) and the literature data they collected.

Appendix C. Chemical analysis of waters

Table C1

Summary of test case data.

River water ¹		Seawater ¹		Groundwater ²		Oil field brine ³		Dead Sea brine ⁴		Stream flow contaminated with hazardous metals		Geothermal water ⁶	
Species	mg/L	Species	mg/L	Species	mg/L	Species	mg/L	Species	mg/L	Species	mg/L	Species	mg/L
Na	12	Na	11,019.54	Na	30	Na	22,300	Na	39,330	Na	3100	Na	16,250
K	1.4	K	408.423	K	3	K	143	K	6500	K	120	K	140
Ca	12.2	Ca	421.931	Ca	50	Ca	1130	Ca	17,750	Ca	600	Ca	380
Mg	7.5	Mg	1321.976	Mg	7	Mg	363	Mg	40,450	Mg	270	Mg	70
Si	8.52	SiO ₂	4.38	SiO ₂	16	SiO ₂	162	SiO ₂	35	SiO ₂	35	SiO ₂	68
HCO ₃ ^{-*}	75.2	HCO ₃ ^{-*}	144.992	HCO ₃ ⁻	300	HCO ₃ ⁻	504	HCO ₃ ⁻	290	HCO ₃ ⁻	361	HCO ₃ ⁻	361
Cl	9.9	Cl	19,805.09	Cl	20	Cl	37,700	Cl	212,600	Cl	5000	Cl	24,000
SO ₄	7.7	SO ₄	2775.35	SO ₄	30	SO ₄	14.8	SO ₄	760	SO ₄	2900	SO ₄	43
B	0.05	B	4.5540	B	0.01	B	37	T (°C)	25	F	3.2	B	45
Br	0.006	Br	68.872	Br	0.02	Br	185	pH	6	Br	6.5		
I	0.0018	I	0.06345	I	0.007	I	5.6					NH ₃	10.5
F	0.1	F	1.4225	F	0.1	F	13.1					Ba	11
PO ₄	0.21	PO ₄	0.0614	PO ₄	0.02	S(-2)	0.85					Fe	1.4
NO ₃	0.898	NO ₃	0.2968	Au	0.000002							Mn	25
NO ₂	0.019	NO ₂	0.0205	Be	0.005							Al	51
NH ₃	0.144	NH ₃	0.0307	Bi	0.000005	NH ₃	112					Al	0.000703
Fe(+2)	0.015	Ba	0.0205	Ba	0.02	Ba	90					Zn	170
Fe(+3)	0.0007	Fe	0.00205	Fe	0.1	Fe	13.9					Cd	0.69
Mn	0.0044	Mn	0.000205	Mn	0.015	Mn	0.29					Pb	0.004
Al	0.005	Al	0.00205	Al	0.01	Al	1					Cu	13
Zn	0.00049	Zn	0.005014	Zn	0.02								
Cd	0.0001	Cd	0.000102	Cd	0.00003								
Hg	0.00001	Hg	0.0000307	Hg	0.00007								
Pb	0.00003	Pb	0.0000512	Pb	0.003								
Cu	0.0005	Cu	0.000716	Cu	0.003								
Co	0.0005	Co	0.0000512	Co	0.0001								
Ni	0.0018	Ni	0.00174	Ni	0.0015								

(continued on next page)

Table C1 (continued)

River water ¹		Seawater ¹		Groundwater ²		Oil field brine ³		Dead Sea brine ⁴		Stream flow contaminated with hazardous metals		Geothermal water ⁶	
Species	mg/L	Species	mg/L	Species	mg/L	Species	mg/L	Species	mg/L	Species	mg/L	Species	mg/L
Cr	0.0005	Cr	0.000307	Cr	0.001								
Ag	0.00004	Ag	0.0000409	Ag	0.0003					Ag	0.001		
Mo	0.0005	Mo	0.00512	Mo	0.0015					Eh(V)	0.484		
As	0.002	As	0.000409	As	0.002					T (°C)	18.5		
H ₂ S	0.002	Sr	8.3302	Sr	0.4	Sr	66			pH	4.1	Sr	25
DO	10.94	Sb	0.0003377	Sb	0.002								
Eh(V)	0.44	Li	0.18523	Li	0.003	Li	1.79						
DOC	2.5	Rb	0.11973	Rb	0.001	Rb	0.17						
T (°C)	9.5	Cs	0.00409	Cs	0.00002	Cs	0.07						
pH	8.01	DO	6.6	La	0.0002	Acetate	221.9					Acetate	1290
Density	1.00	Eh(V)	0.5	Nb	0.001	Propionate	34.6					T (°C)	94
		T (°C)	25	Rb	0.001	Butyrate	11.3					pH	6.31 ⁷
		pH	8.22	Se	0.0004	Valerate	11.1						
		Density	1.02336	Sn	0.0001	T (°C)	77						
				Th	0.0001	pH	7.6 ⁷						
				Ti	0.003								
				W	0.00003								
				U	0.0005								
				V	0.002								
				T (°C)	25								
				pH	7.4								

*Titration alkalinity as HCO_3^- . ¹Nordstrom et al. (1979). ²Langmuir (1997). ³Kharaka et al. (1986). ⁴Jones and Deocampo (2003). ⁵Hamlin and Alpers (1995). ⁶Kharaka et al. (1977). ⁷pH corrected to subsurface temperatures.

Appendix D. Calculated concentrations of species and saturation indices of minerals for the river water test case

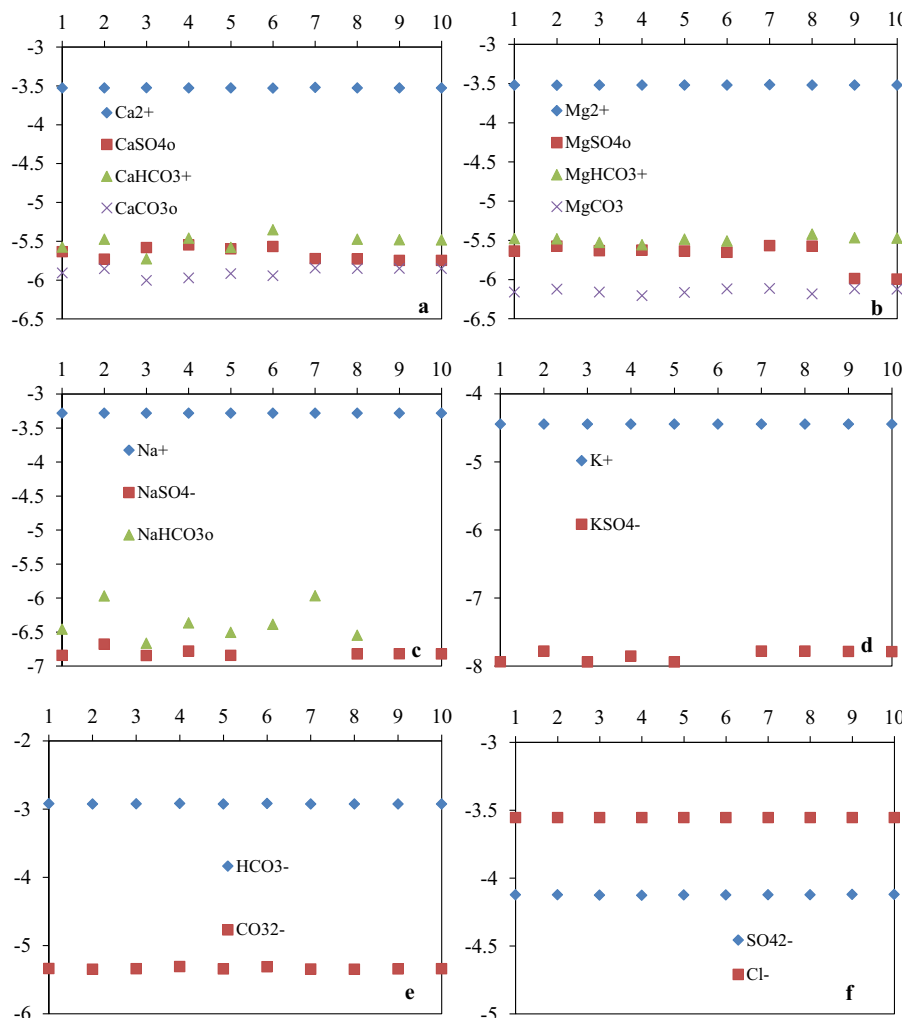


Fig. D1. Modeled concentrations (log molalities; Y-axis) of selected major species in the river water test case using different TDFs. (a) Ca-bearing species, (b) Mg-bearing species, (c) Na-bearing species, (d) K-bearing species, (e) C-bearing species, (f) SO_4^{2-} and Cl^- . For X-axis: 1 = *phreeqc.dat*, 2 = *llnl.dat*, 3 = *minteq.dat*, 4 = *minteq.v4.dat*, 5 = *wateq4f.dat*, 6 = *sit.dat*, 7 = *core10.dat*, 8 = *carbfix.dat*, 9 = *geothermal.dat*, 10 = *diagenesis.dat*.

Concentrations of Mn-bearing species are quite consistent, except those calculated using *sit.dat* (Fig. D2a). This arises because $\text{Mn}(\text{CO}_3)^0$ is the dominant species using *sit.dat*, whereas Mn^{2+} is dominant when using other files. For Fe-bearing species, the calculated concentrations using *sit.dat* and *core10.dat* differ significantly from those using other TDFs (Fig. D2b) because FeCO_3OH^0 is the dominant Fe-bearing species in *sit.dat* and $\text{Fe}(\text{OH})_4^-$ is omitted in *core10.dat*.

Only *minteq.dat*, *minteq.v4.dat*, *wateq4f.dat* and *sit.dat* include the NiCO_3^0 species (Fig. D2c). NiCO_3^0 is the dominant species when using *minteq.dat* and *wateq4f.dat*, whereas Ni^{2+} is dominant when using other TDFs.

Concentrations of Cu^{2+} are $\sim 2\text{--}3$ log units lower when calculated from *phreeqc.dat*, *minteq.dat*, *minteq.v4.dat* and *wateq4f.dat* than from other TDFs (Fig. D2d). The concentration of $\text{Cu}(\text{OH})_2^0$ from *minteq.v4.dat* is $\sim 2\text{--}3$ log units lower than those from all other TDFs with this species. The dominant Cu-bearing species is $\text{Cu}(\text{HS})_3^-$ for *phreeqc.dat*, *minteq.dat*, *minteq.v4.dat* and *wateq4f.dat*, but is Cu^{2+} for other TDFs incorporating Cu.

The dominant Ag species using *minteq.dat*, *minteq.v4.dat* and *wateq4f.dat* is AgHS^0 , whereas it is Ag^+ for *llnl.dat*, *sit.dat*, *geothermal.dat* and *diagenesis.dat*. This causes the log molalities of Ag^+ to be ~ 6 units lower in *minteq.dat*, *minteq.v4.dat* and *wateq4f.dat* when compared with those from *llnl.dat*, *sit.dat*, *geothermal.dat* and *diagenesis.dat* (Fig. D2e). The AgHS^0 , log molality from *sit.dat* is exceptionally low (Fig. D2e).

The concentrations of Zn-bearing species are generally consistent, except for $\text{Zn}(\text{HS})_2^0$ from *minteq.v4.dat*, which is ~ 2 log units lower than those for all other databases with this species (Fig. D2f).

Concentrations of Cd^{2+} from *phreeqc.dat*, *minteq.dat* and *wateq4f.dat* are ~ 2 log units lower than those from all other databases incorporating this species (Fig. D2g). For CdOH^+ , values from *phreeqc.dat*, *minteq.dat* and *wateq4f.dat* are ~ 3 log units lower than for all other databases with this species, because CdHS^+ is the dominant species using these TDFs. The CdHS^+ concentration from *sit.dat* is exceptionally low (-33.467 M ; not shown in Fig. D2g).

For Al-bearing species, $\text{Al}(\text{OH})_3^0$ is the calculated dominant species only when using *minteq.dat* (Fig. D2h). Calculated concentrations for this species from *llnl.dat*, *sit.dat*, *core10.dat* and *carbfix.dat* are consistent with each other, whereas those from *phreeqc.dat*, *wateq4f.dat*, *geothermal.dat* and *diagenesis.dat* differ, but are also consistent.

Pb as a component is not present in *core10.dat* and *carbfix.dat* (Fig. D2i). PbCO_3^0 is not present in *geothermal.dat* and *diagenesis.dat*, where PbOH^+ is the dominant species (Fig. D2i).

The calculated concentrations of N- and P-bearing species are quite consistent, differing by less than ~ 0.2 log unit (Figs. D2j, D2k; Table D1). Values for Hg^{2+} are quite different between all databases with this species (Table D1).

For As-bearing species, values from all databases except *llnl.dat* are quite consistent. The latter incorporates $\text{As}(\text{AsO}_3\text{F}^{2-})$ as the dominant species (Table D1).

For S(-2), the dominant species in *llnl.dat*, *sit.dat*, *core10.dat*, *carbfix.dat*, *geothermal.dat* and *diagenesis.dat* is S_5^{2-} , whereas in all other databases it is HS^- (Table D1). This leads to large differences in calculated log molalities of S^{2-} , HS^- , and H_2S^0 for the two groups, but within each group, the calculated values are consistent with each other.

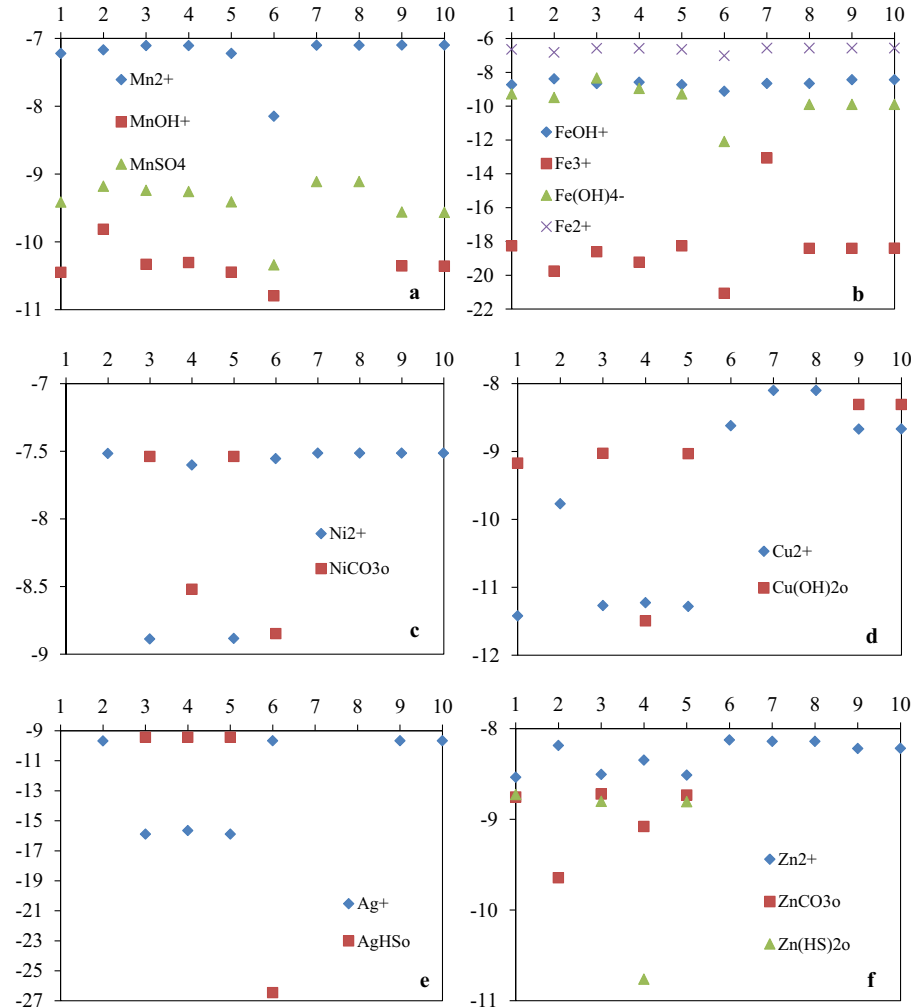


Fig. D2. Modeled concentrations (log molalities; Y-axis) of selected minor species in the river water test case using different TDFs. (a) Mn-bearing species, (b) Fe-bearing species, (c) Ni-bearing species, (d) Cu-bearing species, (e) Ag-bearing species, (f) Zn-bearing species, (g) Cd-bearing species, (h) Al-bearing species, (i) Pb-bearing species, (j) N-bearing species, (k) P-bearing species. For X-axis: 1 = phreeqc.dat, 2 = llnl.dat, 3 = minteq.dat, 4 = minteq.v4.dat, 5 = wateq4f.dat, 6 = sit.dat, 7 = core10.dat, 8 = carbfix.dat, 9 = geothermal.dat, 10 = diagenesis.dat.

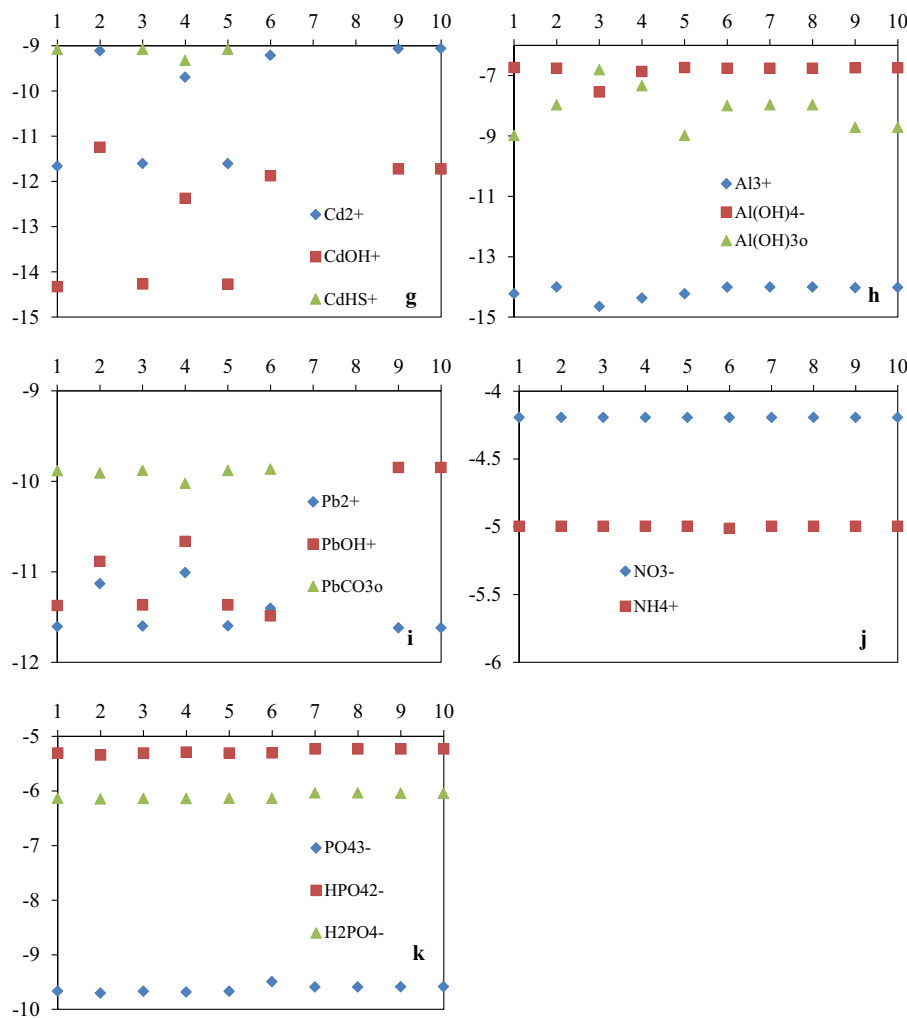


Fig. D2. (continued).

Table D1

Log concentrations (molalities) of selected major and minor species in the river water test case.

Major species	phreeqc.dat	llnl.dat	minEQ.dat	minEQ.v4.dat	wateq4f.dat	sit.dat	core10.dat	carbfix.dat	geothermal.dat	diagenesis.dat
Ca ²⁺	-3.526	-3.527	-3.525	-3.528	-3.526	-3.529	-3.521	-3.526	-3.526	-3.526
CaSO ₄ ^o	-5.634	-5.730	-5.582	-5.547	-5.598	-5.567	-5.724	-5.729	-5.746	-5.747
CaHCO ₃ ⁺	-5.574	-5.474	-5.726	-5.460	-5.580	-5.353	-	-5.473	-5.480	-5.483
CaCO ₃ ^o	-5.909	-5.854	-6.004	-5.973	-5.916	-5.945	-5.846	-5.853	-5.851	-5.853
Mg ²⁺	-3.521	-3.522	-3.520	-3.520	-3.521	-3.520	-3.516	-3.521	-3.519	-3.519
MgSO ₄ ^o	-5.637	-5.575	-5.632	-5.626	-5.638	-5.653	-5.569	-5.574	-5.988	-5.996
MgHCO ₃ ⁺	-5.479	-5.480	-5.526	-5.557	-5.485	-5.508	-	-5.422	-5.467	-5.472
MgCO ₃	-6.161	-6.123	-6.161	-6.206	-6.166	-6.119	-6.115	-6.184	-6.118	-6.123
Na ⁺	-3.283	-3.283	-3.283	-3.283	-3.283	-3.283	-3.283	-3.283	-3.282	-3.282
NaSO ₄ ⁻	-6.842	-6.678	-6.845	-6.781	-6.843	-	-	-6.821	-6.818	-6.821
NaHCO ₃ ^o	-6.458	-5.970	-6.664	-6.364	-6.504	-6.387	-5.967	-6.547	-	-
K ⁺	-4.446	-4.446	-4.446	-4.446	-4.446	-4.446	-4.446	-4.446	-4.446	-4.446
KSO ₄ ⁻	-7.938	-7.781	-7.941	-7.854	-7.939	-	-7.780	-7.781	-7.784	-7.787
SO ₄ ²⁻	-4.123	-4.122	-4.125	-4.126	-4.124	-4.124	-4.122	-4.122	-4.120	-4.120
Cl ⁻	-3.554	-3.554	-3.554	-3.554	-3.554	-3.554	-3.554	-3.554	-3.554	-3.554
HCO ₃ ⁻	-2.919	-2.926	-2.921	-2.918	-2.925	-2.918	-2.924	-2.926	-2.925	-2.925
CO ₃ ²⁻	-5.336	-5.348	-5.338	-5.307	-5.342	-5.311	-5.345	-5.348	-5.341	-5.338
SiO ₂ ^o	-3.522	-3.521	-3.520	-3.522	-3.522	-3.522	-3.521	-3.521	-3.525	-3.525
H ⁺	-7.989	-7.989	-7.989	-7.987	-7.989	-7.987	-7.989	-7.989	-7.989	-7.989
OH ⁻	-6.518	-6.524	-6.501	-6.500	-6.520	-6.503	-6.524	-6.524	-6.519	-6.516
Ionic Strength	2.434e-3	2.422e-3	2.433e-3	2.436e-3	2.425e-3	2.433e-3	2.438e-3	2.428e-3	2.436e-3	2.437e-3
Minor species	phreeqc.dat	llnl.dat	minEQ.dat	minEQ.v4.dat	wateq4f.dat	sit.dat	core10.dat	carbfix.dat	geothermal.dat	diagenesis.dat
H ₃ BO ₃	-5.354	-5.353	-5.354	-5.355	-5.354	-5.355	-5.352	-5.352	-5.352	-5.353
H ₂ BO ₃ ⁻	-6.691	-6.746	-6.689	-6.682	-6.690	-6.692	-6.745	-6.745	-6.738	-6.734
Br ⁻	-7.124	-7.124	-7.124	-7.124	-7.124	-7.124	-	-	-7.124	-7.124

(continued on next page)

Table D1 (continued)

Major species	<i>phreeqc.dat</i>	<i>llnl.dat</i>	<i>minteq.dat</i>	<i>minteq.v4.dat</i>	<i>wateq4f.dat</i>	<i>sit.dat</i>	<i>core10.dat</i>	<i>carbfix.dat</i>	<i>geothermal.dat</i>	<i>diagenesis.dat</i>
F ⁻	-5.284	-5.284	-5.284	-5.288	-5.285	-5.284	-	-5.279	-5.282	-5.282
Cr ³⁺	-	-36.495	-32.042	-34.133	-	-35.805	-36.495	-36.495	-35.075	-35.069
Mn ²⁺	-7.223	-7.168	-7.106	-7.107	-7.221	-8.147	-7.101	-7.101	-7.098	-7.098
MnOH ⁺	-10.448	-9.815	-10.331	-10.306	-10.447	-10.796	-	-	-10.355	-10.358
MnSO ₄	-9.412	-9.180	-9.239	-9.258	-9.411	-10.339	-9.112	-9.112	-9.559	-9.566
Fe ²⁺	-6.650	-6.827	-6.581	-6.587	-6.649	-7.028	-6.574	-6.574	-6.577	-6.577
FeOH ⁺	-8.737	-8.383	-8.669	-8.586	-8.736	-9.118	-8.661	-8.661	-8.440	-8.442
Fe ³⁺	-18.266	-19.759	-18.609	-19.227	-18.266	-21.065	-13.072	-18.410	-18.410	-18.397
Fe(OH) ₄ ⁻	-9.279	-9.490	-8.340	-8.959	-9.279	-12.090	-	-9.895	-9.895	-9.894
Ni ²⁺	-	-7.516	-8.887	-7.601	-8.884	-7.554	-7.513	-7.513	-7.513	-7.513
NiCO ₃ ⁰	-	-	-7.538	-8.520	-7.539	-8.848	-	-	-	-
Cu ²⁺	-11.422 ^{\$}	-9.773	-11.272 ^{\$}	-11.228 ^{\$}	-11.283 ^{\$}	-8.623	-8.104	-8.104	-8.672	-8.671
Cu(OH) ₂ ⁰	-9.172 ^{\$}	-	-9.026 ^{\$}	-11.494 ^{\$}	-9.033 ^{\$}	-	-	-	-8.307	-8.307
Ag ⁺	-	-9.673	-15.884	-15.651	-15.887	-9.665	-	-	-9.672	-9.671
AgHS ⁰	-	-	-9.431	-9.432	-9.431	-26.458	-	-	-	-
Zn ²⁺	-8.537	-8.186	-8.504	-8.348	-8.512	-8.125	-8.140	-8.140	-8.219	-8.218
ZnCO ₃ ⁰	-8.754	-9.644	-8.722	-9.079	-8.734	-	-	-	-	-
Zn(HS) ₂ ⁰	-8.727	-	-8.802	-10.763	-8.805	-	-	-	-	-
Cd ²⁺	-11.661	-9.112	-11.604	-9.694	-11.606	-9.210	-	-	-9.063	-9.062
CdOH ⁺	-14.327	-11.246	-14.270	-12.375	-14.272	-11.875	-	-	-11.724	-11.725
CdHS ⁺	-9.079	-	-9.077	-9.325	-9.077	-33.476	-	-	-	-
Hg ²⁺	-	-10.302	-35.873	-34.742	-	-10.302	-	-	-19.708 [†]	-19.706 [†]
Al ³⁺	-14.230	-14.003	-14.645	-14.367	-14.230	-14.010	-14.002	-14.003	-14.027	-14.016
Al(OH) ₄ ⁻	-6.735	-6.758	-7.546	-6.864	-6.735	-6.760	-6.758	-6.759	-6.740	-6.740
Al(OH) ₃ ⁰	-8.984	-7.971	-6.808	-7.336	-8.984	-7.996	-7.971	-7.971	-8.710	-8.713
Pb ²⁺	-11.604	-11.130	-11.598	-11.008	-11.597	-11.401	-	-	-11.619	-11.618
PbOH ⁺	-11.373	-10.884	-11.367	-10.663	-11.366	-11.487	-	-	-9.847	-9.847
PbCO ₃ ⁰	-9.883	-9.909	-9.879	-10.022	-9.881	-9.865	-	-	-	-
NO ₃ ⁻	-4.193	-4.194	-4.193	-4.193	-4.193	-4.193	-4.193	-4.193	-4.193	-4.193
NH ₄ ⁺	-4.996	-4.996	-4.996	-4.996	-4.996	-5.012	-4.996	-4.996	-4.996	-4.996
PO ₄ ³⁻	-9.668	-9.705	-9.671	-9.684	-9.671	-9.495	-9.592	-9.592	-9.590	-9.587
HPO ₄ ²⁻	-5.307	-5.344	-5.307	-5.291	-5.307	-5.304	-5.232	-5.232	-5.231	-5.231
H ₂ PO ₄ ⁻	-6.138	-6.151	-6.139	-6.142	-6.138	-6.138	-6.039	-6.039	-6.043	-6.046
HASO ₄ ²⁻	-	-41.318 [#]	-7.595	-7.607	-7.626	-7.615	-	-	-7.675	-7.673
H ₂ AsO ₄ ⁻	-	-42.584 [#]	-8.885	-8.702	-8.514	-8.892	-	-	-8.647	-8.648
S ²⁻	-12.823	-36.861 [*]	-12.877	-17.245	-12.875	-30.308 [*]	-*	-*	-*	-*
HS ⁻	-7.496	-31.538 [*]	-7.551	-7.547	-7.548	-31.554 [*]	-31.538 [*]	-31.538 [*]	-31.538 [*]	-31.537 [*]
H ₂ S ⁰	-8.355	-32.334 [*]	-8.409	-8.350	-8.407	-32.383 [*]	-32.334 [*]	-32.334 [*]	-32.338 [*]	-32.340 [*]
I ⁻	-	-21.703 ^{&}	-7.848	-7.848	-7.848	-20.060 ^{&}	-	-	-21.707 ^{&}	-21.709 ^{&}

*The dominant species is S₅²⁻. [#]The dominant species is AsO₃F²⁻. [&]The dominant species is IO₃⁻. ^{\$}The dominant species is Cu(HS)₃⁻. [†]The dominant species is HgO.

Table D2

Saturation indices for selected minerals in the river water test case.

	Formula	<i>phreeqc.dat</i>	<i>amm.dat</i>	<i>iso.dat</i>	<i>llnl.dat</i>	<i>minteq.dat</i>	<i>minteq.v4.dat</i>	<i>wateq4f.dat</i>	<i>sit.dat</i>	<i>core10.dat</i>	<i>carbfix.dat</i>	<i>geothermal.dat</i>	<i>diagenesis.dat</i>
Calcite	CaCO ₃	-0.64	-0.64	-0.64	-0.63	-0.64	-0.62	-0.64	-0.64	-0.62	-0.63	-0.56	-0.56
Dolomite	CaMg(CO ₃) ₂	-1.38	-1.38	-1.38	-0.16	-1.41	-1.32	-1.38	-1.26	-0.14	-0.66	-1.10	-1.11
Siderite	FeCO ₃	-1.38	-1.38	-1.38	-1.95	-1.76	-2.00	-1.38	-1.84	-1.70	-1.06	-1.08	-1.08
Rhodochrosite	MnCO ₃	-1.67	-1.67	-1.67	-	-2.19	-2.30	-2.04	-1.67	-2.57	-2.12	-2.12	-2.12
Gypsum	CaSO ₄ •2H ₂ O	-3.23	-3.23	-3.24	-3.32	-3.21	-3.22	-3.24	-3.24	-3.31	-3.32	-3.26	-3.26
Hydroxyapatite	Ca ₅ (PO ₄) ₃ OH	-0.27	-0.26	-0.27	-0.97	4.51	4.57	-0.27	3.42	-0.61	-0.63	1.47	1.43
Fluorite	CaF ₂	-3.43	-3.43	-3.43	-4.05	-3.42	-3.67	-3.43	-3.45	-	-	-	-
Ferric Hydrix. (am)	Fe(OH) ₃	0.68	0.68	0.68	-2.38	0.34	0.70	0.68	0.22	4.31	-1.03	-	-
Goethite	FeO(OH)	5.99	5.99	5.99	2.95	4.15	3.52	5.99	1.78	9.64	4.30	4.75	4.75
Hematite	Fe ₂ O ₃	13.91	13.91	13.91	6.83	13.22	9.37	13.91	5.35	20.21	9.53	9.19	9.18
FeS (am)	FeS	-2.33	-2.33	-2.10	-26.80	-2.32	-3.40	-2.39	-27.74	-26.55	-26.55	-26.55	-26.52
Machinawite	FeS	-1.60	-1.60	-1.36	-	-1.59	-2.65	-1.65	-27.09	-	-	-	-
Gibbsite	Al(OH) ₃	0.58	0.58	0.58	1.11	-0.49	0.25	0.58	1.09	1.11	1.11	1.09	1.08
Chalcedony	SiO ₂	0.22	0.22	0.22	0.56	0.19	0.22	0.22	-	0.56	0.56	-	-
Quartz	SiO ₂	0.70	0.70	0.70	0.85	0.74	0.69	0.70	0.42	0.85	0.85	0.71	0.71
Kaolinite	Al ₂ Si ₂ O ₅ (OH) ₄	3.32	3.32	3.32	4.48	4.20	3.01	3.32	4.45	4.49	4.48	6.47	6.46
Sepiolite	Mg ₂ SiO _{7.5} (OH)	-1.94	-1.94	-1.94	-3.12	-2.75	-2.61	-1.94	-	-3.09	-3.11	-	-
	•3H ₂ O												

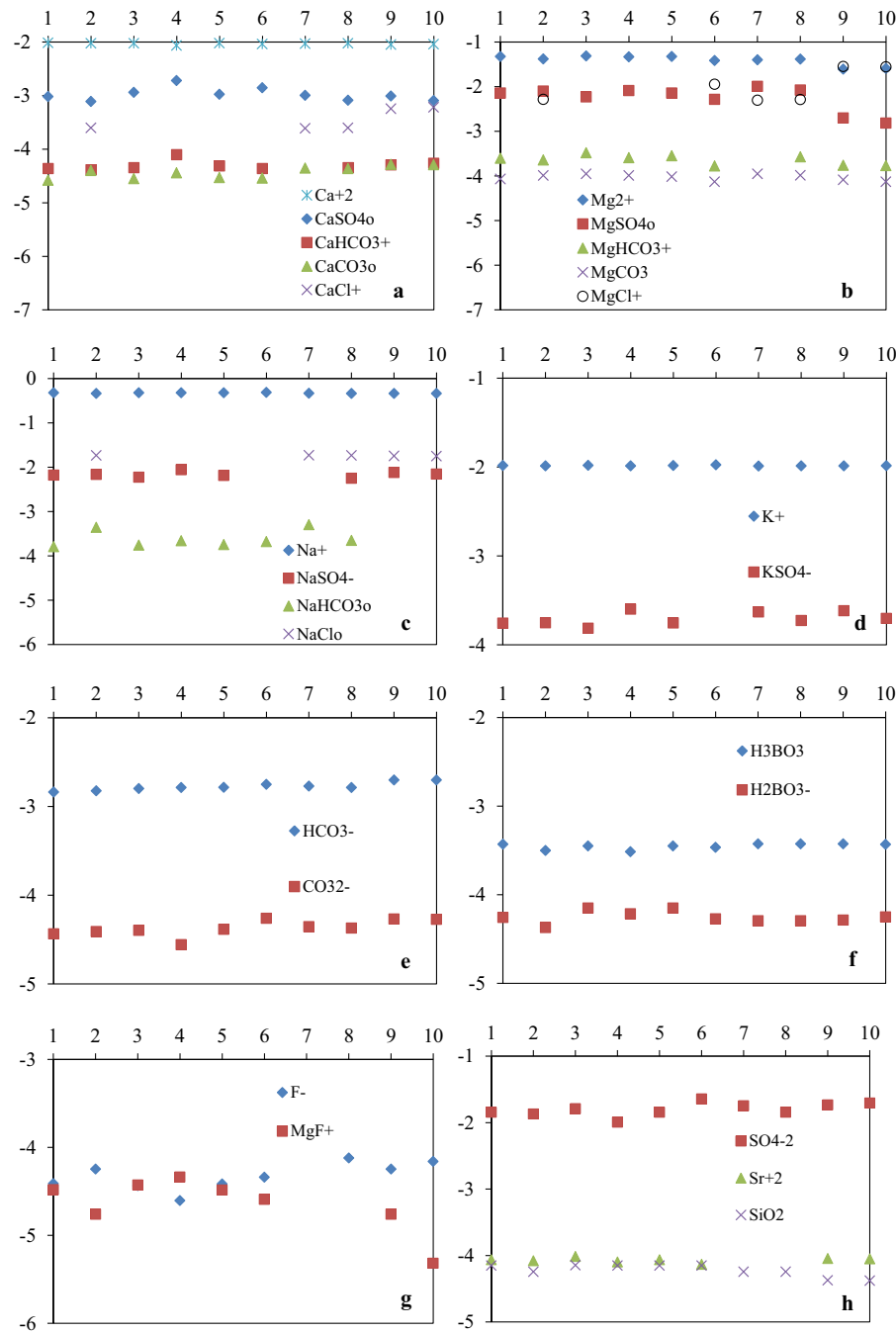
Appendix E. Calculated concentrations of species and saturation indices of minerals for the seawater test case


Fig. E1. Modeled concentrations (log molalities; Y-axis) of selected major species in the seawater test case using different TDFs. (a) Ca-bearing species, (b) Mg-bearing species, (c) Na-bearing species, (d) K-bearing species, (e) C-bearing species, (f) B-bearing species, (g) F-bearing species, (h) SO_4^{2-} , Sr^{2+} , and SiO_2 . For X-axis: 1 = *phreeqc.dat*, 2 = *llnl.dat*, 3 = *minteq.dat*, 4 = *minteq.v4.dat*, 5 = *wateq4f.dat*, 6 = *sit.dat*, 7 = *core10.dat*, 8 = *carbfix.dat*, 9 = *geothermal.dat*, 10 = *diagenesis.dat*.

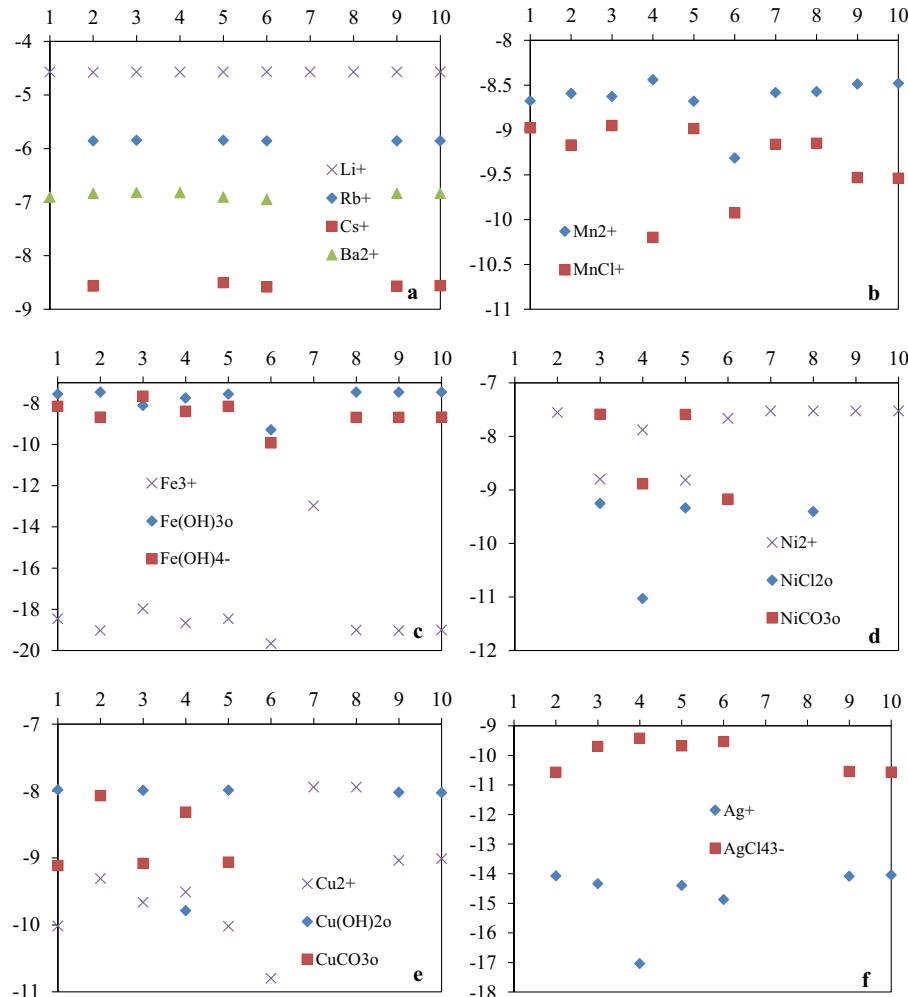


Fig. E2. Modeled concentrations (log molalities; Y-axis) of selected minor species in the seawater test case using different TDFs. (a) Li^+ , Rb^+ , Sr^{2+} and Ba^{2+} , (b) Mn-bearing species, (c) Fe-bearing species, (d) Ni-bearing species, (e) Cu-bearing species, (f) Ag-bearing species, (g) Zn-bearing species, (h) Cd-bearing species, (i) Hg-bearing species, (j) Al-bearing species, (k) Pb-bearing species, (l) P-bearing species. For X-axis: 1 = *phreeqc.dat*, 2 = *llnl.dat*, 3 = *minseq.dat*, 4 = *minseq.v4.dat*, 5 = *wateq4f.dat*, 6 = *sit.dat*, 7 = *core10.dat*, 8 = *carbfix.dat*, 9 = *geothermal.dat*, 10 = *diagenesis.dat*.

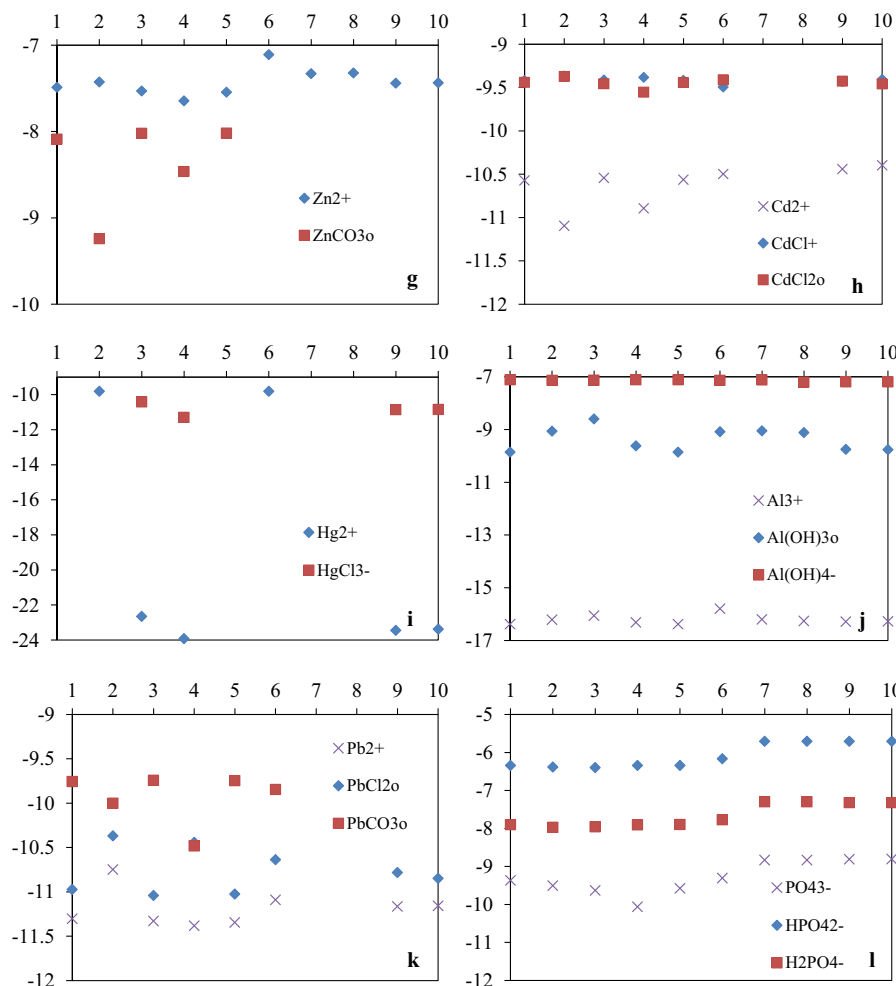


Fig. E2. (continued).

Table E1
Log concentrations (molalities) of selected major and minor species in the Seawater test case.

Major species	phreeqc.dat	llnl.dat	miniteq.dat	miniteq.v4.dat	wateq4f.dat	sit.dat	core10.dat	carbfix.dat	geothermal.dat	diagenesis.dat
Ca ²⁺	-2.016	-2.023	-2.025	-2.064	-2.021	-2.037	-2.032	-2.025	-2.048	-2.041
CaSO ₄ ^o	-3.020	-3.111	-2.940	-2.719	-2.975	-2.853	-2.997	-3.087	-3.010	-3.094
CaHCO ₃ ⁺	-4.362	-4.385	-4.348	-4.103	-4.314	-4.362	-	-4.348	-4.295	-4.266
CaCO ₃ ^o	-4.579	-4.399	-4.549	-4.442	-4.532	-4.540	-4.355	-4.363	-4.283	-4.292
CaCl ⁺	-	-3.601	-	-	-	-	-3.611	-3.603	-3.244	-3.220
Mg ²⁺	-1.323	-1.381	-1.312	-1.333	-1.323	-1.417	-1.399	-1.385	-1.610	-1.591
MgSO ₄ ^o	-2.145	-2.099	-2.231	-2.088	-2.145	-2.285	-1.994	-2.077	-2.702	-2.818
MgHCO ₃ ⁺	-3.603	-3.644	-3.483	-3.591	-3.550	-3.775	-	-3.571	-3.762	-3.767
MgCO ₃	-4.069	-3.991	-3.954	-3.990	-4.017	-4.132	-3.955	-3.985	-4.087	-4.131
MgCl ⁺	-	-2.286	-	-	-	-1.945	-2.304	-2.289	-1.548	-1.558
Na ⁺	-0.320	-0.338	-0.319	-0.322	-0.320	-0.314	-0.331	-0.336	-0.337	-0.337
NaSO ₄ ⁻	-2.178	-2.161	-2.226	-2.055	-2.185	-	-	-2.251	-2.120	-2.154
NaHCO ₃ ^o	-3.791	-3.355	-3.758	-3.658	-3.745	-3.678	-3.295	-3.651	-	-
NaCl ^o	-	-1.735	-	-	-	-	-1.729	-1.733	-1.745	-1.750
K ⁺	-1.983	-1.986	-1.982	-1.986	-1.983	-1.976	-1.988	-1.986	-1.986	-1.984
KSO ₄ ⁻	-3.756	-3.752	-3.813	-3.599	-3.755	-	-3.631	-3.726	-3.617	-3.703

(continued on next page)

Table E1 (continued)

Major species	<i>phreeqc.dat</i>	<i>llnl.dat</i>	<i>minteq.dat</i>	<i>minteq.v4.dat</i>	<i>wateq4f.dat</i>	<i>sit.dat</i>	<i>core10.dat</i>	<i>carbfix.dat</i>	<i>geothermal.dat</i>	<i>diagenesis.dat</i>
SO_4^{2-}	-1.844	-1.871	-1.792	-1.995	-1.844	-1.645	-1.747	-1.845	-1.733	-1.705
Cl^-	-0.247	-0.266	-0.247	-0.247	-0.247	-0.256	-0.266	-0.266	-0.285	-0.284
HCO_3^-	-2.839	-2.826	-2.799	-2.789	-2.786	-2.752	-2.773	-2.788	-2.704	-2.703
CO_3^{2-}	-4.436	-4.409	-4.396	-4.558	-4.384	-4.261	-4.354	-4.370	-4.269	-4.273
H_3BO_3	-3.430	-3.501	-3.449	-3.514	-3.449	-3.466	-3.425	-3.425	-3.426	-3.431
$\text{H}_2\text{BO}_3^-/\text{B(OH)}_4^-$	-4.256	-4.370	-4.150	-4.215	-4.151	-4.273	-4.294	-4.294	-4.286	-4.250
Br^-	-3.059	-3.063	-3.059	-3.059	-3.059	-3.062	-	-	-3.063	-3.063
F^-	-4.412	-4.247	-4.436	-4.605	-4.415	-4.339	-	-4.120	-4.247	-4.161
MgF^+	-4.481	-4.761	-4.428	-4.337	-4.485	-4.591	-	-	-4.761	-5.318
Sr^{2+}	-4.063	-4.080	-4.016	-4.097	-4.063	-4.133	-	-	-4.046	-4.051
$\text{H}_4\text{SiO}_4^0/\text{SiO}_2^0$	-4.151	-4.245	-4.147	-4.151	-4.151	-4.152	-4.246	-4.245	-4.375	-4.379
H^+	-8.098	-8.125	-8.098	-8.093	-8.098	-8.099	-8.125	-8.125	-8.137	-8.099
OH^-	-5.568	-5.618	-5.571	-5.571	-5.573	-5.620	-5.617	-5.618	-5.613	-5.572
Ionic Strength	0.6754	0.6427	0.6812	0.6629	0.6753	0.6728	0.6469	0.6431	0.6187	0.6240
Minor species	<i>phreeqc.dat</i>	<i>llnl.dat</i>	<i>minteq.dat</i>	<i>minteq.v4.dat</i>	<i>wateq4f.dat</i>	<i>sit.dat</i>	<i>core10.dat</i>	<i>carbfix.dat</i>	<i>geothermal.dat</i>	<i>diagenesis.dat</i>
Li^+	-4.573	-4.578	-4.573	-4.575	-4.573	-4.568	-4.572	-4.572	-4.572	-4.571
Rb^+	-	-5.858	-5.848	-	-5.848	-5.858	-	-	-5.858	-5.857
Cs^+	-	-8.569	-	-	-8.506	-8.585	-	-	-8.570	-8.563
Ba^{2+}	-6.909	-6.837	-6.821	-6.824	-6.907	-6.951	-	-	-6.838	-6.837
Cr^{3+}	-	-38.224	-33.969	-31.314	-	-37.075	-38.224	-38.224	-36.932	-36.891
Mn^{2+}	-8.677	-8.593	-8.627	-8.440	-8.680	-9.313	-8.584	-8.573	-8.488	-8.481
MnCl^+	-8.977	-9.169	-8.951	-10.198	-8.985	-9.925	-9.161	-9.149	-9.531	-9.539
Fe^{3+}	-18.464	-19.031	-17.970	-18.673	-18.464	-19.673	-12.978	-19.013	-19.039	-19.003
Fe(OH)_3^0	-7.557	-7.464	-8.105	-7.746	-7.557	-9.285	-	-7.465	-7.464	-7.465
Fe(OH)_4^-	-8.148	-8.679	-7.655	-8.392	-8.148	-9.926	-	-8.684	-8.688	-8.680
Ni^{2+}	-	-7.560	-8.806	-7.882	-8.820	-7.667	-7.528	-7.528	-7.529	-7.528
NiCl_2^0	-	-	-9.256	-11.032	-9.340	-	-	-9.406	-	-
NiCO_3^0	-	-	-7.589	-8.888	-7.590	-9.173	-	-	-	-
Cu^{2+}	-10.018	-9.309	-9.662	-9.508	-10.022	-10.797	-7.942	-7.942	-9.037	-9.010
Cu(OH)_2^0	-7.983	-	-7.990	-9.788	-7.987	-	-	-	-8.020	-8.025
CuCO_3^0	-9.114	-8.071	-9.083	-8.315	-9.065	-	-	-	-	-
Ag^+	-	-14.074	-14.340	-17.041	-14.396	-14.878	-	-	-14.084	-14.043
AgCl_4^{3-}	-	-10.569	-9.696	-9.420	-9.683	-9.533	-	-	-10.548	-10.566
Zn^{2+}	-7.488	-7.426	-7.531	-7.646	-7.545	-7.110	-7.330	-7.322	-7.440	-7.437
ZnCO_3^0	-8.088	-9.243	-8.020	-8.464	-8.019	-	-	-	-	-
Cd^{2+}	-10.571	-11.096	-10.544	-10.893	-10.563	-10.499	-	-	-10.441	-10.397
CdCl^+	-9.419	-9.367	-9.413	-9.383	-9.416	-9.494	-	-	-9.433	-9.406
CdCl_2^0	-9.441	-9.372	-9.457	-9.553	-9.443	-9.411	-	-	-9.427	-9.458
Hg^{2+}	-	-9.810	-22.652	-23.927	-	-9.810	-	-	-23.449	-23.385
HgCl_3^-	-	-	-10.414	-11.297	-	-	-	-	-10.859	-10.846
Al^{3+}	-16.385	-16.218	-16.063	-16.315	-16.385	-15.796	-16.200	-16.263	-16.292	-16.273
Al(OH)_3^0	-9.859	-9.064	-8.598	-9.619	-9.859	-9.086	-9.048	-9.118	-9.757	-9.770
Al(OH)_4^-	-7.115	-7.136	-7.129	-7.116	-7.115	-7.136	-7.120	-7.199	-7.196	-7.195
Pb^{2+}	-11.303	-10.749	-11.330	-11.383	-11.345	-11.091	-	-	-11.165	-11.158
PbCl_2^0	-10.973	-10.369	-11.042	-10.442	-11.025	-10.638	-	-	-10.782	-10.848
PbCO_3^0	-9.756	-10.001	-9.743	-10.482	-9.746	-9.846	-	-	-	-
NO_3^-	-5.314	-5.319	-5.314	-5.322	-5.314	-5.314	-5.314	-5.314	-5.314	-5.314
PO_4^{3-}	-9.369	-9.509	-9.632	-10.063	-9.577	-9.309	-8.833	-8.834	-8.812	-8.809
HPO_4^{2-}	-6.344	-6.383	-6.400	-6.344	-6.343	-6.165	-5.709	-5.709	-5.708	-5.708
H_2PO_4^-	-7.900	-7.973	-7.957	-7.907	-7.899	-7.772	-7.300	-7.299	-7.320	-7.323
AsO_4^{3-}	-	-44.010	-10.008	-8.488	-10.069	-9.783	-	-	-10.858	-10.843
HASO_4^{2-}	-	-41.637	-7.264	-7.285	-7.273	-7.341	-	-	-8.272	-8.261
I^-	-	-18.526	-6.296	-6.296	-6.296	-18.374	-	-	-18.537	-18.442

Table E2

Log activity coefficients of selected major species in the seawater test case.

	<i>phreeqc.dat</i>	<i>llnl.dat</i>	<i>minteq.dat</i>	<i>minteq.v4.dat</i>	<i>wateq4f.dat</i>	<i>sit.dat</i>	<i>core10.dat</i>	<i>carbfix.dat</i>	<i>geothermal.dat</i>	<i>diagenesis.dat</i>
Ca^{2+}	-0.602	-0.609	-0.529	-0.510	-0.602	-0.673	-0.610	-0.609	-0.593	-0.598
CaSO_4^0	0.068	0.000	0.068	0.000	0.068	0.000	0.000	0.000	0.000	0.000
CaHCO_3^+	-0.160	-0.173	-0.160	-0.159	-0.160	-0.188	-	-0.173	-0.160	-0.198
CaCO_3^0	0.068	0.000	0.068	0.000	0.068	0.000	0.000	0.000	0.000	0.000
Mg^{2+}	-0.540	-0.501	-0.473	-0.510	-0.540	-0.645	-0.502	-0.501	-0.486	-0.539

(continued on next page)

Table E2 (continued)

	<i>phreeqc.dat</i>	<i>llnl.dat</i>	<i>minteq.dat</i>	<i>minteq.v4.dat</i>	<i>wateq4f.dat</i>	<i>sit.dat</i>	<i>core10.dat</i>	<i>carbfix.dat</i>	<i>geothermal.dat</i>	<i>diagenesis.dat</i>
MgSO ₄ ⁰	0.068	0.000	0.068	0.000	0.068	0.000	0.000	0.000	0.000	0.000
MgHCO ₃ ⁺	-0.202	-0.173	-0.202	-0.201	-0.202	-0.188	-	-0.173	-0.160	-0.198
MgCO ₃	0.068	0.000	0.068	0.000	0.068	0.000	0.000	0.000	0.000	0.000
Na ⁺	-0.144	-0.173	-0.151	-0.127	-0.151	-0.174	-0.173	-0.173	-0.160	-0.151
NaSO ₄ ⁻	-0.171	-0.173	-0.171	-0.170	-0.171	-	-	-0.173	-0.160	-0.198
NaHCO ₃ ⁰	0.068	0.000	0.068	0.000	0.068	0.000	0.000	0.000	-	-
K ⁺	-0.205	-0.203	-0.222	-0.127	-0.205	-0.188	-0.203	-0.203	-0.188	-0.202
KSO ₄ ⁻	-0.171	-0.173	-0.171	-0.170	-0.171	-	-0.173	-0.173	-0.160	-0.168
SO ₄ ²⁻	-0.741	-0.772	-0.835	-0.510	-0.740	-0.808	-0.773	-0.772	-0.753	-0.860
Cl ⁻	-0.200	-0.203	-0.222	-0.127	-0.205	-0.164	-0.203	-0.203	-0.188	-0.202
HCO ₃ ⁻	-0.171	-0.173	-0.171	-0.170	-0.171	-0.188	-0.173	-0.173	-0.160	-0.168
CO ₃ ²⁻	-0.682	-0.724	-0.683	-0.510	-0.682	-0.789	-0.725	-0.724	-0.706	-0.743
H ₃ BO ₃	0.068	0.000	0.068	0.066	0.068	0.000	0.000	0.000	0.000	0.000
H ₂ BO ₃ ⁻ /B(OH) ₄ ⁻	-0.127	-0.173	-0.251	-0.249	-0.250	-0.222	-0.173	-0.173	-0.160	-0.198
Br ⁻	-0.232	-0.203	-0.202	-0.127	-0.127	-0.163	-	-	-0.188	-0.230
F ⁻	-0.216	-0.187	-0.216	-0.127	-0.216	-0.178	-	-0.187	-0.173	-0.211
MgF ⁺	-0.189	-0.173	-0.190	-0.188	-0.189	-0.188	-	-	-0.160	-0.186
Si ²⁺	-0.611	-0.681	-0.715	-0.510	-0.611	-0.750	-	-	-0.664	-0.606
H ₄ SiO ₄ ⁰ /SiO ₂ ⁰	0.068	0.000	0.068	0.066	0.068	0.000	0.000	0.000	0.000	0.000
H ⁺	-0.122	-0.095	-0.122	-0.127	-0.122	-0.121	-0.095	-0.095	-0.082	-0.121
OH ⁻	-0.216	-0.187	-0.216	-0.214	-0.216	-0.168	-0.187	-0.187	-0.173	-0.211
Ionic Strength	0.6754	0.6427	0.6821	0.6629	0.6753	0.6728	0.6469	0.6431	0.6187	0.6240

Table E3

Saturation index for selected minerals in the seawater test case.

	Formula	Phreeqc. dat	Amm. dat	Iso.dat	llnl.dat	Minteq. dat	Minteq. v4.dat	Wateq4f. dat	Sit.dat	Core10. dat	Carbfix. dat	Geothermal. dat	Diagenesis. dat
Calcite	CaCO ₃	0.74	0.80	0.82	0.76	0.84	0.84	0.79	0.72	0.81	0.80	0.84	0.83
Dolomite	CaMg(CO ₃) ₂	2.37	2.48	2.54	3.45	2.50	2.54	2.47	2.25	3.53	2.86	2.58	2.52
Siderite	FeCO ₃	-13.18	-13.12	-13.06	-14.02	-12.97	-14.00	-13.12	-14.96	-7.92	-13.50	-13.34	-13.34
Rhodochrosite	MnCO ₃	-3.31	-3.26	-	-3.76	-3.94	-4.59	-3.26	-3.91	-3.70	-3.71	-3.54	-3.58
Gypsum	CaSO ₄ •2H ₂ O	-0.64	-0.64	-0.63	-0.76	-0.59	-0.49	-0.64	-0.57	-0.65	-0.74	-0.59	-0.67
Celestite	SrSO ₄	-0.60	-0.60	-	-1.68	-0.89	-0.49	-0.63	-0.72	-	-	-	-
Barite	BaSO ₄	-0.35	-0.35	-	-0.15	-0.19	0.14	-0.23	-0.15	-	-	-	-
Hydroxyapatite	Ca ₅ (PO ₄) ₃ OH	2.03	2.03	1.95	1.47	5.92	6.04	2.01	5.64	3.44	3.48	5.41	5.28
Fluorite	CaF ₂	-1.27	-1.27	-1.23	-1.43	-1.26	-1.54	-1.28	-1.14	-	-	-	-
Ferric Hydrix. (am)	Fe(OH) ₃	0.18	0.18	0.19	-1.10	0.67	1.62	0.18	2.08	4.95	-1.09	-	-
Goethite	FeO(OH)	6.08	6.08	6.09	4.01	5.07	4.33	6.08	2.89	10.07	4.03	4.45	4.44
Hematite	Fe ₂ O ₃	14.17	14.17	14.20	9.02	15.16	11.07	14.17	7.59	21.13	9.06	8.71	8.70
Gibbsite	Al(OH) ₃	-0.96	-0.96	-0.89	-0.39	-1.30	-1.12	-0.96	-0.41	-0.37	-0.44	-0.44	-0.45
Birnessite	MnO ₂	-	-	-	-12.00	0.85	0.15	4.75	5.60	-	-	-	-
Manganite	MnO(OH)	2.39	2.38	-	-	-1.44	1.58	2.39	1.74	-	-	-	-
Chalcedony	SiO ₂	-0.52	-0.52	-0.51	-0.49	-0.54	-0.52	-0.52	-1.43	-0.49	-0.49	-	-
Quartz	SiO ₂	-0.09	-0.09	-0.08	-0.22	-0.06	-0.07	-0.09	-0.40	-0.22	-0.22	-0.49	-0.49
Kaolinite	Al ₂ Si ₂ O ₅ (OH) ₄	-1.26	-1.26	-1.11	-0.50	1.10	-1.22	-1.26	-0.10	-0.47	-0.59	1.02	0.98
Sepiolite	Mg ₂ SiO _{7.5} (OH) ₄ •3H ₂ O	1.15	1.15	1.12	2.45	1.16	1.19	1.15	-	2.37	2.43	-	-

Appendix F. Calculated concentrations (molalities) of species and saturation indices of minerals for the groundwater test case

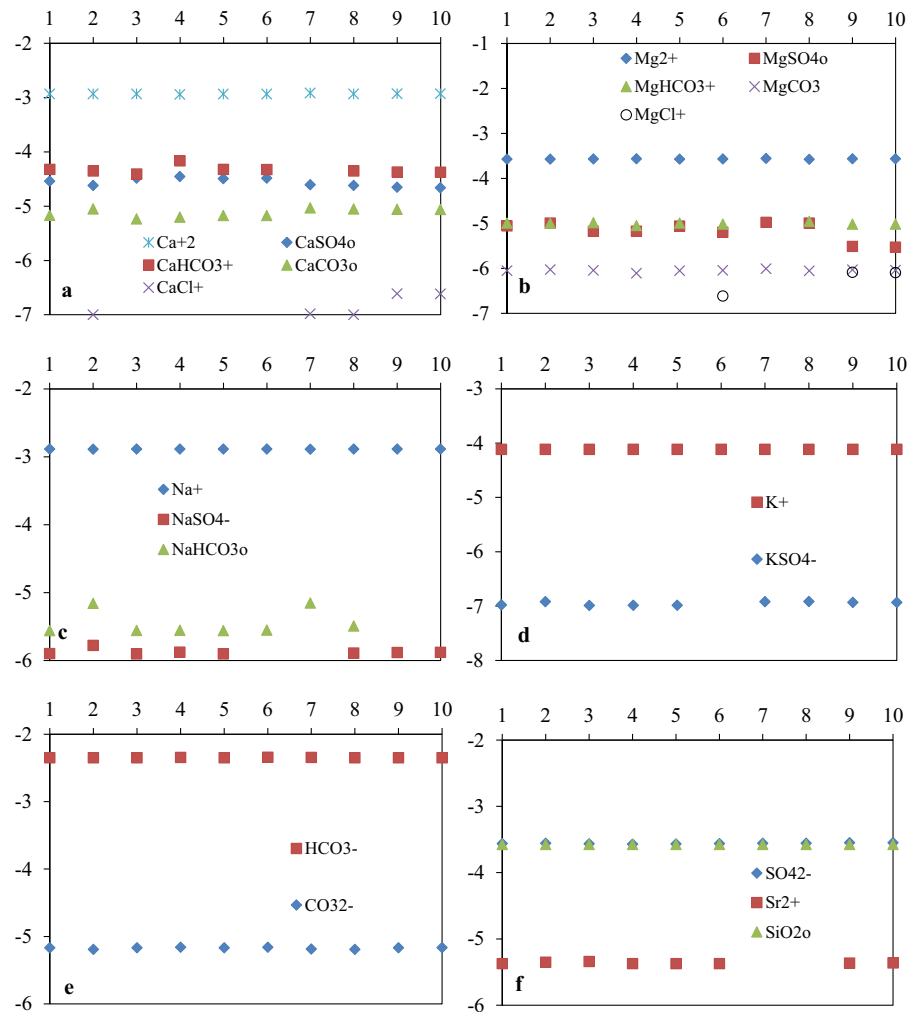


Fig. F1. Modeled concentrations (log molalities; Y-axis) of selected major species in the groundwater test case using different TDFs. (a) Ca-bearing species, (b) Mg-bearing species, (c) Na-bearing species, (d) K-bearing species, (e) C-bearing species, (f) SO_4^{2-} , Sr^{2+} , and SiO_2 . For X-axis: 1 = *phreeqc.dat*, 2 = *llnl.dat*, 3 = *minteq.dat*, 4 = *minteq.v4.dat*, 5 = *wateq4f.dat*, 6 = *sit.dat*, 7 = *core10.dat*, 8 = *carbfix.dat*, 9 = *geothermal.dat*, 10 = *diagenesis.dat*.

For Cr^{3+} , the differences range up to 7.5 log units for relevant TDFs (Fig. F2a). This arises because the dominant species in *core10.dat* and *carbfix.dat* is CrO_4^{2-} instead of Cr^{3+} . Values calculated from *sit.dat* differ from all other databases for Mn-bearing (Fig. F2b), Fe^{3+} -bearing (Fig. F2c), and U-bearing (Fig. F2m) species, and for Th(OH)_4° (not illustrated), varying by up to 1.2, 3, 2.5 and 1.3 log units, respectively. Values calculated from *sit.dat* and *minteq.v4.dat* also differ from all other TDFs for NiCl^- species by up to 1.5 log units, where NiCO_3° is included, but only where Ni^{2+} is dominant (Fig. F2d). Values calculated from *llnl.dat* differ from all other databases for Au^+ (~5 log unit), CdCl^+ , CdCl_2° , and Co^{2+} (up to 1 log unit), and AsO_4^{3-} and HAsO_4^{2-} (~40 log unit), due to the dominance of AsO_4^{3-} . Sb(OH)_3° and SeO_3^{2-} concentrations in *llnl.dat*, *geothermal.dat* and *diagenesis.dat* differ from *minteq.dat*, *minteq.v4.dat*, *wateq4f.dat* and *sit.dat* (Table F1) by up to 9 and 1 log unit, respectively.

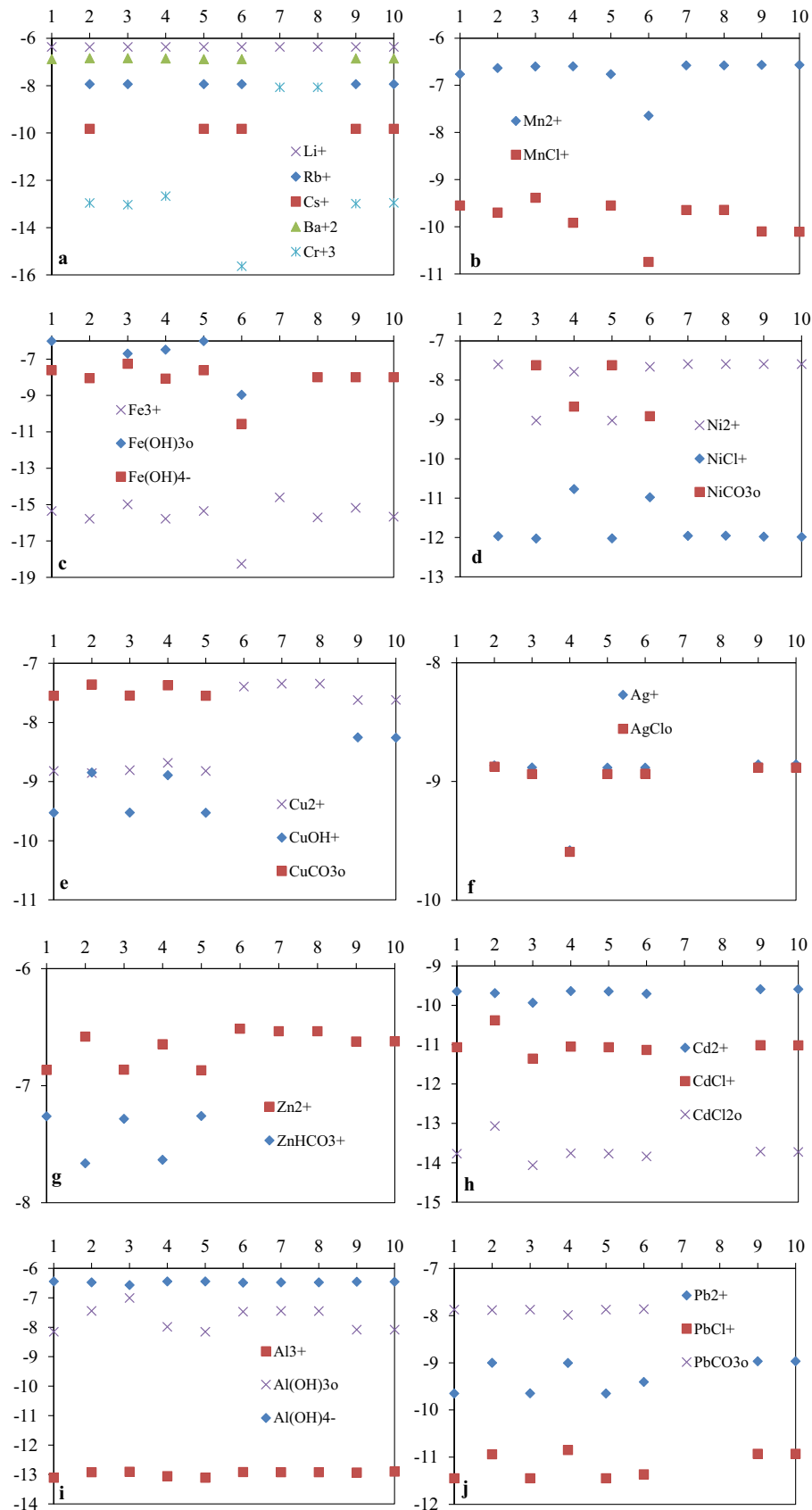


Fig. F2. Modeled concentrations (log molalities; Y-axis) of selected minor species in the groundwater test case using different TDFs. (a) Li⁺, Rb⁺, Cs⁺, Cr³⁺ and Ba²⁺, (b) Mn-bearing species, (c) Fe-bearing species, (d) Ni-bearing species, (e) Cu-bearing species, (f) Ag-bearing species, (g) Zn-bearing species, (h) Cd-bearing species, (i) Al-bearing species, (j) Pb-bearing species, (k) Se-bearing species, (l) La-bearing species, (m) U-bearing species, (n) V-bearing species, (o) P-bearing species, (p) B-

bearing species, (q) F-bearing species,. For X-axis: 1 = *phreeqc.dat*, 2 = *lnl.dat*, 3 = *minseq.dat*, 4 = *minseq.v4.dat*, 5 = *wateq4f.dat*, 6 = *sit.dat*, 7 = *core10.dat*, 8 = *carbfix.dat*, 9 = *geothermal.dat*, 10 = *diagenesis.dat*.

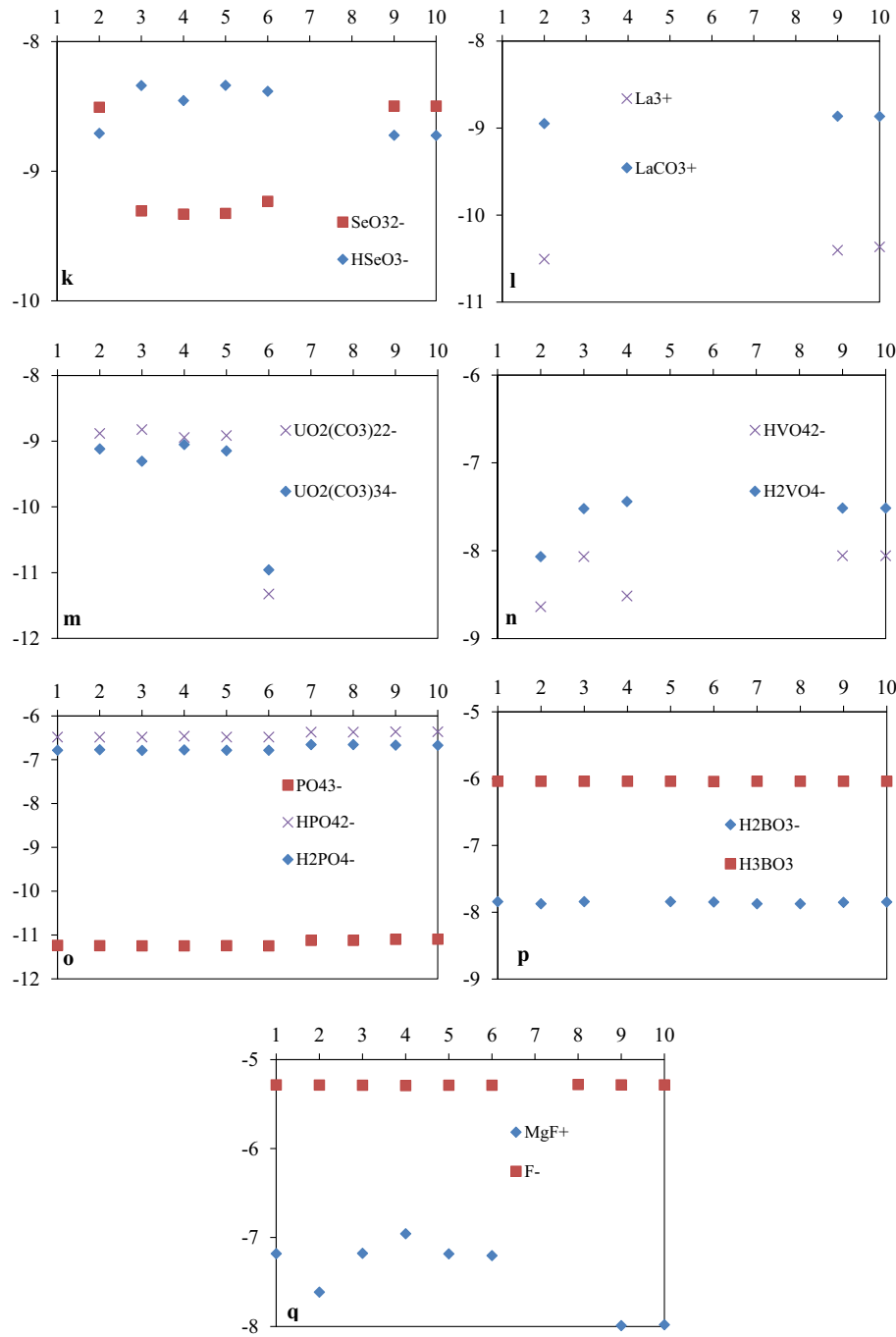


Fig. F2. (continued).

Table F1
Log concentrations (molalities) of selected major and minor species in the groundwater test case.

Major species	<i>phreeqc.dat</i>	<i>lnl.dat</i>	<i>minseq.dat</i>	<i>minseq.v4.dat</i>	<i>wateq4f.dat</i>	<i>sit.dat</i>	<i>core10.dat</i>	<i>carbfix.dat</i>	<i>geothermal.dat</i>	<i>diagenesis.dat</i>
Ca ²⁺	-2.934	-2.932	-2.932	-2.944	-2.935	-2.935	-2.916	-2.932	-2.930	-2.930
CaSO ₄ ⁰	-4.541	-4.620	-4.483	-4.454	-4.496	-4.486	-4.605	-4.619	-4.653	-4.662
CaHCO ₃ ⁺	-4.323	-4.352	-4.408	-4.168	-4.325	-4.326	-	-4.352	-4.373	-4.376
CaCO ₃ ⁰	-5.169	-5.051	-5.237	-5.202	-5.172	-5.173	-5.031	-5.051	-5.059	-5.062
CaCl ⁺	-	-6.999	-	-	-	-	-6.984	-6.999	-6.614	-6.618
Mg ²⁺	-3.572	-3.574	-3.569	-3.566	-3.571	-3.567	-3.558	-3.575	-3.563	-3.563
MgSO ₄ ⁰	-5.057	-4.994	-5.177	-5.176	-5.061	-5.198	-4.979	-4.994	-5.514	-5.527
MgHCO ₃ ⁺	-4.995	-4.996	-4.986	-5.048	-4.995	-5.018	-	-4.959	-5.015	-5.017

(continued on next page)

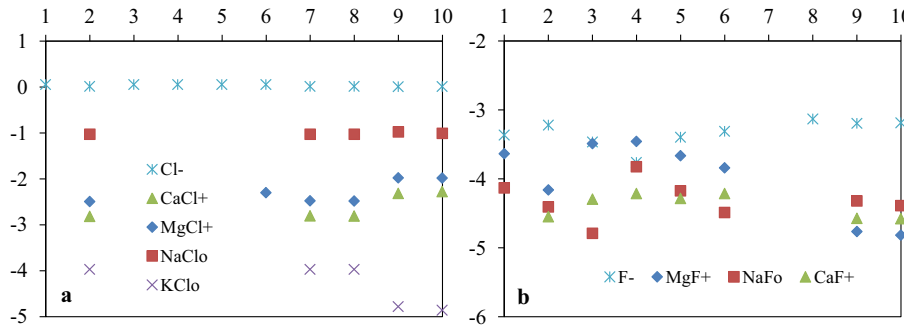
Table F1 (continued)

Major species	<i>phreeqc.dat</i>	<i>llnl.dat</i>	<i>miniteq.dat</i>	<i>miniteq.v4.dat</i>	<i>wateq4f.dat</i>	<i>sit.dat</i>	<i>core10.dat</i>	<i>carbfix.dat</i>	<i>geothermal.dat</i>	<i>diagenesis.dat</i>
MgCO ₃	-6.051	-6.027	-6.045	-6.105	-6.051	-6.045	-6.008	-6.057	-6.034	-6.041
MgCl ⁺	-	-7.068	-	-	-	-6.614	-7.054	-7.069	-6.088	-6.097
Na ⁺	-2.886	-2.887	-2.886	-2.886	-2.886	-2.885	-2.887	-2.886	-2.885	-2.885
NaSO ₄ ⁻	-5.897	-5.776	-5.903	-5.877	-5.902	-	-	-5.891	-5.882	-5.880
NaHCO ₃ ⁰	-5.559	-5.157	-5.558	-5.553	-5.559	-5.551	-5.152	-5.491	-	-
K ⁺	-4.115	-4.116	-4.115	-4.115	-4.115	-4.115	-4.116	-4.116	-4.115	-4.115
KSO ₄ ⁻	-6.981	-6.919	-6.988	-6.987	-6.986	-	-6.919	-6.918	-6.933	-6.934
SO ₄ ²⁻	-3.563	-3.558	-3.566	-3.570	-3.568	-3.563	-3.557	-3.558	-3.549	-3.548
Cl ⁻	-3.248	-3.249	-3.248	-3.248	-3.248	-3.249	-3.249	-3.249	-3.249	-3.249
HCO ₃ ⁻	-2.349	-2.350	-2.348	-2.344	-2.349	-2.342	-2.345	-2.350	-2.348	-2.348
CO ₃ ²⁻	-5.169	-5.192	-5.169	-5.159	-5.169	-5.160	-5.186	-5.192	-5.168	-5.164
H ₄ SiO ₄ ⁰ /SiO ₂ ⁰	-3.576	-3.576	-3.576	-3.576	-3.576	-3.576	-3.576	-3.576	-3.576	-3.576
H ⁺	-7.366	-7.367	-7.366	-7.363	-7.366	-7.363	-7.366	-7.400	-7.367	-7.366
OH ⁻	-6.557	-6.578	-6.560	-6.559	-6.562	-6.563	-6.578	-6.616	-6.559	-6.556
Ionic Strength	6.680e-3	6.686e-3	6.694e-3	6.665e-3	6.668e-3	6.717e-3	6.782e-3	6.679e-3	6.740e-3	6.744e-3
Minor species	<i>phreeqc.dat</i>	<i>llnl.dat</i>	<i>miniteq.dat</i>	<i>miniteq.v4.dat</i>	<i>wateq4f.dat</i>	<i>sit.dat</i>	<i>core10.dat</i>	<i>carbfix.dat</i>	<i>geothermal.dat</i>	<i>diagenesis.dat</i>
H ₃ BO ₃	-6.040	-6.040	-6.040	-6.041	-6.040	-6.043	-6.040	-6.040	-6.040	-6.040
H ₂ BO ₃ ⁻ /B(OH) ₄ ⁻	-7.842	-7.874	-7.842	7.837	-7.841	-7.846	-7.873	-7.873	-7.851	-7.847
Br ⁻	-6.601	-6.601	-6.601	-6.601	-6.601	-6.601	-	-	-6.601	-6.601
F ⁻	-5.284	-5.285	-5.287	-5.292	-5.287	-5.288	-	-5.279	-5.283	-5.283
MgF ⁺	-7.181	-7.614	-7.178	-6.958	-7.184	-7.204	-	-	-7.990	-7.981
Sr ²⁺	-5.373	-5.353	-5.340	-5.374	-5.373	-5.374	-	-	-5.365	-5.364
Li ⁺	-6.364	-6.365	-6.364	-6.364	-6.364	-6.364	-6.364	-6.364	-6.364	-6.364
Rb ⁺	-	-7.932	-7.932	-	-7.932	-7.932	-	-	-7.932	-7.932
Cs ⁺	-	-9.822	-	-	-9.822	-9.822	-	-	-9.822	-9.822
Ba ²⁺	-6.878	-6.837	-6.837	-6.850	-6.878	-6.879	-	-	-6.852	-6.851
Cr ³⁺	-	-12.957	-13.031	-12.668	-	-15.628	-8.070	-8.070	-12.983	-12.948
Mn ²⁺	-6.765	-6.634	-6.600	-6.599	-6.765	-7.647	-6.579	-6.579	-6.569	-6.569
MnCl ⁺	-9.548	-9.699	-9.387	-9.915	-9.548	-10.745	-9.645	-9.644	-10.099	-10.108
Fe ³⁺	-15.349	-15.779	-14.991	-15.783	-15.349	-18.263	-14.608	-15.706	-15.178	-15.670
Fe(OH) ₃ ⁰	-6.012	-5.882	-6.694	-6.481	-6.012	-8.959	-	-5.828	-5.827	-5.828
Fe(OH) ₄ ⁻	-7.615	-8.045	-7.257	-8.072	-7.615	-10.561	-	-7.994	-7.994	-7.992
Ni ²⁺	-	-7.601	-9.027	-7.786	-9.027	-7.662	-7.592	-7.592	-7.592	-7.592
NiCl ⁺	-	-11.967	-12.027	-10.772	-12.026	-10.979	-11.959	-11.958	-11.981	-11.988
NiCO ₃ ⁰	-	-	-7.622	-8.673	-7.622	-8.920	-	-	-	-
Cu ²⁺	-8.820	-8.854	-8.806	-8.684	-8.820	-7.394	-7.344	-7.344	-7.621	-7.618
CuOH ⁺	-9.526	-8.848	-9.525	-8.893	-9.526	-	-	-	-8.253	-8.257
CuCO ₃ ⁰	-7.548	-7.359	-7.547	-7.373	-7.548	-	-	-	-	-
Ag ⁺	-	-8.864	-8.882	-9.579	-8.883	-8.883	-	-	-8.856	-8.855
AgCl ⁰	-	-8.875	-8.937	-9.592	-8.937	-8.935	-	-	-8.883	-8.883
Au ⁺	-	-10.993	-	-	-	-	-	-	-15.601	-15.599
Zn ²⁺	-6.867	-6.581	-6.864	-6.646	-6.869	-6.514	-6.536	-6.536	-6.623	-6.622
ZnHCO ₃ ⁺	-7.262	-7.663	-7.284	-7.634	-7.260	-	-	-	-	-
Cd ²⁺	-9.647	-9.691	-9.937	-9.638	-9.646	-9.707	-	-	-9.590	-9.590
CdCl ⁺	-11.065	-10.382	-11.357	-11.052	-11.065	-11.134	-	-	-11.014	-11.019
CdCl ₂ ⁰	-13.770	-13.069	-14.062	-13.759	-13.770	-13.837	-	-	-13.716	-13.725
Co ²⁺	-	-9.678	-	-8.894	-	-8.901	-8.770	-8.770	-8.772	-8.772
Cs ⁺	-	-9.822	-	-	-9.822	-9.822	-	-	-9.822	-9.822
Hg ²⁺	-	-16.210	-23.634	-23.256	-	-22.647	-	-	-17.980	-17.975
Al ³⁺	-13.111	-12.924	-12.905	-13.057	-13.111	-12.919	-12.921	-12.924	-12.934	-12.901
Al(OH) ₃ ⁰	-8.155	-7.448	-7.008	-7.986	-8.155	-7.474	-7.447	-7.449	-8.081	-8.085
Al(OH) ₄ ⁻	-6.442	-6.476	-6.570	-6.446	-6.442	-6.487	-6.475	-6.477	-6.454	-6.454
Pb ²⁺	-9.649	-9.000	-9.648	-9.005	-9.649	-9.406	-	-	-8.969	-8.968
PbCl ⁺	-11.448	-10.938	-11.447	-10.849	-11.448	-11.363	-	-	-10.928	-10.930
PbCO ₃ ⁰	-7.874	-7.885	-7.873	-7.986	-7.874	-7.864	-	-	-	-
Sb(OH) ₃ ⁰	-	-7.784	-15.176	-16.648	-	-13.561	-	-	-7.784	-7.784
SeO ₃ ²⁻	-	-8.507	-9.307	-9.331	-9.325	-9.232	-	-	-8.498	-8.497
HSeO ₃ ⁻	-	-8.708	-8.340	-8.456	-8.338	-8.384	-	-	-8.723	-8.724
La ³⁺	-	-10.505	-	-	-	-	-	-	-10.404	-10.366
LaCO ₃ ⁺	-	-8.948	-	-	-	-	-	-	-8.864	-8.865
Sn(OH) ₄ ⁰	-	-9.074	-	-	-	-	-	-	-	-
Th(OH) ₄ ⁰	-	-9.369	-	-	-	-10.686	-9.365	-9.365	-	-
Ti(OH) ₄ ⁰	-	-7.203	-	-	-	-	-7.203	-7.203	-	-
UO ₂ (CO ₃) ₂ ²⁻	-	-8.882	-8.822	-8.942	-8.913	-11.326	-	-	-	-
UO ₂ (CO ₃) ₃ ⁴⁻	-	-9.117	-9.304	-9.051	-9.148	-10.958	-	-	-	-
HVO ₄ ²⁻	-	-8.640	-8.068	-8.516	-	-	-	-	-8.058	-8.058
H ₂ VO ₄ ⁻	-	-8.069	-7.521	-7.441	-	-	-	-	-7.515	-7.515
WO ₄ ²⁻	-	-9.787	-	-	-	-	-	-	-9.787	-9.787
PO ₄ ³⁻	-11.238	-11.245	-11.248	-11.249	-11.246	-11.249	-11.125	-11.126	-11.100	-11.097
HPO ₄ ²⁻	-6.484	-6.490	-6.485	-6.464	-6.484	-6.485	-6.371	-6.371	-6.364	-6.364
H ₂ PO ₄ ⁻	-6.787	-6.775	-6.789	-6.777	-6.787	-6.787	-6.657	-6.656	-6.670	-6.671
AsO ₄ ³⁻	-	-45.888	-11.652	-11.570	-11.796	-11.710	-	-	-11.992	-11.987
HAsO ₄ ²⁻	-	-41.886	-7.644	-7.678	-7.733	-7.696	-	-	-7.775	-7.772
AsO ₃ F ²⁻	-	-7.583	-	-	-	-	-	-	-	-
I ⁻	-	-7.258	-7.260	-7.259	-7.260	-7.261	-	-	-7.258	-7.258

Table F2

Saturation indices for selected minerals in the groundwater test case.

	Formula	phreeqc.dat	amm.dat	iso.dat	llnl.dat	minetq.dat	minetq.v4.dat	wateq4f.dat	sit.dat	core10.dat	carbfix.dat	geothermal.dat	diagenesis.dat
Calcite	CaCO ₃	0.09	0.09	0.08	0.11	0.09	0.08	0.08	0.09	0.13	0.11	0.06	0.06
Aragonite	CaCO ₃	-0.06	-0.06	-	-0.03	-0.05	-0.10	-0.06	-0.08	-0.01	-0.03	0.02	0.01
Dolomite	CaMg(CO ₃) ₂	-0.33	-0.33	-0.34	0.76	-0.41	-0.34	-0.33	-0.30	0.80	-0.68	-0.15	-0.16
Siderite	FeCO ₃	-1.06	-1.06	-1.06	-1.83	-1.03	-2.16	-1.06	-4.10	-0.66	-1.29	-1.22	-1.22
Magnesite	MgCO ₃	-	-	-	-0.97	-0.99	-1.56	-1.00	-0.11	-0.95	-0.97	-1.04	-1.05
Dawsonite	NaAlCO ₃ (OH) ₂	-	-	-	-0.68	-	-	-	-0.69	-0.67	-0.68	-1.31	-1.32
Rhodochrosite	MnCO ₃	-1.09	-1.09	-	-1.55	-1.65	-1.49	-1.09	-1.98	-1.49	-1.49	-1.52	-1.53
Witherite	BaCO ₃	-3.78	-3.78	-	1.04	-3.71	-3.74	-3.78	-3.78	-	-	-	-
Gypsum	CaSO ₄ •2H ₂ O	-2.21	-2.21	-2.21	-2.25	-2.18	-2.20	-2.22	-2.19	-2.24	-2.25	-2.22	-2.22
Anhydrite	CaSO ₄	-2.51	-2.51	-2.43	-2.43	-2.15	-2.45	-2.43	-2.36	-2.42	-2.43	-2.44	-2.45
Barite	BaSO ₄	-0.89	-0.89	-	-0.68	-0.72	-0.74	-0.77	-0.77	-	-	-	-
Hydroxyapatite	Ca ₅ (PO ₄) ₃ OH	-2.27	-2.27	-2.28	-2.48	1.49	1.51	-2.27	1.56	-2.05	-2.12	-0.19	-0.24
Fluorite	CaF ₂	-3.12	-3.12	-3.13	-3.65	-3.13	-3.25	-3.13	-3.13	-	-	-	-
Ferric Hydrix. (am)	Fe(OH) ₃	1.66	1.66	-	0.48	2.02	2.89	1.66	2.41	1.65	0.55	-	-
Goethite	FeO(OH)	7.55	7.55	7.55	5.59	6.41	5.59	7.55	3.21	6.76	5.66	6.08	6.08
Hematite	Fe ₂ O ₃	17.10	17.10	17.10	12.16	17.82	13.58	17.11	8.22	14.50	12.31	11.97	11.97
Gibbsite	Al(OH) ₃	0.68	0.68	0.68	1.23	0.22	0.51	0.68	1.21	1.23	1.23	1.23	1.23
Birnessite	MnO ₂	-	-	-	-68.82	-12.74	-12.61	-12.91	-	-	-	-	-
Chalcedony	SiO ₂	-0.02	-0.02	-0.02	0.18	-0.05	-0.03	-0.02	-	0.18	0.18	-	-
Quartz	SiO ₂	0.41	0.41	0.41	0.45	0.43	0.42	0.41	0.16	0.45	0.45	0.18	0.17
Albite	NaAlSi ₃ O ₈	-2.13	-2.13	-2.13	0.06	-0.76	-	-2.13	-0.04	0.07	0.07	-0.13	-0.14
K-Feldspar	KAlSi ₃ O ₈	-0.79	-0.79	-0.79	1.87	0.90	-	-0.79	1.42	1.87	1.87	1.67	1.67
Anorthite	CaAl ₂ (SiO ₄) ₂	-3.47	-3.47	-3.48	-3.96	-2.87	-	-3.47	-2.85	-3.94	-3.96	-1.83	-1.85
Kaolinite	Al ₂ Si ₂ O ₅ (OH) ₄	2.99	2.99	2.99	4.08	5.11	3.02	2.99	4.23	4.08	4.08	5.69	5.68
Muscovite	KAl ₃ Si ₃ O ₁₀ (OH) ₂	6.18	6.18	6.18	5.99	6.51	-	6.18	6.32	6.00	5.99	6.03	6.02
Illite	K _{0.6} Mg _{0.25} Al _{1.8} Al _{0.5} Si _{3.5} O ₁₀ (OH) ₂	0.55	0.55	0.55	3.97	-	-	0.55	3.97	-	-	-	-
Beidellite-Ca	Ca _{0.165} Al _{2.33} Si _{3.67} O ₁₀ (OH) ₂	-	-	-	4.28	-	-	1.27	4.07	6.01	6.00	3.22	3.21
Montmorillonite-Ca	Ca _{0.165} Mg _{0.33} Al _{1.67} Si ₄ O ₁₀ (OH) ₂	1.50	1.50	1.50	3.93	5.99	-	1.50	2.11	4.28	4.27	3.22	3.19
Nontronite-Ca	Ca _{0.165} Fe ₂ Al _{0.33} Si _{3.67} H ₂ O ₁₂	-	-	-	15.74	-	-	-	3.74	16.28	14.09	15.31	15.29
Sepiolite	Mg ₂ SiO _{7.5} (OH) • 3H ₂ O	-4.32	-4.32	-4.32	-7.32	-4.46	-4.32	-4.32	-	-7.26	-7.33	-	-
Rutile	TiO ₂	-	-	-	2.44	-	-	-	-	2.44	2.44	-	-
Uraninite	UO ₂	-	-	-	-9.45	-9.43	-9.51	-9.59	-11.58	-5.03	-5.03	-	-
Zincite	ZnO	-	-	-	-3.12	-3.35	-3.33	-3.35	-	-3.08	-3.08	-	-

Appendix G. Calculated concentrations of species and saturation indices of minerals for the organic-rich oil field brine test case**Fig. G1.** Modeled concentrations (log molal; Y-axis) of selected species in oil field brine test case using different TDFs. (a) Cl-bearing species, (b) F-bearing species. For X-axis: 1 = phreeqc.dat, 2 = llnl.dat, 3 = minetq.dat, 4 = minetq.v4.dat, 5 = wateq4f.dat, 6 = sit.dat, 7 = core10.dat, 8 = carbfix.dat, 9 = geothermal.dat, 10 = diagenesis.dat.

For Acetate⁻, concentrations computed from all databases containing this species are quite consistent, except that for minetq.v4.dat, which is 0.4–0.5 log units lower. For Na(Acetate)⁰, the concentration differences are small (within 0.2 log unit) between the only three TDFs containing this species (llnl.dat, minetq.dat and minetq.v4.dat). For Ca(Acetate)⁺, concentrations from llnl.dat and minetq.dat are similar, but from minetq.v4.dat it is 0.5–0.7 log units higher, and from sit.dat it is 0.4–0.6 log units lower. For Mg(Acetate)⁺, the concentrations from llnl.dat and minetq.dat are similar, but from minetq.v4.dat it is 0.3–0.5 log units higher.

For Butyrate⁻, the difference between minetq.dat and minetq.v4.dat is ~0.15 log unit. Concentrations for Ca(Butyrate)⁺ and Mg(Butyrate)⁺ from minetq.dat are ~1 log unit lower than those from minetq.v4.dat. Only two TDFs (minetq.dat and minetq.v4.dat) incorporate Propionate-bearing species, where the differences in saturated concentrations are small. However, for Ca(Propionate)⁺ and Mg(Propionate)⁺, saturated concentrations from minetq.dat are 1 log unit lower than that from minetq.v4.dat. Only minetq.dat and minetq.v4.dat include Valerate⁻ and saturation indices (SI) that are quite consistent. Only minetq.v4.dat includes Ca(Valerate)⁺.

Table G1

Log concentrations (molalities) of selected major and minor species in the oil field brine test case.

Major species	<i>phreeqc.dat</i>	<i>llnl.dat</i>	<i>minteq.dat</i>	<i>minteq.v4.dat</i>	<i>wateq4f.dat</i>	<i>sit.dat</i>	<i>core10.dat</i>	<i>carbfix.dat</i>	<i>geothermal.dat</i>	<i>diagenesis.dat</i>
Ca ²⁺	-1.535	-1.572	-1.555	-1.600	-1.535	-1.532	-1.561	-1.566	-1.629	-1.635
CaHCO ₃ ⁺	-3.260	-3.264	-2.846	-2.566	-3.287	-3.753	-	-3.346	-3.208	-3.173
CaCO ₃ ⁰	-3.478	-3.348	-3.361	-3.282	-3.507	-3.598	-3.291	-3.430	-3.262	-3.308
CaCl ⁺	-	-2.816	-	-	-	-	-2.805	-2.809	-2.315	-2.278
Mg ²⁺	-1.819	-1.920	-1.822	-1.844	-1.818	-1.975	-1.905	-1.911	-2.287	-2.281
MgHCO ₃ ⁺	-3.394	-3.462	-3.665	-3.429	-3.420	-3.920	-	-3.555	-3.771	-3.776
MgCO ₃	-4.226	-4.082	-4.243	-3.910	-4.252	-4.381	-4.020	-4.140	-4.327	-4.412
MgCl ⁺	-	-2.493	-	-	-	-2.302	-2.477	-2.483	-1.978	-1.980
Na ⁺	0.014	-0.028	0.014	0.014	0.014	0.014	0.027	-0.028	-0.032	-0.028
NaHCO ₃ ⁰	-3.123	-2.895	-2.923	-3.258	-3.053	-3.279	-2.849	-2.622	-	-
NaCl ⁰	-	-1.028	-	-	-	-	-1.028	-1.028	-0.978	-1.011
K ⁺	-2.409	-2.421	-2.409	-2.409	-2.661	-2.409	-2.421	-2.421	-2.410	-2.410
KSO ₄ ⁻	-6.350	-6.473	-6.411	-6.313	-6.559	-	-6.313	-6.512	-6.402	-6.530
KCl ⁰	-	-3.970	-	-	-	-	-3.970	-3.969	-4.781	-4.859
SO ₄ ²⁻	-4.160	-4.142	-4.069	-4.594	-4.162	-3.849	-3.982	-4.181	-4.121	-4.064
Cl ⁻	0.055	0.015	0.055	0.055	0.055	0.053	0.015	0.015	0.006	0.009
HCO ₃ ⁻	-2.303	-2.232	-2.409	-2.364	-2.330	-2.311	-2.186	-2.321	-2.153	-2.155
CO ₃ ²⁻	-4.207	-4.051	-4.310	-4.541	-4.235	-3.873	-4.005	-4.140	-3.976	-3.939
H ⁺	-7.457	-7.506	-7.457	-7.505	-7.457	-7.501	-7.506	-7.506	-7.538	-7.459
OH ⁻	-4.794	-4.861	-4.692	-4.692	-4.817	-4.771	-4.861	-4.861	-4.894	-4.816
Ionic Strength	1.187	1.082	1.186	1.179	1.186	1.181	1.079	1.077	1.052	1.060
Minor and organic species										
H ₃ BO ₃	-2.472	-2.489	-2.498	-2.558	-2.495	-2.504	-2.472	-2.472	-2.469	-2.476
H ₂ BO ₃ ⁻	-3.549	-3.575	-3.324	-3.416	-3.344	-3.503	-3.557	-3.557	-3.584	-3.512
Br ⁻	-2.607	-2.620	-2.607	-2.607	-2.607	-2.608	-	-	-2.621	-2.619
F ⁻	-3.367	-3.222	-3.465	-3.761	-3.398	-3.311	-	-3.133	-3.194	-3.187
MgF ⁺	-3.635	-4.160	-3.488	-3.457	-3.665	-3.840	-	-	-4.765	-4.817
NaF ⁰	-4.132	-4.408	-4.791	-3.824	-4.174	-4.488	-	-	-4.322	-4.388
CaF ⁺	-	-4.548	-4.294	-4.214	-4.285	-4.213	-	-	-4.574	-4.578
SiO ₂ ⁰	-2.563	-2.649	-2.574	-2.560	-2.563	-2.573	-2.649	-2.649	-2.682	-2.683
Sr ²⁺	-3.134	-3.169	-3.095	-3.169	-3.132	-3.231	-	-	-3.204	-3.234
SrHCO ₃ ⁺	-4.178	-	-	-4.257	-4.204	-4.641	-	-	-4.229	-4.126
Mn ²⁺	-5.562	-5.673	-5.506	-5.256	-5.555	-6.702	-5.657	-5.657	-5.459	-5.445
MnCl ⁺	-5.694	-5.482	-5.673	-7.441	-5.696	-6.622	-5.466	-5.466	-5.675	-5.697
Fe ²⁺	-7.785	-5.205	-4.742	-6.085	-7.785	-8.293	-3.696	-8.551	-8.634	-8.559
FeOH ⁺	-8.818	-7.637	-5.775	-8.694	-8.818	-9.474	-4.691	-9.545	-9.535	-9.459
Fe ³⁺	-15.232	-13.158	-12.166	-15.619	-15.232	-15.065	-11.649	-16.504	-16.553	-16.478
Fe(OH) ₃ ⁰	-3.752	-3.638	-4.425	-3.580	-3.752	-4.283	-	-3.652	-3.649	-3.655
Al ³⁺	-15.539	-15.584	-15.474	-15.935	-15.539	-15.127	-15.525	-15.722	-15.765	-15.703
Al(OH) ₄ ⁻	-4.404	-4.465	-4.403	-4.403	-4.404	-4.459	-4.406	-4.635	-4.694	-4.675
NH ₄ ⁺	-2.142	-2.177	-2.142	-2.178	-2.218	-2.075	-2.176	-2.176	-2.184	-2.166
S ²⁻	-7.965	-17.976	-8.271	-13.935	-8.323	-22.254	-	-	-	-
S ₅ ²⁻	-	-5.248	-	-4.713	-5.719	-5.248	-5.248	-5.248	-5.248	-5.248
HS ⁻	-4.564	-14.565	-4.870	-5.774	-4.922	-15.364	-14.565	-14.565	-14.591	-14.528
H ₂ S ⁰	-6.004	-15.830	-6.310	-7.542	-6.362	-16.788	-15.830	-15.830	-15.823	-15.838
I ⁻	-	-4.335	-4.327	-4.327	-4.327	-4.341	-	-	-4.336	-4.334
Ba ²⁺	-3.169	-3.209	-3.157	-3.204	-3.166	-3.169	-	-	-3.235	-3.228
BaHCO ₃ ⁺	-4.711	-	-	-4.330	-4.788	-4.752	-	-	-4.497	-4.528
BaCO ₃ ⁰	-5.974	-5.731	-	-5.376	-6.051	-5.823	-	-	-5.636	-5.749
Li ⁺	-3.560	-3.571	-3.560	-3.560	-3.560	-3.560	-3.570	-3.570	-3.571	-3.568
Acetate ⁻	-	-2.593	-2.571	-2.870	-	-2.406	-	-	-2.397	-2.397
Na(Acetate) ⁰	-	-2.973	-3.111	-2.913	-	-	-	-	-	-
Ca(Acetate) ⁺	-	-3.705	-3.521	-3.043	-	-4.100	-	-	-	-
Mg(Acetate) ⁺	-	-3.816	-3.615	-3.301	-	-	-	-	-	-
Butyrate ⁻	-	-	-3.876	-4.053	-	-	-	-	-	-
Ca(Butyrate) ⁺	-	-	-5.496	-4.484	-	-	-	-	-	-
Mg(Butyrate) ⁺	-	-	-5.660	-4.795	-	-	-	-	-	-
Propionate ⁻	-	-	-3.314	-3.505	-	-	-	-	-	-
Ca(Propionate) ⁺	-	-	-4.944	-3.946	-	-	-	-	-	-
Mg(Propionate) ⁺	-	-	-5.088	-4.125	-	-	-	-	-	-
Valerate ⁻	-	-	-3.932	-3.961	-	-	-	-	-	-
Ca(Valerate) ⁺	-	-	-	-5.118	-	-	-	-	-	-

Table G2

Saturation indices for selected minerals in the oil field brine test case.

	Formula	<i>phreeqc.dat</i>	<i>amm.dat</i>	<i>iso.dat</i>	<i>llnl.dat</i>	<i>minteq.dat</i>	<i>minteq.v4.dat</i>	<i>wateq4f.dat</i>	<i>sit.dat</i>	<i>core10.dat</i>	<i>carbfix.dat</i>	<i>geothermal.dat</i>	<i>diagenesis.dat</i>
Calcite	CaCO_3	1.71	1.71	1.76	1.79	1.80	1.79	1.68	1.55	1.85	1.71	1.90	1.86
Aragonite	CaCO_3	1.59	1.59	—	1.65	1.57	1.71	1.57	1.38	1.71	1.57	1.79	1.75
Dolomite	$\text{CaMg}(\text{CO}_3)_2$	3.44	3.44	3.54	4.76	3.18	4.08	3.39	3.26	4.88	3.96	3.88	3.75
Siderite	FeCO_3	−2.43	−2.43	−2.29	0.37	0.48	−2.81	−2.46	−3.01	1.93	−2.69	−2.50	−2.54
Magnesite	MgCO_3	—	—	—	1.61	1.25	−0.20	1.24	1.95	1.67	1.53	1.33	1.25
Dawsonite	$\text{NaAlCO}_3(\text{OH})_2$	—	—	—	0.90	—	—	—	0.83	1.00	0.67	0.52	0.47
Rhodochrosite	MnCO_3	−0.08	−0.08	—	−0.39	−0.78	−2.01	−0.10	−1.10	−0.33	−0.46	−0.10	−0.21
Witherite	BaCO_3	−0.21	−0.21	—	3.83	−0.62	−0.04	−0.29	−0.44	—	—	—	—
Gypsum	$\text{CaSO}_4 \cdot 2\text{H}_2\text{O}$	−2.60	−2.60	−2.56	−2.68	−2.70	−2.40	−2.60	−2.62	−2.51	−2.71	−2.63	−2.76
Anhydrite	CaSO_4	−2.35	−2.35	−2.33	−2.36	−2.20	−2.40	−2.37	−2.31	−2.18	−2.39	−2.29	−2.42
Barite	BaSO_4	0.45	0.45	—	0.43	0.15	0.83	0.42	0.34	—	—	—	—
Fluorite	CaF_2	0.74	0.74	0.76	0.73	0.62	0.60	0.68	0.73	—	—	—	—
Ferric Hydrix. (am)	Fe(OH)_3	1.34	1.34	1.37	4.90	4.40	5.00	1.34	3.04	6.41	1.55	—	—
Goethite	$\text{FeO}(\text{OH})$	8.82	8.82	8.86	9.43	10.39	7.38	8.82	6.80	10.94	6.09	6.46	6.45
Hematite	Fe_2O_3	19.87	19.87	19.95	20.11	26.00	17.38	19.87	15.44	23.13	13.42	13.07	13.06
Gibbsite	$\text{Al}(\text{OH})_3$	0.29	0.29	0.45	0.93	−0.30	0.15	0.29	0.82	0.99	0.79	0.73	0.71
Boehmite	AlOOH	—	—	—	1.36	0.49	0.46	0.42	1.24	1.42	1.22	1.17	1.16
Birnessite	MnO_2	—	—	—	−11.95	−14.31	−9.99	−11.56	—	—	—	—	—
Chalcedony	SiO_2	0.63	0.63	0.63	0.40	0.60	0.63	0.63	—	0.40	0.40	—	—
Quartz	SiO_2	0.92	0.92	0.92	0.63	0.91	1.01	0.92	0.65	0.63	0.63	0.52	0.51
Albite	$\text{NaAlSi}_3\text{O}_8$	3.21	3.21	3.36	4.36	4.86	—	3.20	5.11	4.41	4.22	4.49	4.46
K-Feldspar	KAlSi_3O_8	2.72	2.72	2.88	4.24	4.38	—	2.72	4.66	4.30	4.11	4.37	4.33
Anorthite	$\text{CaAl}_2(\text{SiO}_4)_2$	2.22	2.22	2.50	1.14	2.49	—	2.22	2.49	1.27	0.87	2.92	2.88
Kaolinite	$\text{Al}_2\text{Si}_2\text{O}_5(\text{OH})_4$	3.44	3.44	3.77	4.00	5.26	3.54	3.44	4.62	4.12	3.72	5.37	5.35
Muscovite	$\text{KAl}_3\text{Si}_3\text{O}_{10}(\text{OH})_2$	9.28	9.28	9.75	8.03	9.13	—	9.28	9.19	8.20	7.61	8.15	8.08
Illite	$\text{K}_{0.6}\text{Mg}_{0.25}\text{Al}_{1.8}\text{Al}_{0.5}\text{Si}_{3.5}\text{O}_{10}(\text{OH})_2$	3.97	3.97	4.33	6.50	—	—	3.97	6.95	—	—	—	—
Beidellite-Ca	$\text{Ca}_{16.5}\text{Al}_{12.33}\text{Si}_{3.67}\text{O}_{10}(\text{OH})_2$	—	—	—	5.45	—	—	—	6.34	7.03	6.56	4.72	4.67
Montmorillonite-Ca	$\text{Ca}_{16.5}\text{Mg}_{3.3}\text{Al}_{1.67}\text{Si}_4\text{O}_{10}(\text{OH})_2$	3.54	3.54	3.92	6.32	6.66	—	3.54	5.93	6.82	6.50	5.43	5.37
Nontronite-Ca	$\text{Ca}_{16.5}\text{Fe}_{2}\text{Al}_{3.33}\text{Si}_{3.67}\text{H}_2\text{O}_{12}$	—	—	—	24.26	28.68	—	—	12.82	26.08	16.30	16.99	16.97
Sepiolite	$\text{Mg}_2\text{SiO}_7(\text{OH}) \bullet 3\text{H}_2\text{O}$	3.68	3.68	3.64	8.96	5.47	5.85	3.68	—	9.03	9.00	—	—

Appendix H. Calculation results for the very high salinity water test case

The mean ion-activity coefficient of CaCl_2 as a function of CaCl_2 concentration using different TDFs is compared in Fig. H1. Those calculated using *pitzer.dat* and *coldchem.dat* match the experimental data very well. Values calculated using *frezchem.dat* begin to deviate from the experimental data and underpredict the activity coefficients when the CaCl_2 concentrations are higher than 1.2 M. For those using ion association models, i.e., *phreeqc.dat*, *wateq4f.dat* and *sit.dat*, values deviate from the experiment at a CaCl_2 concentration > 1 M, but fit better than when using the remaining TDFs illustrated in the figure.

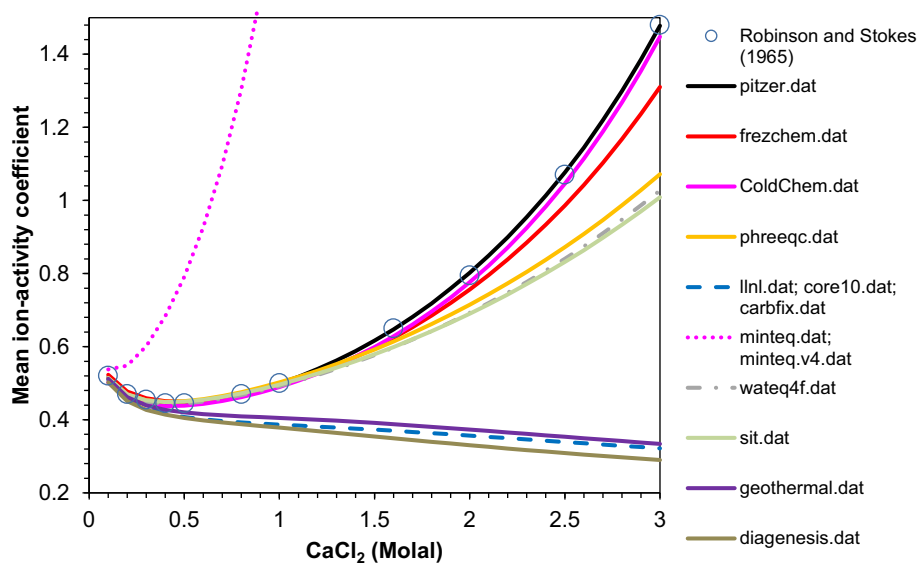


Fig. H1. The mean ion-activity coefficient of CaCl_2 at 25 °C and 1 bar as a function of CaCl_2 concentration derived using different PHREEQC TDFs. The experimental data are from Robinson and Stokes (1965).

For the mean ion-activity coefficient of MgSO_4 , values calculated using *pitzer.dat*, *frezchem.dat* and *coldchem.dat* match experimental data best (Fig. H2). All other TDFs overpredict the mean ion-activity coefficient of MgSO_4 when the MgSO_4 concentration is ~ 1.5 M.

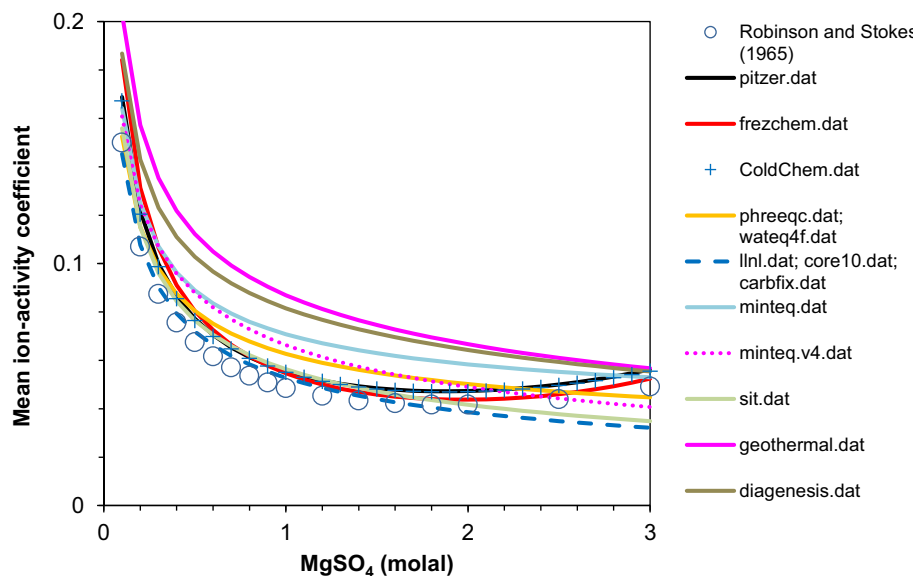


Fig. H2. The mean-ion activity coefficient of MgSO_4 at 25°C and 1 bar as a function of MgSO_4 concentrations calculated using different PHREEQC TDFs. The experimental data are from [Robinson and Stokes \(1965\)](#).

For the calculation of Na_2SO_4 mean-ion activity coefficient, the performances of all TDFs using Pitzer equations (*frezchem.dat*, *ColdChem.dat* and *pitzer.dat*) agree remarkably well (Fig. H3). *sit.dat* slightly overpredicts the activity coefficient when the Na_2SO_4 concentrations <1.6 and under-predicts it when Na_2SO_4 concentrations >1.6 . All other TDFs using ion association models generally overpredict the activity coefficients of Na_2SO_4 and the deviations become larger with the increasing Na_2SO_4 concentrations. The applicable salinity ranges for TDFs in NaCl , CaCl_2 , MgSO_4 , and Na_2SO_4 solution are listed in Table 3.

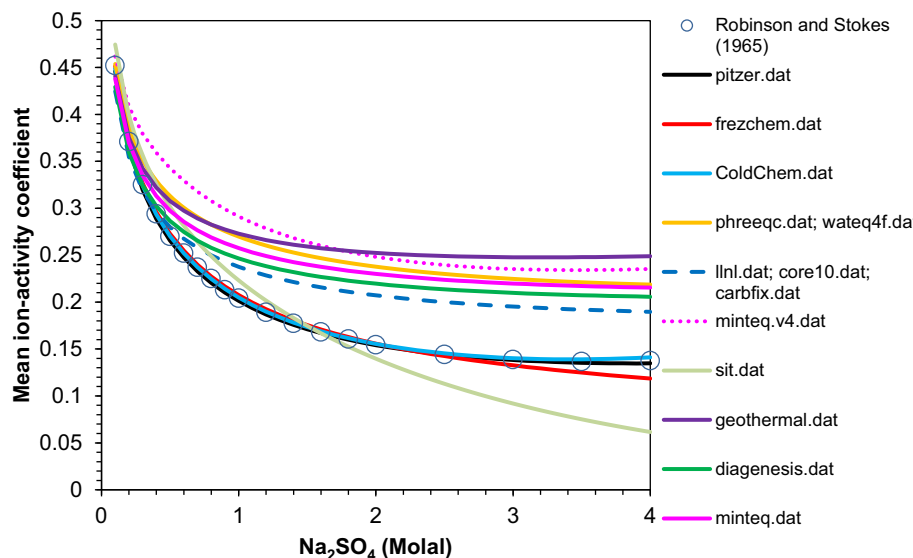


Fig. H3. The mean-ion activity coefficient of Na_2SO_4 at 25°C and 1 bar as a function of Na_2SO_4 concentrations calculated using different PHREEQC TDFs. The experimental data are from [Robinson and Stokes \(1965\)](#).

Appendix I. Calculated concentrations of species and saturation indices of minerals for the stream flow contaminated with hazardous metals test case

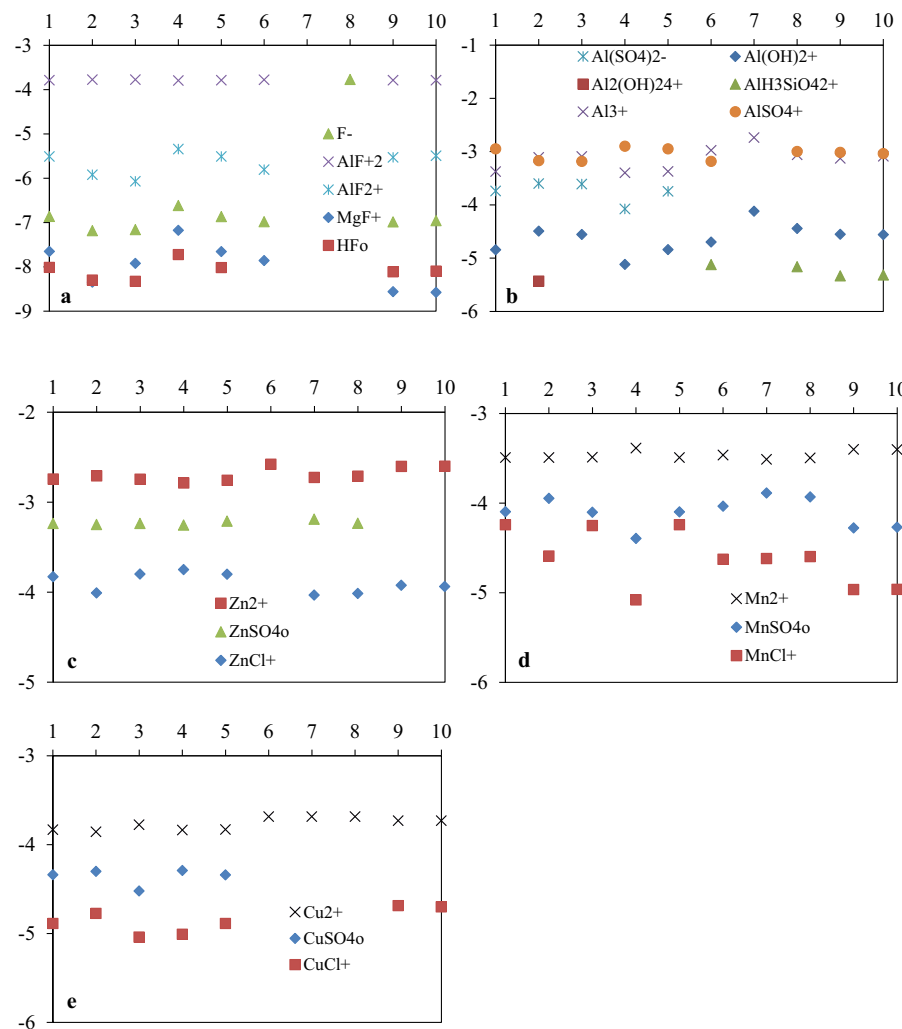


Fig. I1. Modeled concentrations (log molalities; Y-axis) of selected species in the stream flow contaminated with hazardous metals test case using different data files. (a) F-bearing species, (b) Al-bearing species, (c) Zn-bearing species, (d) Mn-bearing species, (e) Cu-bearing species. For X-axis: 1 = *phreeqc.dat*, 2 = *llnl.dat*, 3 = *minseq.dat*, 4 = *minseq.v4.dat*, 5 = *wateq4f.dat*, 6 = *sit.dat*, 7 = *core10.dat*, 8 = *carbfix.dat*, 9 = *geothermal.dat*, 10 = *diagenesis.dat*.

Table II

Log concentrations (molalities) of selected major and minor species in stream flow contaminated with hazardous metals test case.

Major species	<i>phreeqc.dat</i>	<i>llnl.dat</i>	<i>minseq.dat</i>	<i>minseq.v4.dat</i>	<i>wateq4f.dat</i>	<i>sit.dat</i>	<i>core10.dat</i>	<i>carbfix.dat</i>	<i>geothermal.dat</i>	<i>diagenesis.dat</i>
Ca ²⁺	-1.922	-1.908	-1.935	-1.951	-1.931	-1.946	-1.922	-1.911	-1.917	-1.907
CaSO ₄ ⁰	-2.497	-2.575	-2.451	-2.401	-2.465	-2.415	-2.511	-2.559	-2.553	-2.602
CaCl ⁺	-	-3.946	-	-	-	-	-3.967	-3.951	-3.596	-3.594
Mg ²⁺	-2.074	-2.111	-2.058	-2.058	-2.073	-2.088	-2.135	-2.117	-2.137	-2.117
MgSO ₄ ⁰	-2.551	-2.496	-2.604	-2.602	-2.554	-2.636	-2.440	-2.483	-2.948	-3.024
MgCl ⁺	-	-3.503	-	-	-	-3.113	-3.532	-3.510	-2.548	-2.575
Na ⁺	-0.876	-0.883	-0.875	-0.877	-0.876	-0.865	-0.870	-0.880	-0.881	-0.881
NaSO ₄ ⁻	-2.470	-2.381	-2.511	-2.418	-2.477	-	-	-2.490	-2.440	-2.459
NaCl ⁰	-	-2.806	-	-	-	-	-2.797	-2.804	-2.823	-2.821
K ⁺	-2.521	-2.524	-2.520	-2.523	-2.521	-2.508	-2.527	-2.525	-2.525	-2.523
KSO ₄ ⁻	-4.025	-3.963	-4.071	-3.956	-4.029	-	-3.882	-3.944	-3.912	-3.954
SO ₄ ²⁻	-1.729	-1.733	-1.714	-1.756	-1.734	-1.627	-1.640	-1.712	-1.661	-1.647
Cl ⁻	-0.846	-0.852	-0.846	-0.846	-0.846	-0.848	-0.852	-0.852	-0.860	-0.852
Br ⁻	-4.084	-4.086	-4.084	-4.085	-4.084	-4.085	-	-	-4.086	-4.085
F ⁻	-6.860	-7.182	-7.158	-6.614	-6.864	-6.979	-	-3.768	-6.985	-6.956
AlF ₂ ⁺	-3.785	-3.775	-3.773	-3.793	-3.785	-3.777	-	-	-3.784	-3.785
AlF ₂ ⁺	-5.507	-5.922	-6.067	-5.340	-5.510	-5.805	-	-	-5.528	-5.491
MgF ⁺	-7.653	-8.347	-7.920	-7.173	-7.655	-7.859	-	-	-8.559	-8.577
HF ⁰	-8.013	-8.298	-8.325	-7.724	-8.016	-	-	-	-8.110	-8.097
H ₄ SiO ₄ ⁰ /SiO ₂ ⁰	-3.229	-3.229	-3.229	-3.229	-3.229	-3.232	-3.229	-3.234	-3.233	-3.233
H ⁺	-4.000	-4.009	-4.000	-3.972	-4.000	-3.975	-4.008	-4.009	-4.012	-3.999
OH ⁻	-9.964	-9.990	-9.962	-9.963	-9.968	-9.983	-9.988	-9.989	-9.977	-9.961

(continued on next page)

Table I1 (continued)

Major species	<i>phreeqc.dat</i>	<i>llnl.dat</i>	<i>minteq.dat</i>	<i>minteq.v4.dat</i>	<i>wateq4f.dat</i>	<i>sit.dat</i>	<i>core10.dat</i>	<i>carbfix.dat</i>	<i>geothermal.dat</i>	<i>diagenesis.dat</i>
Ionic Strength	0.2271	0.2262	0.2300	0.2239	0.2262	0.2394	0.2373	0.2279	0.2327	0.2356
Minor species	<i>phreeqc.dat</i>	<i>llnl.dat</i>	<i>minteq.dat</i>	<i>minteq.v4.dat</i>	<i>wateq4f.dat</i>	<i>sit.dat</i>	<i>core10.dat</i>	<i>carbfix.dat</i>	<i>geothermal.dat</i>	<i>diagenesis.dat</i>
Mn ²⁺	-3.493	-3.492	-3.489	-3.386	-3.492	-3.465	-3.512	-3.497	-3.401	-3.402
MnSO ₄ ⁰	-4.096	-3.947	-4.103	-4.394	-4.099	-4.034	-3.888	-3.932	-4.278	-4.269
MnCl ⁺	-4.241	-4.592	-4.251	-5.081	-4.242	-4.628	-4.619	-4.598	-4.965	-4.964
Fe ²⁺	-4.882	-4.872	-4.854	-4.823	-4.882	-4.876	-4.777	-4.778	-4.778	-4.777
FeSO ₄ ⁰	-5.483	-5.479	-5.496	-5.688	-5.486	-5.511	-	-	-	-
FeCl ⁺	-6.106	-6.379	-	-	-6.101	-6.145	-6.290	-6.285	-6.299	-6.315
Fe ³⁺	-9.294	-9.214	-9.283	-9.460	-9.294	-8.971	-9.116	-9.119	-9.110	-8.870
Fe(OH) ₂ ⁺	-7.818	-7.443	-7.529	-6.883	-7.817	-7.864	-	-7.646	-7.637	-7.671
Fe(OH) ²⁺	-7.916	-7.642	-7.905	-8.328	-7.916	-7.972	-7.846	-7.848	-7.721	-7.790
Al ³⁺	-3.374	-3.109	-3.090	-3.400	-3.371	-2.974	-2.736	-3.061	-3.126	-3.089
AlSO ₄ ⁺	-2.948	-3.171	-3.183	-2.900	-2.949	-3.183	-	-2.999	-3.015	-3.038
Al(SO ₄) ₂ ⁻	-3.740	-3.599	-3.612	-4.076	-3.745	-	-	-	-	-
Al(OH) ²⁺	-4.843	-4.492	-4.555	-5.119	-4.840	-4.699	-4.119	-4.444	-4.554	-4.558
Al ₂ (OH) ₂ ⁴⁺	-	-5.434	-	-	-	-	-	-	-	-
AlH ₃ SiO ₄ ²⁺	-	-	-	-	-	-5.123	-	-5.160	-5.334	-5.316
Cu ²⁺	-3.832	-3.855	-3.777	-3.837	-3.831	-3.684	-3.684	-3.684	-3.731	-3.730
CuSO ₄ ⁰	-4.339	-4.302	-4.522	-4.292	-4.342	-	-	-	-	-
CuCl ⁺	-4.887	-4.775	-5.041	-5.009	-4.888	-	-	-	-4.687	-4.701
Ag ⁺	-	-11.532	-11.506	-11.969	-11.527	-11.657	-	-	-11.519	-11.511
AgCl ₂ ⁻	-	-8.141	-8.186	-8.494	-8.189	-8.234	-	-	-8.141	-8.132
AgCl ⁰	-	-9.332	-9.351	-9.715	-9.362	-9.440	-	-	-9.326	-9.354
Zn ²⁺	-2.744	-2.708	-2.745	-2.788	-2.757	-2.580	-2.726	-2.712	-2.602	-2.601
ZnSO ₄ ⁰	-3.237	-3.249	-3.236	-3.254	-3.210	-	-3.189	-3.235	-	-
ZnCl ⁺	-3.829	-4.009	-3.799	-3.749	-3.800	-	-4.033	-4.014	-3.923	-3.937
Cd ²⁺	-6.027	-6.637	-6.012	-6.133	-6.025	-6.043	-	-	-6.013	-6.040
CdCl ⁺	-5.438	-5.341	-5.435	-5.405	-5.438	-5.456	-	-	-5.415	-5.412
CdCl ₂ ⁰	-5.976	-5.860	-5.984	-6.006	-5.977	-5.909	-	-	-5.897	-5.891
Pb ²⁺	-8.259	-8.077	-8.242	-8.357	-8.257	-8.259	-	-	-8.067	-8.062
PbCl ⁺	-8.112	-8.061	-8.106	-8.089	-8.112	-8.234	-	-	-8.067	-8.068
PbCl ₂ ⁰	-9.005	-8.642	-9.011	-8.664	-9.007	-8.812	-	-	-8.653	-8.671

Table I2

Saturation indices for selected minerals in stream flow contaminated with hazardous metals test case.

	Formula	<i>phreeqc.dat</i>	<i>amm.dat</i>	<i>iso.dat</i>	<i>llnl.dat</i>	<i>minteq.dat</i>	<i>minteq.v4.dat</i>	<i>wateq4f.dat</i>	<i>sit.dat</i>	<i>core10.dat</i>	<i>carbfix.dat</i>	<i>geothermal.dat</i>	<i>diagenesis.dat</i>
Gypsum	CaSO ₄ •2H ₂ O	-0.12	-0.12	-0.12	-0.20	-0.10	-0.12	-0.14	-0.11	-0.13	-0.18	-0.10	-0.15
Fluorite	CaF ₂	-5.78	-5.78	-5.77	-6.94	-6.35	-5.42	-5.79	-6.06	-	-	-	-
Ferric Hydrix. (am)	Fe(OH) ₃	-2.79	-2.79	-2.80	-3.78	-2.78	-1.80	-2.79	-0.50	-3.70	-3.69	-	-
Goethite	FeO(OH)	2.86	2.86	2.86	1.42	1.37	0.95	2.87	1.41	1.50	1.51	1.95	1.94
Hematite	Fe ₂ O ₃	7.71	7.71	7.69	3.80	7.73	4.28	7.71	4.63	3.97	3.98	3.66	3.63
Gibbsite	Al(OH) ₃	-0.46	-0.46	-0.47	0.15	-0.84	-0.92	-0.46	-0.06	0.51	0.19	0.15	0.16
Chalcedony	SiO ₂	0.43	0.43	0.43	0.66	0.40	0.42	0.43	-	0.66	0.65	-	-
Quartz	SiO ₂	0.88	0.88	0.88	0.93	0.91	0.89	0.88	0.60	0.93	0.93	0.79	0.78
Albite	NaAlSi ₃ O ₈	-3.42	-3.42	-3.43	-1.16	-2.04	-	-3.42	-1.56	-0.79	-1.13	-0.95	-0.94
Alunite	KAl ₃ (OH) ₆ (SO ₄) ₂	5.11	5.11	5.13	4.82	6.70	4.32	5.12	-	6.08	5.00	-	-
Beidellite-Ca	Ca _{1.65} Al _{2.33} Si _{3.67} O ₁₀ (OH)2	-	-	-	2.37	-	-	-0.41	1.50	4.90	4.14	1.78	1.80
Illite	K _{0.6} Mg _{0.25} Al _{1.8} Al _{0.5} Si _{3.5} O ₁₀ (OH)2	-3.05	-3.05	-3.07	0.51	-	-	-3.04	-1.23	-	-	-	-
K-Feldspar	KAlSi ₃ O ₈	-2.44	-2.44	-2.45	0.33	-0.70	-	-2.43	-0.41	0.69	0.36	0.54	0.54
Kaolinite	Al ₂ Si ₂ O ₅ (OH)4	1.63	1.63	1.61	2.82	3.90	1.06	1.63	2.55	3.55	2.90	4.73	4.75
Montmorillonite-Ca	Ca _{1.65} Mg _{0.33} Al _{1.67} Si ₄ O ₁₀ (OH)2	-0.55	-0.55	-	1.04	2.56	-	-0.54	-1.43	1.80	1.27	0.29	0.27
Muscovite	KAl ₃ Si ₃ O ₁₀ (OH)2	2.21	2.21	2.19	2.23	2.77	-	2.23	1.91	3.32	2.35	2.66	2.70
Nontronite-Ca	Ca _{1.65} Fe ₂ Al ₃ Si ₃ O ₁₀ (OH)2	-	-	-	7.82	10.74	-	-	0.25	6.11	5.99	7.43	7.39
Sepiolite	Mg ₂ Si _{7.5} O _{17.5} (OH)•3H ₂ O	-14.25	-14.25	-14.26	-27.54	-14.56	-14.57	-14.24	-	-27.65	-27.59	-	-
Manganite	MnO(OH)	-8.67	-8.67	-	-8.95	-8.18	-9.02	-8.67	-9.17	-	-	-	-
MnCl ₂ •4H ₂ O	MnCl ₂ •4H ₂ O	-	-	-	-8.80	-8.44	-9.06	-8.42	-8.70	-8.83	-8.81	-	-
MnSO ₄	MnSO ₄	-	-	-	-9.16	-9.23	-9.45	-9.19	-3.55	-9.10	-9.15	-	-
Rhodonite	MnSiO ₃	-	-	-	-8.95	-	-	-	-	-8.98	-8.96	-9.05	-9.06
Delafosseite	CuFeO ₂	-	-	-	-2.58	-	-	5.06	-	2.84	2.84	-	-
Tenorite	CuO	-	-	-	-4.05	-4.14	-4.05	-4.00	-	-3.88	-3.88	-3.85	-3.87
Chalcanthite	CuSO ₄ •5H ₂ O	-	-	-	-4.02	-4.14	-3.97	-3.96	-	-3.77	-3.83	-	-
Ferrite-Cu	CuFe ₂ O ₄	-	-	-	-2.88	1.44	0.40	1.56	-	-2.54	-2.52	-	-
Cd(OH)Cl	Cd(OH)Cl	-	-	-	-7.73	-7.08	-7.18	-7.08	-	-	-	-	-
CdCl ₂ •H ₂ O	CdCl ₂ •H ₂ O	-	-	-	-7.53	-6.86	-6.93	-6.86	-6.90	-	-	-	-
Ferrite-Zn	ZnFe ₂ O ₄	-	-	-	-3.21	-	-	-	-	-3.06	-3.03	-	-
Bianchite	ZnSO ₄ •6H ₂ O	-	-	-	-3.83	-	-	-3.79	-	-	-	-	-
Goslarite	ZnSO ₄ •7H ₂ O	-	-	-	-3.60	-3.56	-3.52	-3.54	-	-	-	-	-

(continued on next page)

Table I2 (continued)

	Formula	<i>phreeqc.dat</i>	<i>amm.dat</i>	<i>iso.dat</i>	<i>llnl.dat</i>	<i>minteq.dat</i>	<i>minteq.v4.dat</i>	<i>wateq4f.dat</i>	<i>sit.dat</i>	<i>core10.dat</i>	<i>carbfix.dat</i>	<i>geothermal.dat</i>	<i>diagenesis.dat</i>
Zincite	ZnO	–	–	–	–6.55	–6.54	–6.79	–6.55	–	–6.57	–6.55	–	–
Anglesite	PbSO ₄	–3.23	–3.23	–	–3.00	–3.25	–3.30	–3.23	–3.14	–	–	–	–
Chlorargyrite	AgCl	–	–	–	–2.68	–	–3.07	–2.65	–2.77	–	–	–	–

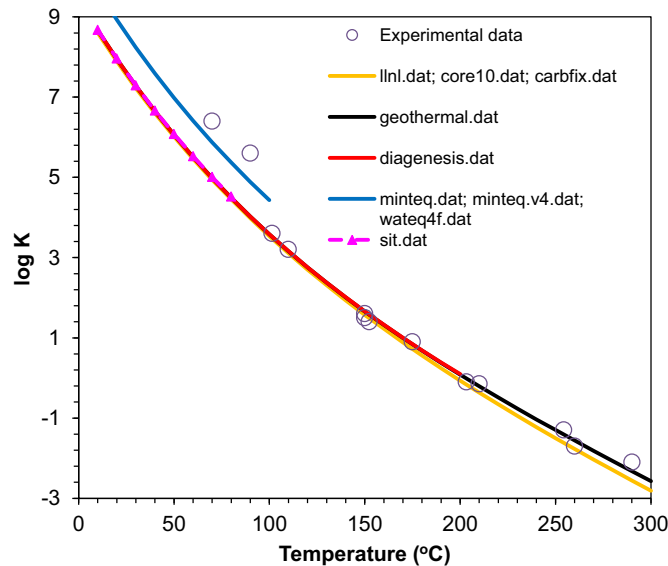
Appendix J. Selected results of mineral solubility or solubility product constants calculations

Fig. J1. Boehmite solubility product constants as a function of temperature in acidic solutions. Symbols represent experimental data for comparison. The experimental data are from Verdes et al. (1992), Castet et al. (1993), Bourcier et al. (1993) and Bénédith et al. (2001).

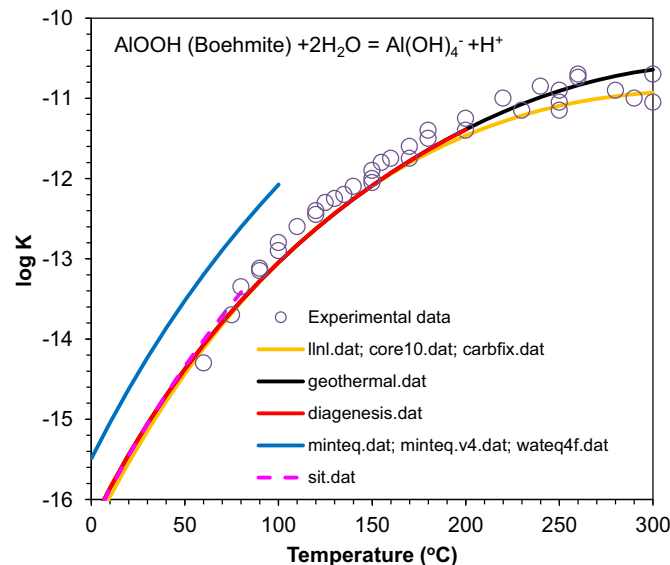


Fig. J2. Boehmite solubility product constants as a function of temperature in basic solutions. Circular symbols represent experimental data for comparison. The experimental data are taken from Russell et al. (1955), Kuyunko et al. (1983), Apps et al. (1989), Verdes et al. (1992), Bourcier et al. (1993), Castet et al. (1993) and Bénédith et al. (2001).

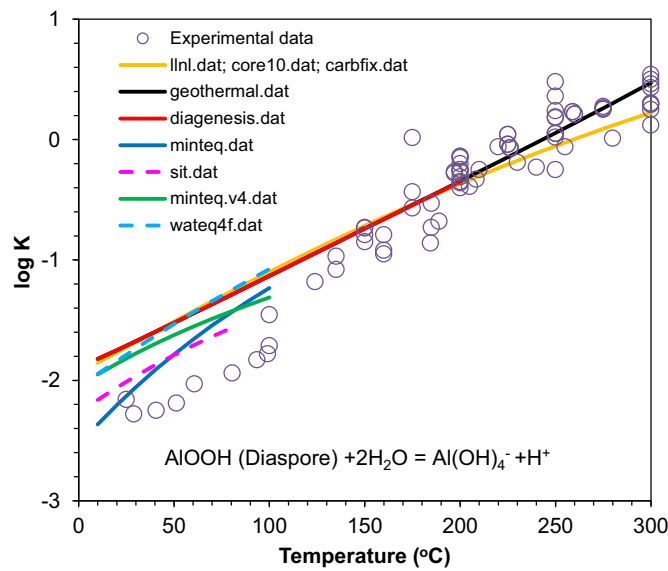


Fig. J3. Diasporite solubility product constants as a function of temperature. The experimental data were compiled by Apps et al. (1989) and Verdes et al. (1992).

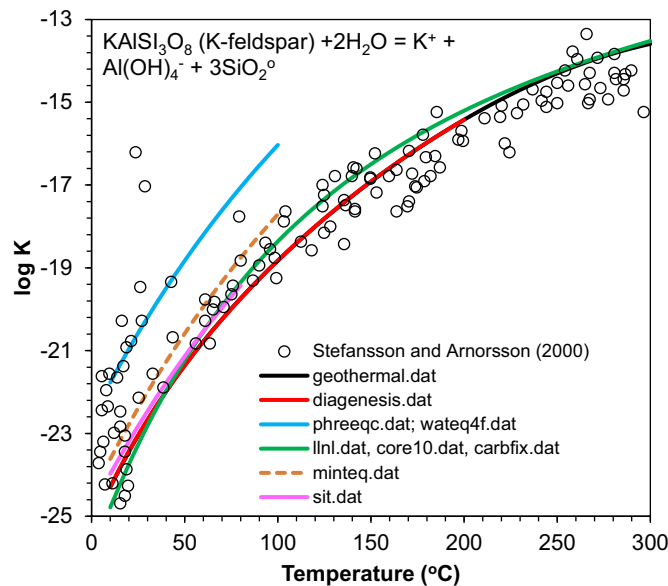


Fig. J4. K-feldspar (microcline) solubility product constants as a function of temperature. Symbols are the saturation state of the natural waters with respect to K-feldspar collected and calculated by Stefánsson and Arnórsson (2000).

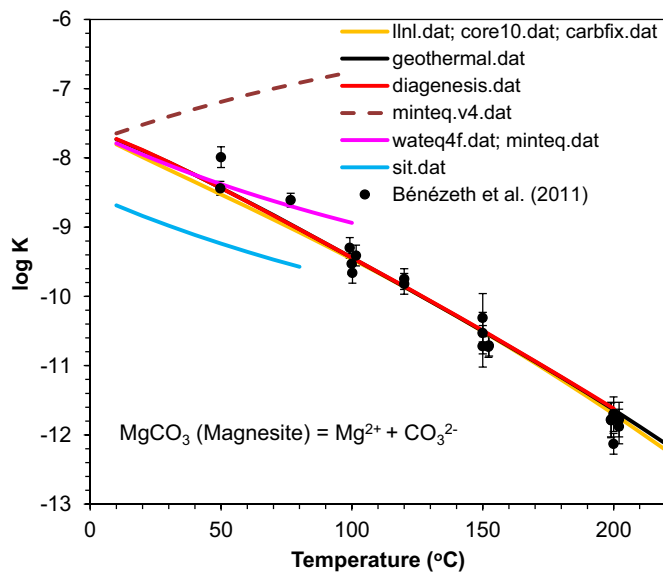


Fig. J5. Magnesite solubility product constants as a function of temperature. The experimental data are from Bénédeth et al. (2011). The errors of Bénédeth et al. (2011) are ± 0.1 and ± 0.15 at 50°C , ± 0.1 at 75°C , ± 0.15 at 100°C and 120°C , ± 0.2 – 0.35 at 150°C , and ± 0.15 – 0.25 at 200°C . The models represent a system closed to atmosphere without the presence of CO_2 gas phase. Bénédeth et al. (2011)'s experiments were at 4–30 bars $p\text{CO}_2$.

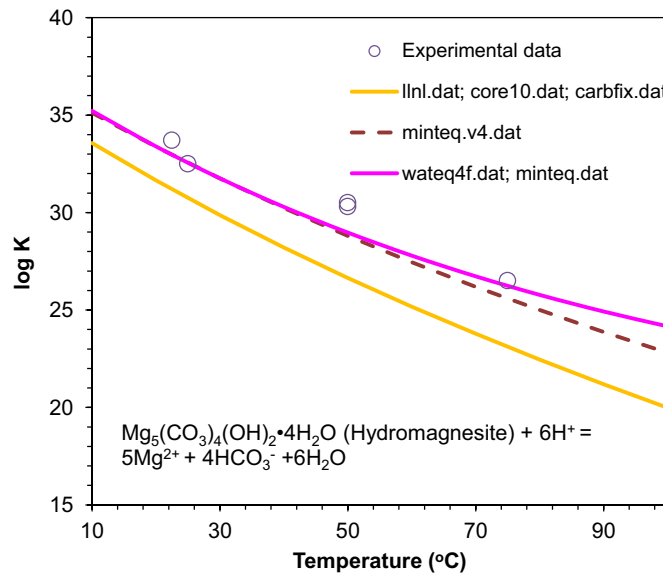


Fig. J6. Hydromagnesite solubility product constants as a function of temperature. The experimental data are from Berninger et al. (2014).

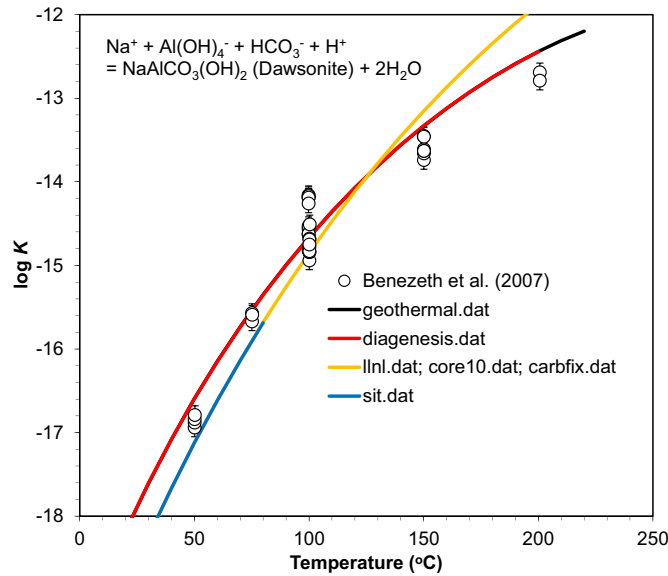


Fig. J7. Dawsonite solubility product constants as a function of temperature. The experimental data are from Bénédeth et al. (2007). The errors of Bénédeth et al. (2007) are ± 0.11 . The models represent a system closed to atmosphere without the presence of CO_2 gas phase. Bénédeth et al. (2007)'s experiments were at 10 bars $p\text{CO}_2$.

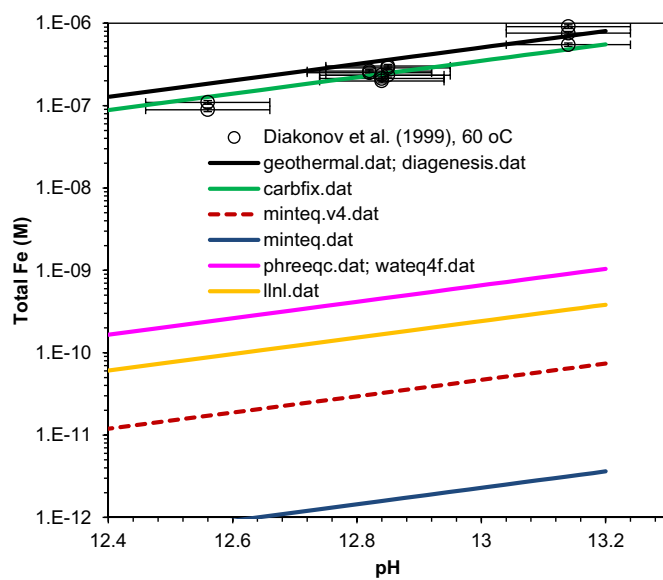


Fig. J11. Calculated total Fe (Molal) concentration at 60 °C in equilibrium with hematite using different data files. The experimental data are from Diakonov et al. (1999) in $\text{NaOH}-\text{NaCl}$ solutions (0.007–0.2 m NaOH). The experimental error is $\pm 1\%$ for total Fe.

Appendix K. Thermodynamic properties of minerals and relevant aqueous species

Table K1

Thermodynamic properties of minerals and relevant aqueous species.

		geothermal.dat / diagenesis.dat	llnl.dat/core10.dat	carbfix.dat	sit.dat	wateq4f.dat / phreeqc.dat
Brucite	ΔG_f^0 _Brucite	−834.62; Holland and Powell (2011)	−835.32; Helgeson et al. (1978)	−835.32; Helgeson et al. (1978)	−832.00; Blanc (2008)	Nordstrom et al. (1990)
	ΔG_f^0 _Mg ²⁺	−456.01; Miron et al. (2017)	−453.99; Shock and Helgeson (1988)	−453.99; Shock and Helgeson (1988)	−455.38; Blanc (2008)	Nordstrom et al. (1990)
Gibbsite	ΔG_f^0 _Gibbsite	−1154.90; Robie et al. (1978)	−1154.90; Helgeson et al. (1978)	−1154.90; Helgeson et al. (1978)	−1154.90; Helgeson et al. (1978)	Nordstrom et al. (1990)
	ΔG_f^0 _Al ³⁺	−487.48; Tagirov and Schott (2001)	−487.62; Pokrovskii and Helgeson (1995)	−487.62; Pokrovskii and Helgeson (1995)	−487.62; Pokrovskii and Helgeson (1995)	Nordstrom et al. (1990)
Boehmite	ΔG_f^0 _Boehmite	−918.40; Hemingway et al. (1991)	−918.80; Helgeson et al. (1978)	−918.80; Helgeson et al. (1978)	−918.41; Robie and Hemingway (1995)	−910.75; Robie and Waldbaum (1968)
	ΔG_f^0 _Diaspore	−921.06; Holland and Powell (2011)	−921.11; Helgeson et al. (1978)	−921.11; Helgeson et al. (1978)	−922.74; Robie and Hemingway (1995)	−920.89; Wagman et al. (1982)
Hematite	ΔG_f^0 _Hematite	−743.68; Holland and Powell (2011)	−745.40; Helgeson et al. (1978)	−745.40; Helgeson et al. (1978)	−744.25; Hemingway (1990)	−743.61; Wagman et al. (1982)
	ΔG_f^0 _Fe ³⁺	−17.24; Shock and Helgeson (1988)	−17.24; Shock and Helgeson (1988)	−17.24; Shock and Helgeson (1988)	−16.28; Parker and Khodakovsky (1995)	Nordstrom et al. (1990)
Quartz	ΔG_f^0 _Quartz	−856.28; Holland and Powell (2011)	−856.24; Helgeson et al. (1978)	−856.24; Helgeson et al. (1978)	−856.28; Helgeson et al. (1978)	Nordstrom et al. (1990)
	ΔG_f^0 _SiO ₂ ,aq	−834.88; Apps and Spycher (2004)	−833.41; Shock and Helgeson (1988)	−833.41; Shock and Helgeson (1988)	−834.86; Blanc (2008)	Nordstrom et al. (1990)
Kaolinite	ΔG_f^0 _Kaolinite	−3801.57; Holland and Powell (2011)	−3789.09; Helgeson et al. (1978)	−3789.09; Helgeson et al. (1978)	−3793.94; Robie and Hemingway (1995)	Nordstrom et al. (1990)
	ΔG_f^0 _Al(OH) ₄ [−]	−1305.77; Tagirov and Schott (2001)	−1305.72; Pokrovskii and Helgeson (1995)	−1305.72; Pokrovskii and Helgeson (1995)	−1305.74; Blanc (2008)	Nordstrom et al. (1990)
Albite	ΔG_f^0 _Albite	−3712.10; Holland and Powell (2011)	−3708.31; Helgeson et al. (1978)	−3708.31; Helgeson et al. (1978)		

(continued on next page)

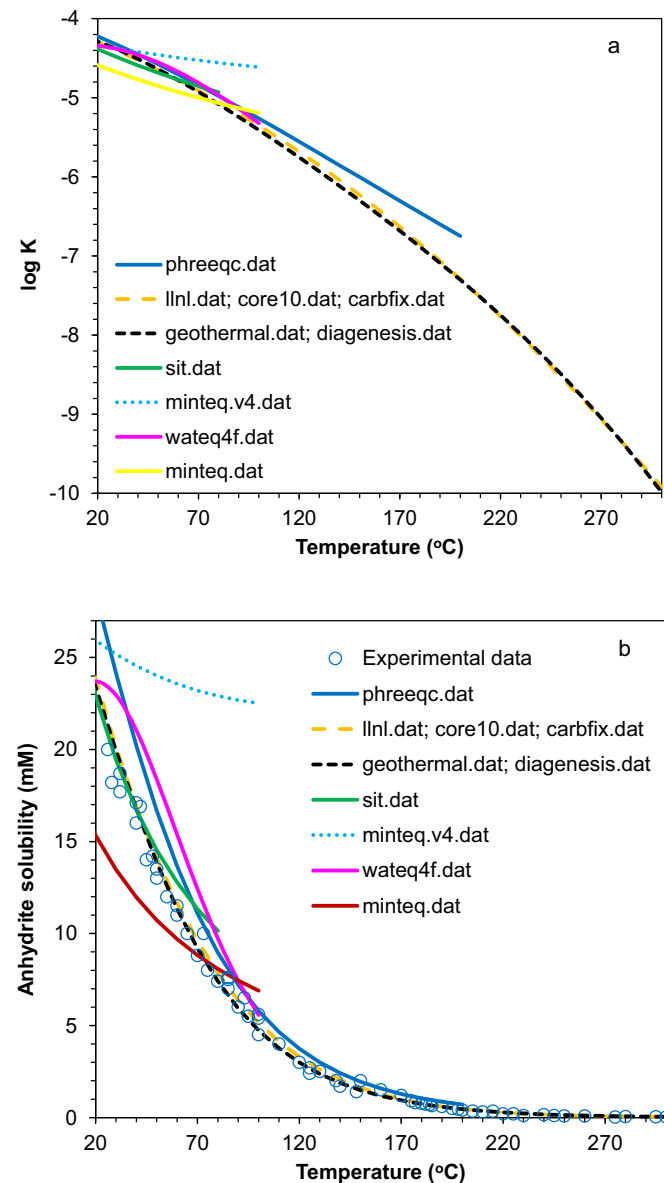


Fig. J8. Calculated anhydrite solubility product constants (a) and solubility (mM) (b) using different data files as a function of temperature. The experimental data are from [Azimi and Papangelakis \(2010\)](#) and the literature data they collected.

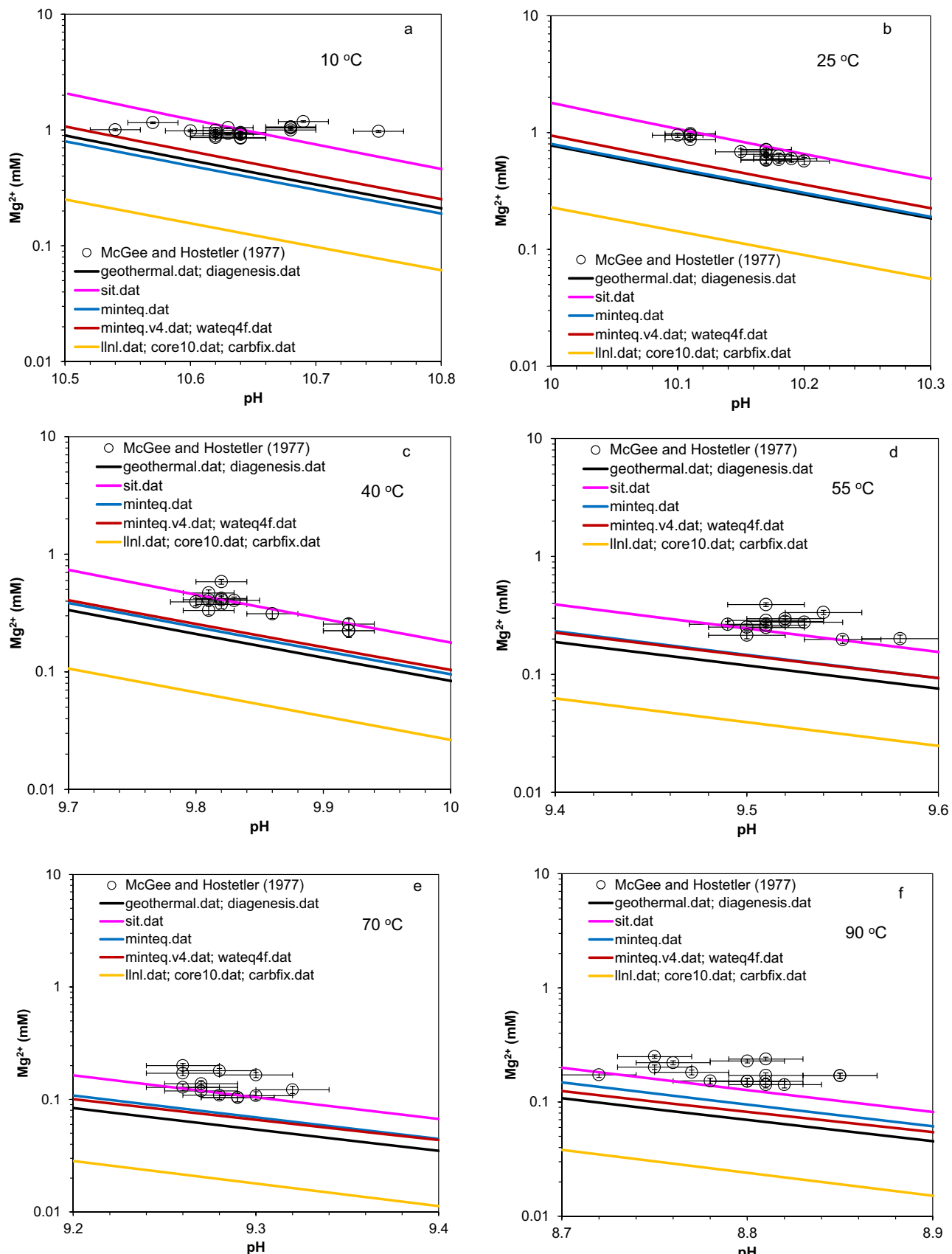


Fig. J9. Calculated total Mg (mM) concentration in equilibrium with brucite in pure water as a function of temperature using different data files. The experimental data are from McGee and Hostetler (1977). The experimental error is $\pm 1\%$ for total Mg^{2+} . (a) 10 °C; (b) 25 °C; (C) 40 °C, (d) 55 °C, (e) 70 °C, and (f) 90 °C.

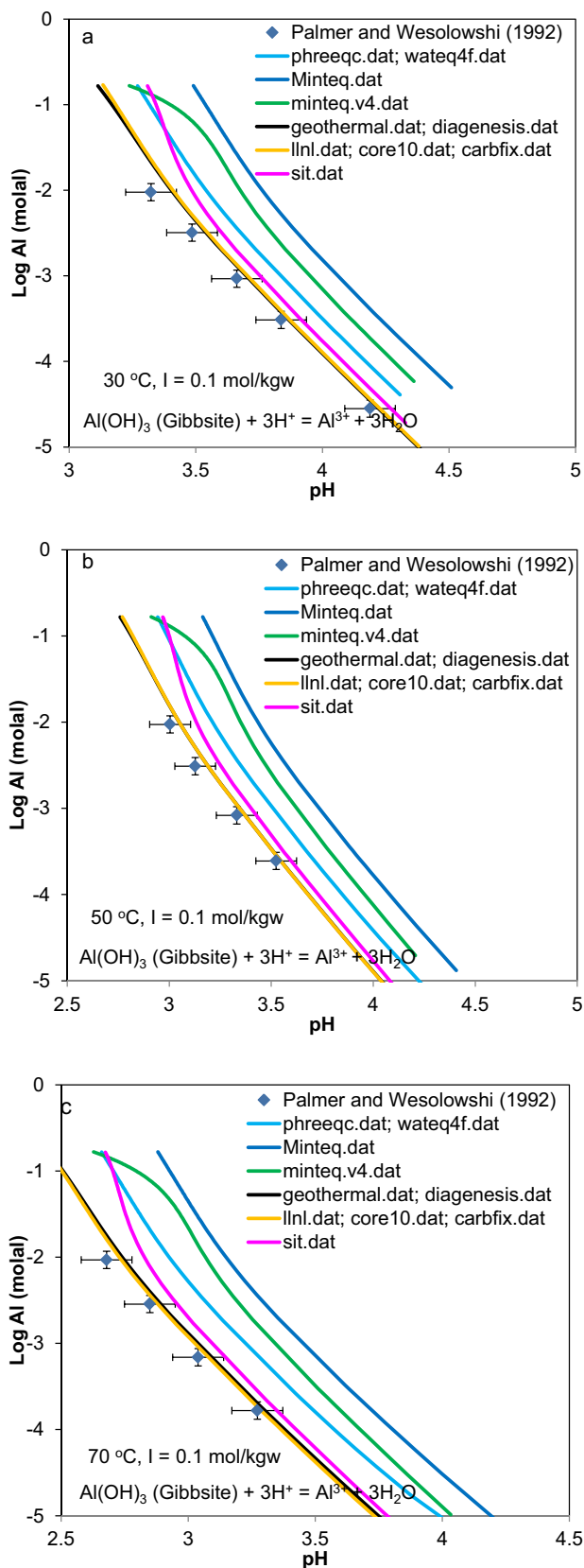


Fig. J10. Calculated total Al (M) concentration at pH 2.5–4.5 in equilibrium with gibbsite using different data files as a function of temperature. The experimental data are from Palmer and Wesolowski (1992) in mixed HCl (0.0003–0.03 mol/kgw) and NaCl solution with an ionic strength of 0.1 mol/kgw. The experimental error is $\pm 0.084\text{--}0.113$ log unit. (a) 30 °C; (b) 50 °C; (C) 70 °C.

Table K1 (*continued*)

(continued on next page)

Table K1 (continued)

		<i>geothermal.dat /diagenesis.dat</i>	<i>lhl.dat/core10.dat</i>	<i>carbfix.dat</i>	<i>sit.dat</i>	<i>wateq4f.dat/ phreeqc.dat</i>
Gypsum	ΔG_f^0 Gypsum	–1797.57; Matschei et al. (2007) (Appendix F)	–527.98; Shock and Helgeson (1988)	–527.98; Shock and Helgeson (1988)	–1797.39; Cox et al. (1989)	Nordstrom et al. (1990)
	ΔG_f^0 SO_4^{2-}	–744.46; Shock and Helgeson (1988)	–744.46; Shock and Helgeson (1988)	–744.46; Shock and Helgeson (1988)	–744.00; Cox et al. (1989)	Nordstrom et al. (1990)
	ΔG_f^0 Ca^{2+}	–552.79; Shock and Helgeson (1988)	–552.79; Shock and Helgeson (1988)	–552.79; Shock and Helgeson (1988)	–552.80; Cox et al. (1989)	Plummer and Busenberg (1982)
Anhydrite	ΔG_f^0 Anhydrite	–1321.98; Holland and Powell (2011)	–1321.83; Helgeson et al. (1978)	–1321.83; Helgeson et al. (1978)	–1322.13; Robie and Hemingway (1995)	Nordstrom et al. (1990)
	ΔG_f^0 SO_4^{2-}	–744.46; Shock and Helgeson (1988)	–744.46; Shock and Helgeson (1988)	–744.46; Shock and Helgeson (1988)	–744.00; Cox et al. (1989)	Nordstrom et al. (1990)
	ΔG_f^0 Ca^{2+}	–552.79; Shock and Helgeson (1988)	–552.79; Shock and Helgeson (1988)	–552.79; Shock and Helgeson (1988)	–552.80; Cox et al. (1989)	Plummer and Busenberg (1982)

Notes: Units: kJ/mol; The data source for *minseq.dat/ minseq.v4.dat* is Allison et al. (1991) and for *wateq4f.dat/phreeqc.dat* is mostly from Nordstrom et al. (1990); individual values are difficult to track down.

Appendix L. Selected results from geothermometry calculations

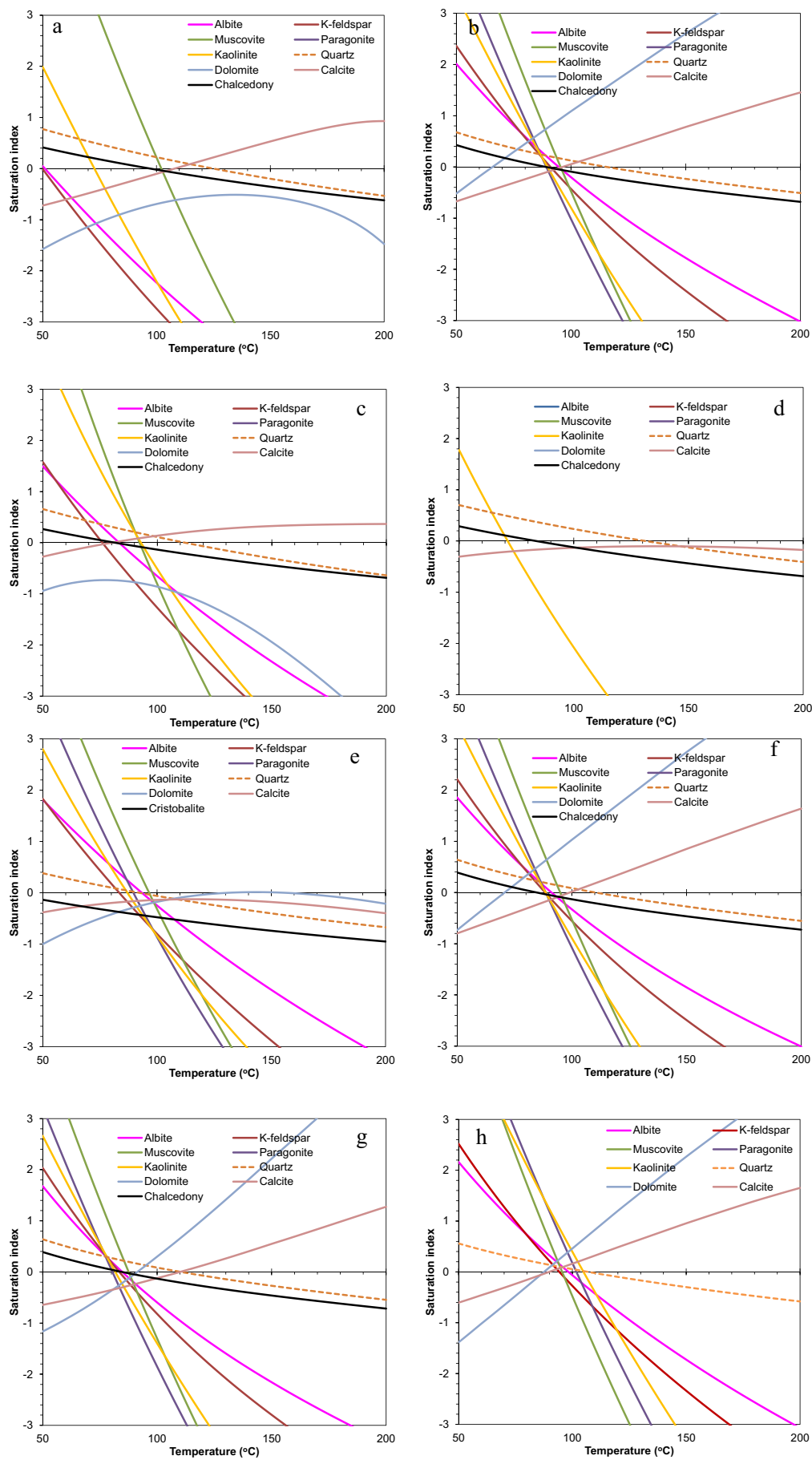


Fig. L1. Mineral saturation indices as a function of temperature over the course of simulating the reheating of formation water. (a) *phreeqc.dat*, (b) *llnl.dat*, (c) *minreq.dat*, (d) *minreq.v4.dat*, (e) *sit.dat*, (f) *core10.dat*, (g) *carbfix.dat*, (h) *geothermal.dat*. Formation water composition of well Bernard #6, Frio Formation zone "A," Brazoria County, Texas from Kharaka et al. (1977).

References

- Baes, C. F. & Mesmer, R. E. (1976). The hydrolysis of cations. Wiley. New York, 177-182.
- Bénézeth, P., Palmer, D. A. & Wesołowski, D. J. (2001). Aqueous high-temperature solubility studies. II. The solubility of boehmite at 0.03 M ionic strength as a function of temperature and pH as determined by in situ measurements. *Geochimica et Cosmochimica Acta*, 65(13), 2097-2111.
- Bourcier, W. L., Knauss, K. G. & Jackson, K. J. (1993). Aluminum hydrolysis constants to 250 °C from boehmite solubility measurements. *Geochimica et Cosmochimica Acta*, 57(4), 747-762.
- Castet, S., Dandurand, J. L., Schott, J. & Gout, R. (1993). Boehmite solubility and aqueous aluminum speciation in hydrothermal solutions (90–350°C): Experimental study and modeling. *Geochimica et Cosmochimica Acta*, 57(20), 4869-4884.
- Cox, E. J., Wagman, D. D. & Medvedev, V. A. (1989). CODATA: Key values for thermodynamics. Hemisphere Publishing Corp., New York, 1989.
- Ferrante, M.J., Stuve, J.M. & Richardson, D.W. (1976). Thermodynamic data for synthetic dawsonite. U.S. Bureau of Mines Report of Investigations No. 8129, 13 pp.
- Matschei, T., Lothenbach, B. & Glasser, F. P. (2007). Thermodynamic properties of Portland cement hydrates in the system CaO-Al₂O₃-SiO₂-CaSO₄-CaCO₃-H₂O. *Cement and Concrete Research*, 37(10), 1379-1410.
- Parker, V.B. & Khodakovskiy, I.L. (1995). Thermodynamic properties of aqueous ions (2+ and 3+) of iron and the key compounds of iron. *Journal of Physical & Chemical Reference Data* 24, 1699-1745.
- Pokrovskii, V.A. & Helgeson, H.C. (1995). Thermodynamic properties of aqueous species and the solubilities of minerals at high pressures and temperatures: The system Al₂O₃-H₂O-NaCl: American Journal of Science, 295, 1255-1342.
- Robie, R.A., Hemingway, B.S. & Fisher, J.R., (1978). Thermodynamic properties of minerals and related substances at 298.15 K and 1 bar (10⁵ Pa) pressure and at higher temperatures. U.S. Geological Survey Bulletin, 1452, 456.
- Wagman, D. D., Evans, W. H., Parker, V. B., Schumm, R. H. & Halow, I. (1982). The NBS tables of chemical thermodynamic properties. Selected values for inorganic and C1 and C2 organic substances in SI units. National Standard Reference Data System.

References

- Aja, S.U., Rosenberg, P.E., Kittrick, J.A., 1991. Illite equilibria in solutions: I. Phase relationships in the system K₂O-Al₂O₃-SiO₂-H₂O between 25 and 250 °C. *Geochim. Cosmochim. Acta* 55 (5), 1353-1364.
- Allison, J.D., Brown, D.S., Novo-Gradac, K.J., 1991. MINTEQA2/PRODEFA2, A Geochemical Assessment Model for Environmental Systems: Version 3.0 Users' Manual. U.S. EPA, Athens, Georgia. EPA/600/3- 91/021.
- Anderson, G.M., Crerar, D.A., 1993. Thermodynamics in Geochemistry: The Equilibrium Model. Oxford University Press on Demand.
- Anthony, J.W., 1990. Handbook of Mineralogy, vol. 4. Mineral Data Publishing.
- Appelo, C.A.J., Parkhurst, D.L., Post, V.E.A., 2014. Equations for calculating hydrogeochemical reactions of minerals and gases such as CO₂ at high pressures and temperatures. *Geochim. Cosmochim. Acta* 125, 49-67.
- Apps, J.A., 1970. The Stability Field of Analcime. Unpublished Ph.D. Dissertation. Harvard University, 347 pp.
- Apps, J., Spycher, N., 2004. Data Qualification for Thermodynamic Data Used to Support THC Calculations. ANL-NBS-HS-000043 REV 00. Bechtel SAIC Company, LLC, Las Vegas, NV, 172 pp. DOC. 20041118.0004.
- Apps, J.A., Neil, J.M., Jun, C.H., 1989. Thermochemical Properties of Gibbsite, Bayerite, Boehmite, Diaspore, and the Aluminate Ion Between 0 and 350 °C. (No. NUREG/CR-5271; LBL-21482). Nuclear Regulatory Commission, Washington, DC (USA). Div. of Waste Management; Lawrence Berkeley Lab., CA.
- Atkins, P., De Paula, J., 2006. Physical Chemistry, (8th ed.). W. H. Freeman and Company, p. 212.
- Azimi, G., Papangelakis, V.G., 2010. The solubility of gypsum and anhydrite in simulated laterite pressure acid leach solutions up to 250 °C. *Hydrometallurgy* 102 (1-4), 1-13.
- Ball, J.W., Nordstrom, D.K., 1991. User's manual for WATEQ4F, with revised thermodynamic data base and text cases for calculating speciation of major, trace, and redox elements in natural waters. USGS Open-File Report 91-183.193 p.
- Bénézeth, P., Palmer, D.A., Anovitz, L.M., Horita, J., 2007. Dawsonite synthesis and reevaluation of its thermodynamic properties from solubility measurements: Implications for mineral trapping of CO₂. *Geochim. Cosmochim. Acta* 71 (18), 4438-4455.
- Bénézeth, P., Dandurand, J.L., Harrichoury, J.C., 2009. Solubility product of siderite (FeCO₃) as a function of temperature (25–250 °C). *Chem. Geol.* 265 (1-2), 3-12.
- Bénézeth, P., Saldi, G.D., Dandurand, J.L., Schott, J., 2011. Experimental determination of the solubility product of magnesite at 50 to 200 °C. *Chem. Geol.* 286 (1-2), 21-31.
- Bénézeth, P., Stefansson, A., Gautier, Q., Schott, J., 2013. Mineral solubility and aqueous speciation under hydrothermal conditions to 300 °C – the carbonate system as an example. *Rev. Mineral. Geochem.* 76 (1), 81-133.
- Bénézeth, P., Berninger, U.N., Bovet, N., Schott, J., Oelkers, E.H., 2018. Experimental determination of the solubility product of dolomite at 50–253 °C. *Geochim. Cosmochim. Acta* 224, 262-275.
- Berezc, E., Szita, L., 1970. Electrochemical method for the solubility and dissolution of solid compounds. Some thermodynamic properties of the system Al(OH)₃-NaOH-H₂O. *Electrochim. Acta* 15 (8), 1407-1419.
- Berner, R.A., 1976. Solubility of calcite and aragonite in seawater at atmospheric pressure and 34. 5‰ salinity. *Am. J. Sci.* 276 (6).
- Berninger, U.N., Jordan, G., Schott, J., Oelkers, E.H., 2014. The experimental determination of hydromagnesite precipitation rates at 22.5–75 °C. *Mineral. Mag.* 78 (6), 1405-1416.
- Bethke, C.M., 2008. Geochemical and Biogeochemical Reaction Modeling, 2nd ed. Cambridge University Press.
- Bethke, C.M., Yeakel, S., 2014. Reaction Modeling Guide, The Geochemist's Workbench, Release 10.0.
- Blanc, P., 2008. Thermoddem: Sélection de propriétés thermodynamiques pour les principales espèces aquées et minérales porteuses de fer (in French). Rapport final. Rapport BRGM/RP-56587-FR, 70p.
- Blasco, M., Gimeno, M.J., Auqué, L.F., 2017. Comparison of different thermodynamic databases used in a geothermometrical modelling calculation. *Proc. Earth Planet. Sci.* 17, 120-123.
- Bloom, P.R., Weaver, R.M., 1982. Effect of the removal of reactive surface material on the solubility of synthetic gibbsite. *Clay Clay Miner.* 30 (4), 281-286.
- Bond, K.A., Heath, T.G., Tweed, C.J., 1997. HATCHES: a referenced thermodynamic database for chemical equilibrium studies. Nirex Report NSS/R379.
- Brinkley Jr., S.R., 1947. Calculation of the equilibrium composition of systems of many constituents. *J. Chem. Phys.* 15 (2), 107-110.
- Brown, P.L., Drummond Jr., S.E., Palmer, D.A., 1996. Hydrolysis of magnesium (II) at elevated temperatures. *J. Chem. Soc. Dalton Trans.* 14, 3071-3075.
- Bychkov, A.Y., Bénézeth, P., Pokrovsky, O.S., Shvarov, Y.V., Castillo, A., Schott, J., 2020. Experimental determination of calcite solubility and the stability of aqueous Ca-and Na-carbonate and bicarbonate complexes at 100–160 °C and 1–50 bar pCO₂ using in situ pH measurements. *Geochim. Cosmochim. Acta* 290, 352-365.
- Chivot, J., 2004. Thermodynamique des produits de corrosion. Fonctions thermodynamiques de la solubilité, diagrammes E-pH des systèmes Fe-H₂O, Fe-CO₂-H₂O, Fe-S-H₂O, Cr-H₂O et Ni-H₂O en fonction de la température. Document ANDRA, Collection Sciences et Techniques.
- Cornell, R.M., Schwertmann, U., 2003. The Iron Oxides: Structure, Properties, Reactions, Occurrences and Uses. John Wiley & Sons.
- Crerar, D.A., Anderson, G.M., 1971. Solubility and solvation reactions of quartz in dilute hydrothermal solutions. *Chem. Geol.* 8, 107-122.
- Daveler, S.A., Wolery, T.J., 1992. EQPT, a data file preprocessor for the EQ3/6 software package: Users guide and related documentation (Version 7.0); Part 2 (No. UCRL-MA-110662-Pt. 2). Lawrence Livermore National Lab., CA (United States).
- Davis, N.F., 1972. Experimental Studies in the System NaAlSi3O8-H2O. Ph.D. thesis. Pennsylvania State University, p. 319.
- Deer, W.A., Howie, R.A., Zussman, J., 1966. An Introduction to the Rock Forming Minerals. Longman, London, p. 469.
- Devidal, J.L., Dandurand, J.L., Gout, R., 1996. Gibbs free energy of formation of kaolinite from solubility measurement in basic solution between 60 and 170 °C. *Geochim. Cosmochim. Acta* 60 (4), 553-564.
- Diakonov, I.I., Schott, J., Martin, F., Harrichoury, J.C., Escalier, J., 1999. Iron (III) solubility and speciation in aqueous solutions. experimental study and modelling: part 1. hematite solubility from 60 to 300 °C in NaOH-NaCl solutions and

- thermodynamic properties of Fe(OH)₄-(aq). *Geochim. Cosmochim. Acta* 63 (15), 2247–2261.
- Dietrich, R.V., 2018. Feldspar. Encyclopaedia Britannica. <https://www.britannica.com/science/feldspar>. Accessed: May 7, 2020.
- Dillenseger, C., 1995. Modelisation experimentale de la dissolution des oxy-hydroxydes d'aluminium et de fer dans une solution 5 m naoh, a 200 et 250 °C : application au procede Bayer de traitement de la bauxite (Doctoral dissertation, Orléans).
- Drummond, S.E., 1981. Boiling and mixing of hydrothermal fluids—Chemical effects on mineral precipitation: University Park, Penn., Pennsylvania State University, Ph.D. thesis, 760 p.
- Duro, L., et al., 2012. ThermoChimie, the ANDRA thermodynamic database. In: MRS Proceedings 1475.
- Drutizac, J.E., 2002. Calcium sulphate solubilities in simulated zinc processing solutions. *Hydrometallurgy* 65 (2–3), 109–135.
- Ellis, A.J., 1963. The solubility of calcite in sodium chloride solutions at high temperatures. *Am. J. Sci.* 261 (3), 259–267.
- Façq, S., Daniel, I., Montagnac, G., Cardon, H., Sverjensky, D.A., 2014. In situ Raman study and thermodynamic model of aqueous carbonate speciation in equilibrium with aragonite under subduction zone conditions. *Geochim. Cosmochim. Acta* 132, 375–390.
- Fournier, R.O., 1960. Solubility of quartz in water in the temperature interval from 25 °C to 300 °C. *Geol. Soc. Am. Bull.* 71, 1867–1868.
- Fournier, R.O., 1985. The behavior of silica in hydrothermal solutions. In: Berger, B.R., Bethke, P.M. (Eds.), *Geology and Geochemistry of Epithermal Systems*. Society of Econ. Geologists, pp. 45–61.
- Fournier, R.O., Potter, R.W., 1982. Revised and expanded silica (quartz) geothermometer. Bulletin, Geothermal Resources Council (Davis, Calif.); (United States) 11 (10).
- Freed, R.L., 1982. Clay mineralogy and depositional history of the Frio formation in two geopressured wells, Brazoria County, Texas. *Trans. Gulf Coast Assoc. Geol. Soc.* 32, 459–463.
- Frink, C.R., Peech, M., 1962. The solubility of gibbsite in aqueous solutions and soil extracts. *Soil Sci. Soc. Am. J.* 26 (4), 346–347.
- Garrels, R., Thompson, M.E., Siever, R., 1960. Stability of some carbonates at 25 °C and one atmosphere total pressure. *Am. J. Sci.* 258, 402–418.
- Giffaut, E., Grivé, M., Blanc, P., Vieillard, P., Colas, E., Gailhanou, H., Marty, N., Made, B., Duro, L., 2014. Andra thermodynamic data for performance assessment: ThermoChimie. *Appl. Geochem.* 49, 225–236.
- Giggenbach, W.F., 1985. Construction of thermodynamic stability diagrams involving dioctahedral potassium clay minerals. *Chem. Geol.* 49 (1–3), 231–242.
- Gledhill, D.K., Morse, J.W., 2006. Calcite solubility in Na-Ca-Mg-Cl brines. *Chem. Geol.* 233 (3–4), 249–256.
- Grenthe, I., Plyasunov, A.V., Spahiu, K., 1997. Estimations of medium effects on thermodynamic data. In: Grenthe, Ingmar, Puigdomenech, Ignasi (Eds.), *Modelling in Aquatic Chemistry*. OECD Nuclear Energy Agency, Paris, pp. 325–426 chap. IX.
- Grivé, M., Duro, L., Colás, E., Giffaut, E., 2015. Thermodynamic data selection applied to radionuclides and chemotoxic elements: an overview of the ThermoChimie-TDB. *Appl. Geochem.* 55, 85–94.
- Halla, V.F., Van Tassel, R., 1965. Auflösungserscheinungen bei erdkalikarbonaten I. (Dissolution phenomena of alkaline earth aquacarbonates) Radex-Rundschau, 4, pp. 595–599 (in German).
- Hamlin, S.N., Alpers, C.N., 1995. Hydrogeology and geochemistry of acid mine drainage in ground water in the vicinity of Penn Mine and Camanche Reservoir, Calaveras County, California: first-year summary (Vol. 94, No. 4040). U.S. Geological Survey.
- Haselton, H.T., Cygan, G.L., Jenkins, D.M., 1995. Experimental study of muscovite stability in pure H₂O and 1 molal KCl-HCl solutions. *Geochim. Cosmochim. Acta* 59, 429–442.
- Hauenberger, C.A., Baumgartner, L.P., Pak, T.M., 2001. Experimental study on the solubility of the “model”-pelite mineral assemblage albite + K-feldspar + andalusite + quartz in supercritical chloride-rich aqueous solutions at 0.2 GPa and 600 °C. *Geochim. Cosmochim. Acta* 65, 4493–4507.
- Helgeson, H.C., 1969. Thermodynamics of hydrothermal systems at elevated temperatures and pressures. *Am. J. Sci.* 267 (7), 729–804.
- Helgeson, H.C., Delany, J.M., Nesbitt, H.W., Bird, D.K., 1978. Summary and critique of the thermodynamic properties of rock-forming minerals. *Am. J. Sci.* 278A, 229.
- Helgeson, H.C., Kirkham, D.H., Flowers, G.C., 1981. Theoretical prediction of the thermodynamic behavior of aqueous electrolytes by high pressures and temperatures; IV, Calculation of activity coefficients, osmotic coefficients, and apparent molal and standard and relative partial molal properties to 600 °C and 5 kb. *Am. J. Sci.* 281 (10), 1249–1516.
- Hem, J.D., 1992. Study and interpretation of the chemical characteristics of natural water. U.S. Gov. Print. Office, Washington, DC.
- Hemingway, B.S., 1990. Thermodynamic properties for bunsenite, NiO, magnetite, Fe3O4, and hematite, Fe2O3, with comments on selected oxygen buffer reactions. *Am. Mineral.* 75 (7–8), 781–790.
- Hemingway, B.S., Haas, J.L., Robinson, J.R., 1982. Thermodynamic properties of selected minerals in the system Al₂O₃-CaO-SiO₂-H₂O at 298.15 K and 1 bar (10⁵ Pascals) pressure and at high temperatures. *U.S. Geol. Surv. Bull.* 1452, 1–70.
- Hemingway, B.S., Robie, R.A., Apps, J.A., 1991. Revised values for the thermodynamic properties of boehmite, Al(OH)₃, and related species and phases in the system Al-H-O. *Am. Mineral.* 76 (3–4), 445–457.
- Hemley, J.J., 1959. Some mineralogical equilibria in the system K₂O-Al₂O₃-SiO₂-H₂O. *Am. J. Sci.* 257 (4), 241–270.
- Hemley, J.J., Montoya, J.W., Marinenco, J.W., Luce, R.W., 1980. Equilibria in the system Al₂O₃-2-H₂O and some general implications for alteration/mineralization processes. *Econ. Geol.* 75 (2), 210–228.
- Holland, T.J.B., Powell, R., 2011. An improved and extended internally consistent thermodynamic dataset for phases of petrological interest, involving a new equation of state for solids. *J. Metamorph. Geol.* 29 (3), 333–383.
- Huang, F., Sverjensky, D.A., 2019. Extended Deep Earth Water Model for predicting major element mantle metasomatism. *Geochim. Cosmochim. Acta* 254, 192–230.
- Hückel, E., 1925. Zur Theorie konzentrierter wasseriger Lösungen starker Elektolyte. *Phys. Z.* 26, 93–147.
- Hummel, W., Berner, U., Curti, E., Pearson, F.J., Thoenen, T., 2002. Nagra/PSI chemical thermodynamics data base 01/01. Technical Report 02-16. National Cooperative for the Disposal of Radioactive Waste, Switzerland.
- IAEA, 2009. Costing of Spent Nuclear Fuel Storage. IAEA NUCLEAR ENERGY SERIES No. NF-T-3.5.
- IPCC, 2005. Special report on carbon dioxide capture and storage. Intergovernmental Panel on Climate Change.
- Jacobson, R.L., Langmuir, D., 1974. Dissociation constants of calcite and CaHC₀₃⁺ from 0 to 50 °C. *Geochim. Cosmochim. Acta* 38 (2), 301–318.
- Johnson, J.W., Oelkers, E.H., Helgeson, H.C., 1992. SUPCRT92: A software package for calculating the standard molal thermodynamic properties of minerals, gases, aqueous species, and reactions from 1 to 5000 bar and 0 to 1000 °C. *Comput. Geosci.* 18 (7), 899–947.
- Jones, B.F., Deocampo, D.M., 2003. Geochemistry of saline lakes. In: Drever, Surface and Ground Water Weathering and Soils, vol. 5. Treatise on Geochemistry, Amsterdam, Elsevier, pp. 393–424.
- Jove-Colon, C., Wolery, T., Rard, J., Wijesinghe, A., Jareck, R., Helean, K., 2007. Pitzer Database Development: Description of the Pitzer Geochemical Thermodynamic Database data0. ypf. R2. Appendix I. In: Drift Precipitates/Salts Model, ANL-EBS-MD-000045 REV 03, DOC. 20070306.0037. Sandia National Laboratories.
- Kamnev, A.A., Ezhov, B.B., Malandin, O.G., Vasev, A.V., 1986. The solubility of goethite in basic solutions (in Russian). *Zh. Prikl. Khim.* 8, 1689–1693.
- Kennedy, G.C., 1950. A portion of the system silica-water. *Econ. Geol.* 45 (7), 629–653.
- Kharaka, Y.K., Callender, E., Carothers, W.W., Meriwether, J., 1977. Geochemistry of geopressured geothermal waters from the Texas Gulf Coast (No. CONF-771153-P1-7).
- Kharaka, Y.K., Law, L.M., Carothers, W.W., Goerlitz, D.F., 1986. Role of organic species dissolved in formation waters from sedimentary basins in mineral diagenesis.
- Kitahara, S., 1960. The solubility of quartz in water at high temperatures and high pressures. *Rev. Physical Chem. Japan* 30, 109–137.
- Kitamura, A., Fujiwara, K., Doi, R., Yoshida, Y., 2012. Update of JAEA-TDB: Additional selection of thermodynamic data for solid and gaseous phases on nickel, selenium, zirconium, technetium, thorium, uranium, neptunium plutonium and americium, update of thermodynamic data on iodine, and some modifications. JAEA-Data/Code, 6, 2012.
- Kittrick, J.A., 1966. The free energy of formation of gibbsite and Al(OH)₄⁻ from solubility measurements. *Soil Sci. Soc. Am. J.* 30 (5), 595–598.
- Kulik, D.A., Wagner, T., Dmytrieva, S.V., Kosakowski, G., Hingerl, F.F., Chudnenko, K.V., Berner, U.R., 2013. GEM-Selktor geochemical modeling package: revised algorithm and GEMS3K numerical kernel for coupled simulation codes. *Comput. Geosci.* 17 (1), 1–24.
- Kuyunko, N.S., Malinin, S.D., Khodakovskiy, I.L., Khodakovskiy, J.I., 1983. An experimental study of aluminium ion hydrolysis at 150, 200, and 250 °C. *Geochem. Int.* 20 (2), 76–86.
- Langmuir, D., 1971. The geochemistry of some carbonate ground waters in central Pennsylvania. *Geochim. Cosmochim. Acta* 35 (10), 1023–1045.
- Langmuir, D., 1997. *Aqueous Environmental Geochemistry*. Prentice Hall, Upper Saddle River, NJ, 600.
- Leal, A.M., 2015. Reaktoro: A unified framework for modeling chemically reactive systems. URL: www.reaktoro.org.
- Lindberg, R.D., Runnels, D.D., 1984. Ground water redox reactions: an analysis of equilibrium state applied to Eh measurements and geochemical modeling. *Science* 225 (4665), 925–927.
- Lothenbach, B., Kulik, D.A., Matschei, T., 2019. Cemdata 18: a chemical thermodynamic database for hydrated Portland cements and alkali-activated materials. *Cem. Concr. Res.* 115, 472–506.
- Mackenzie, F.T., Gees, R., 1971. Quartz: Synthesis at earth surface conditions. *Science* 173, 533–535.
- Manning, C.E., 1994. The solubility of quartz in H₂O in the lower crust and upper mantle. *Geochim. Cosmochim. Acta* 58, 4831–4839.
- Marion, G.M., 2001. Carbonate mineral solubility at low temperatures in the Na-K-Mg-Ca-H-Cl-SO₄-OH-HCO₃-CO₃-H₂O system. *Geochim. Cosmochim. Acta* 65 (12), 1883–1896.
- Marion, G.M., Farren, R.E., 1999. Mineral solubilities in the Na-K-Mg-Ca-Cl-SO₄-H₂O system: A re-evaluation of the sulfate chemistry in the Spencer-Moller-Weare model. *Geochim. Cosmochim. Acta* 63 (9), 1305–1318.
- Marshall, W.L., Slusher, R., 1966. Thermodynamics of calcium sulfate dihydrate in aqueous sodium chloride solutions, 0–110 °C. *J. Phys. Chem.* 70 (12), 4015–4027.
- Matschei, T., Lothenbach, B., Glasser, F.P., 2007. The role of calcium carbonate in cement hydration. *Cem. Concr. Res.* 37 (4), 551–558.
- May, H.M., Helmke, P.A., Jackson, M.L., 1979. Gibbsite solubility and thermodynamic properties of hydroxy-aluminum ions in aqueous solution at 25 °C. *Geochim. Cosmochim. Acta* 43 (6), 861–868.
- May, H.M., Kinniburgh, D.G., Helmke, P.A., Jackson, M.L., 1986. Aqueous dissolution, solubilities and thermodynamic stabilities of common aluminosilicate clay minerals: kaolinite and smectites. *Geochim. Cosmochim. Acta* 50 (8), 1667–1677.
- McGee, K.A., Hosteller, P.B., 1977. Activity-product constants of brucite from 10 to 90 °C. *J. Res. U.S. Geological Survey* 5 (2), 227–233.

- Miron, G.D., Wagner, T., Kulik, D.A., Heinrich, C.A., 2016. Internally consistent thermodynamic data for aqueous species in the system Na-K-Al-Si-O-H-Cl. *Geochim. Cosmochim. Acta* 187, 41–78.
- Miron, G.D., Wagner, T., Kulik, D.A., Lothenbach, B., 2017. An internally consistent thermodynamic dataset for aqueous species in the system Ca-Mg-Na-K-Al-Si-OHC-Cl to 800 °C and 5 kbar. *Am. J. Sci.* 317 (7), 755–806.
- Montoya, J.W., Hemley, J.J., 1975. Activity relations and stabilities in alkali feldspar and mica alteration reactions. *Econ. Geol.* 70, 577–583.
- Morey, G.W., Fournier, R.O., Rowe, J.J., 1962. The solubility of quartz in water in the temperature interval from 25° to 300 °C. *Geochim. Cosmochim. Acta* 26, 1029–1043.
- Müller, B., 2004. Manual of ChemEQL (Version 3.0). Limnological Research. Center EAWAG/ETH, Kastanienbaum, Switzerland.
- Nagy, K.L., Lasaga, A.C., 1992. Dissolution and precipitation kinetics of gibbsite at 80 °C and pH 3: The dependence on solution saturation state. *Geochim. Cosmochim. Acta* 56 (8), 3093–3111.
- Neveu, M., Desch, S.J., Castillo-Rogez, J.C., 2017. Aqueous geochemistry in icy world interiors: Equilibrium fluid, rock, and gas compositions, and fate of antifreezes and radionuclides. *Geochim. Cosmochim. Acta* 212, 324–371.
- Nordstrom, D.K., Munoz, J.L., 1994. Geochemical Thermodynamics, 2nd ed. Blackwell Scientific Publications. 493 pp.
- Nordstrom, D.K., Plummer, L.N., Wigley, T.M.L., Wolery, T.J., Ball, J.W., Jenne, E.A., Bassett, R.L., Crerar, D.A., Florence, T.M., Fritz, B., Hoffman, M., 1979. A comparison of computerized chemical models for equilibrium calculations in aqueous systems.
- Nordstrom, D.K., Plummer, L.N., Langmuir, D., Busenberg, E., May, H.M., Jones, B.F., Parkhurst, D.L., 1990. Revised chemical equilibrium data for water-mineral reactions and their limitations, Chap.31. In: Bassett, R.L., Melchior, D. (Eds.), Chemical Modeling in Aqueous Systems II, pp. 398–413. American Chemical Society Symposium Series 416.
- Oelkers, E.H., Helgeson, H.C., 1990. Triple-ion anions and polynuclear complexing in supercritical electrolyte solutions. *Geochim. Cosmochim. Acta* 54 (3), 727–738.
- Oelkers, E.H., Bénédith, P., Pokrovski, G.S., 2009. Thermodynamic databases for water-rock interaction. *Rev. Mineral. Geochem.* 70 (1), 1–46.
- Packter, A., 1979. Studies on recrystallised aluminum trihydroxide precipitates: the energetics of dissolution by sodium hydroxide solutions. *Colloid Polym. Sci.* 257 (9), 977–980.
- Pak, T.M., Hauzenberger, C.A., Baumgartner, L.P., 2003. Solubility of the assemblage albite+K-feldspar+andalusite +quartz in supercritical aqueous chloride solutions at 650 °C and 2 kbar. *Chem. Geol.* 200, 377–393.
- Palandri, J.L., Reed, M.H., 2001. Reconstruction of in situ composition of sedimentary formation waters. *Geochim. Cosmochim. Acta* 65 (11), 1741–1767.
- Palmer, D.A., Wesolowski, D.J., 1992. Aluminum speciation and equilibria in aqueous solution: II. The solubility of gibbsite in acidic sodium chloride solutions from 30 to 70 °C. *Geochim. Cosmochim. Acta* 56 (3), 1093–1111.
- Parkhurst, D.L., Appelo, C.A.J., 1999. User's guide to PHREEQC (Version 2): A computer program for speciation, batch-reaction, one-dimensional transport, and inverse geochemical calculations. U.S. Geological Survey, p. 312.
- Parkhurst, D.L., Appelo, C.A.J., 2013. Description of input and examples for PHREEQC version 3: a computer program for speciation, batch-reaction, one-dimensional transport, and inverse geochemical calculations (No. 6-A43). U.S. Geological Survey.
- Parkhurst, D.L., Thorstenson, D.C., Plummer, L.N., 1980. PHREEQE—a computer program for geochemical calculations. US Geological Survey Water Resour. Invest. 80-96, 210.
- Partanen, J.I., 2016. Mean activity coefficients and osmotic coefficients in dilute aqueous sodium or potassium chloride solutions at temperatures from (0 to 70) C. *J. Chem. Eng. Data* 61 (1), 286–306.
- Partanen, J.I., Covington, A.K., 2009. Re-evaluation of the thermodynamic activity quantities in aqueous sodium and potassium chloride solutions at 25 C. *J. Chem. Eng. Data* 54 (2), 208–219.
- Peng, D.Y., Robinson, D.B., 1976. A new two-constant equation of state. *Ind. Eng. Chem. Fundam.* 15 (1), 59–64.
- Perryea, F.J., Kittirat, J.A., 1988. Relative solubility of corundum, gibbsite, boehmite, and diaspore at standard state conditions. *Clay Clay Miner.* 36 (5), 391–396.
- Pitzer, K.S., 1973. Thermodynamics of electrolytes. I. Theoretical basis and general equations. *J. Phys. Chem.* 77 (2), 268–277.
- Plummer, L.N., Busenberg, E., 1982. The solubilities of calcite, aragonite and vaterite in CO₂-H₂O solutions between 0 and 90°C, and an evaluation of the aqueous model for the system CaCO₃-CO₂-H₂O. *Geochim. Cosmochim. Acta* 46 (6), 1011–1040.
- Plummer, L.N., Parkhurst, D.L., Fleming, G.W., Dunkle, S.A., 1988. A computer program incorporating Pitzer's equations for calculation of geochemical reactions in brines (Vol. 88, No. 4153). Department of the Interior, U.S. Geological Survey.
- Plyasunov, A.V., Shock, E.L., 2001. Correlation strategy for determining the parameters of the revised Helgeson-Kirkham-Flowers model for aqueous nonelectrolytes. *Geochim. Cosmochim. Acta* 65 (21), 3879–3900.
- Pokrovskii, V.A., Helgeson, H.C., 1995. Thermodynamic properties of aqueous species and the solubilities of minerals at high pressures and temperatures; the system Al₂O₃-H₂O-NaCl. *Am. J. Sci.* 295 (10), 1255–1342.
- Prieto, M., 2009. Thermodynamics of solid solution-aqueous solution systems. *Rev. Mineral. Geochem.* 70, 47–85.
- Reed, M.H., Spycher, N.F., Palandri, J., 2010. Users Guide for CHIM-XPT: A Program for Computing Reaction Processes in Aqueous-Mineral Gas Systems and MINITAB Guide. University of Oregon, Eugene, OR.
- Rimstidt, J.D., 1997. Quartz solubility at low temperatures. *Geochim. Cosmochim. Acta* 61 (13), 2553–2558.
- Robie, R.A., Hemingway, B.S., 1973. The enthalpies of formation of nesquehonite, MgCO₃·3H₂O, and hydromagnesite, 5MgO·4CO₂·5H₂O. *Journal of Research of the US Geological Survey* 1, 543–547.
- Robie, R.A., Hemingway, B.S., 1995. Thermodynamic Properties of Minerals and Related Substances at 298.15 K and 1 bar (10⁵ Pascals) Pressure and at Higher Temperatures, vol. 2131. U.S. Government Printing Office.
- Robie, R.A., Waldbaum, D.R., 1968. Thermodynamic properties of minerals and related substances at 298.15 K (25.0 °C) and one atmosphere (1.013 bars) pressure and at higher temperatures: US Geological Survey Bulletin 1259, p. 256.
- Robie, R.A., Hemingway, B.S., Fisher, J.R., 1978. Thermodynamic properties of minerals and related substances at 298.15 K and 1 bar (10⁵ pascals) pressure and at higher temperatures.
- Robinson, R.A., Stokes, R.H., 1965. Electrolyte Solutions: The Measurement and Interpretation of Conductance, Chemical Potential and Diffusion in Solutions of Simple Electrolytes, 2nd ed. Butterworths, London, p. 571.
- Russell, A.S., Edwards, J.D., Taylor, C.S., 1955. Solubility and density of hydrated aluminas in NaOH solutions. *J. Metals* 7 (10), 1123–1128.
- Sass, E., Morse, J.W., Millero, F.J., 1983. Dependence of the values of calcite and aragonite thermodynamic solubility products on ionic models. *Am. J. Sci.* 283 (3), 218–229.
- Sassani, D.C., Shock, E.L., 1998. Solubility and transport of platinum-group elements in supercritical fluids: Summary and estimates of thermodynamic properties for ruthenium, rhodium, palladium, and platinum solids, aqueous ions, and complexes to 1000 °C and 5 kbar. *Geochim. Cosmochim. Acta* 62 (15), 2643–2671.
- Schecher, W.D., McAvoy, D.C., 1994. MINEQL+: A Chemical Equilibrium Program for Personal Computers. Environmental Research Software.
- Shock, E.L., Helgeson, H.C., 1988. Calculation of the thermodynamic and transport properties of aqueous species at high pressures and temperatures: correlation algorithms for ionic species and equation of state predictions to 5 kb and 1000 °C. *Geochim. Cosmochim. Acta* 52 (8), 2009–2036.
- Shock, E.L., Koretsky, C.M., 1993. Metal-organic complexes in geochemical processes: calculation of standard partial molal thermodynamic properties of aqueous acetate complexes at high pressures and temperatures. *Geochim. Cosmochim. Acta* 57 (20), 4899–4922.
- Shock, E.L., Sassani, D.C., Willis, M., Sverjensky, D.A., 1997. Inorganic species in geologic fluids: correlations among standard molal thermodynamic properties of aqueous ions and hydroxide complexes. *Geochim. Cosmochim. Acta* 61 (5), 907–950.
- Siever, R., 1962. Silica Solubility, 0 °-200 °C, and the diagenesis of siliceous sediments. *J. Geol.* 70, 127–150.
- Singh, S.S., 1974. The solubility product of gibbsite at 15, 25, and 35 °C. *Soil Sci. Soc. Am. J.* 38 (3), 415–417.
- Sipos, P., 2008. Application of the Specific Ion Interaction Theory (SIT) for the ionic products of aqueous electrolyte solutions of very high concentrations. *J. Mol. Liq.* 143 (1), 13–16.
- Smith, B.D., Brinkley, W.K., 1960. Rigorous solution of multicomponent, multistage extraction problems. *AIChE J.* 6 (3), 451–454.
- Spencer, R.J., Moller, N., Weare, J.H., 1990. The prediction of mineral solubilities in natural waters: A chemical equilibrium model for the Na-K-Ca-Mg-Cl-SO₄-H₂O system at temperatures below 25 °C. *Geochim. Cosmochim. Acta* 54 (3), 575–590.
- Steefel, C.I., 2001. CRUNCH Version 1.2. Lawrence Livermore National Laboratory, Livermore, U.S.
- Stefansson, A., 2007. Iron (III) hydrolysis and solubility at 25 C. *Environ. Sci. Technol.* 41 (17), 6117–6123.
- Stefansson, A., Arnórsson, S., 2000. Feldspar saturation state in natural waters. *Geochim. Cosmochim. Acta* 64 (15), 2567–2584.
- Stumm, W., Morgan, J.J., 1996. Aquatic Chemistry: Chemical Equilibria and Rates in Natural Waters, 3rd ed. John Wiley & Sons.
- Suleimenov, O., 1988. The solubility of hematite and the geochemistry of iron in hydrothermal solutions. Doctoral dissertation, Master's thesis. Moscow State Univ.
- Sverjensky, D.A., Harrison, B., Azzolini, D., 2014. Water in the deep Earth: The dielectric constant and the solubilities of quartz and corundum to 60 kb and 1200 degrees C. *Geochim. Cosmochim. Acta* 129, 125–145.
- Sverjensky, D.A., Hemley, J.J., D'Angelo, W.M., 1991. Thermodynamic assessment of hydrothermal alkali feldspar-mica-aluminosilicate equilibria. *Geochim. Cosmochim. Acta* 55, 989–1004.
- Sverjensky, D.A., Shock, E.L., Helgeson, H.C., 1997. Prediction of the thermodynamic properties of aqueous metal complexes to 1000 °C and 5 kb. *Geochim. Cosmochim. Acta* 61 (7), 1359–1412.
- Tagirov, B., Schott, J., 2001. Aluminum speciation in crustal fluids revisited. *Geochim. Cosmochim. Acta* 65 (21), 3965–3992.
- Tanger, J.C., Helgeson, H.C., 1988. Calculation of the thermodynamic and transport properties of aqueous species at high pressures and temperatures; revised equations of state for the standard partial molal properties of ions and electrolytes. *Am. J. Sci.* 288 (1), 19–98.
- Thorstenson, D.C., Parkhurst, D.L., 2002. Calculation of individual isotope equilibrium constants for implementation in geochemical models. *Water-Resources Investigations Report*, 2, 4172. U.S. Geological Survey.
- Thorstenson, D.C., Parkhurst, D.L., 2004. Calculation of individual isotope equilibrium constants for geochemical reactions. *Geochim. Cosmochim. Acta* 68 (11), 2449–2465.
- Toner, J.D., Catling, D.C., 2017. A low-temperature thermodynamic model for the Na-K-Ca-Mg-Cl system incorporating new experimental heat capacities in KCl, MgCl₂, and CaCl₂ solutions. *J. Chem. Eng. Data* 62 (3), 995–1010.
- Truesdell, A.H., Jones, B.F., 1974. WATEQ, a computer program for calculating chemical equilibria of natural waters. *J. Res. U.S. Geological Survey* 2 (2), 233–248.

- Tutolo, B.M., Kong, X.Z., Seyfried Jr., W.E., Saar, M.O., 2014. Internal consistency in aqueous geochemical data revisited: applications to the aluminum system. *Geochim. Cosmochim. Acta* 133, 216–234.
- van der Lee, J., De Windt, L., Lagneau, V., Goblet, P., 2002. Presentation and application of the reactive transport code HYTEC. In: *Developments in Water Science*, vol. 47. Elsevier, pp. 599–606.
- van Lier, J.A., de Bruyn, P.L., Overbeek, J.T.G., 1960. The solubility of quartz. *J. Phys. Chem.* 64, 1675–1682.
- Verdes, G., Gout, R., Castet, S., 1992. Thermodynamic properties of the aluminate ion and of bayierite, boehmite, diaspore and gibbsite. *Eur. J. Mineral.* 767–792.
- Vieillard, P., 2000. A new method for the prediction of Gibbs free energies of formation of hydrated clay minerals based on the electronegativity scale. *Clay Clay Miner.* 48 (4), 459–473.
- Voigt, M., Marieni, C., Clark, D.E., Gíslason, S.R., Oelkers, E.H., 2018. Evaluation and refinement of thermodynamic databases for mineral carbonation. *Energy Procedia* 146, 81–91.
- Wagman, D.D., Evans, W.H., Parker, V.B., Schumm, R.H., Halow, I., 1982. The NBS tables of chemical thermodynamic properties. Selected values for inorganic and C1 and C2 organic substances in SI units. *J. Phys. Chem. Ref. Data* 11, Suppl. 2.
- Walther, J.V., Helgeson, H.C., 1977. Calculation of the thermodynamic properties of aqueous silica and the solubility of quartz and its polymorphs at high pressures and temperatures. *Am. J. Sci.* 277 (10), 1315–1351.
- Walther, J.V., Orville, P.M., 1983. The extraction-quench technique for determination of the thermodynamic properties of solute complexes: application to quartz solubility in fluid mixtures. *Am. Mineral.* 68, 731–741.
- Wang, L., Salah, S., De Soete, H., 2011. MOLDATA: A Thermochemical Data Base for phenomenological and safety assessment studies for disposal of radioactive waste in Belgium—Data compilation strategy. External Report SCK* CEN-ER-121.
- Warren, J.K., 2006. Evaporites: Sediments, Resources and Hydrocarbons. Springer Science & Business Media.
- Weill, D.F., Fyfe, W.S., 1964. The solubility of quartz in H_2O in the range 1000–4000 bars and 400–550 °C. *Geochim. Cosmochim. Acta* 28, 1243–1255.
- Wesolowski, D.J., 1992. Aluminum speciation and equilibria in aqueous solution: I. The solubility of gibbsite in the system Na-K-Cl-OH-Al(OH)₄ from 0 to 100 °C. *Geochim. Cosmochim. Acta* 56 (3), 1065–1091.
- White, W.B., Johnson, S.M., Dantzig, G.B., 1958. Chemical equilibrium in complex mixtures. *J. Chem. Phys.* 28 (5), 751–755.
- Wolery, T.J., Sutton, M., 2013. Evaluation of Thermodynamic Data (No. LLNL-TR-640133). Lawrence Livermore National Lab.(LLNL), Livermore, CA (United States).
- Xu, T., Sonnenthal, E., Spycher, N., Pruess, K., 2004. TOUGHREACT User's Guide: A Simulation Program for Non-Isothermal Multiphase Reactive Geochemical Transport in Variable Saturated Geologic Media (No. LBNL-55460). Lawrence Berkeley National Lab. (LBNL), Berkeley, CA (United States).
- Yanat'eva, O.K., 1952. Solubility of dolomite in water salt solutions. *Izvestiya Sektora FkhA Akademii Nauk SSSR* 20, 252–268.
- Yishan, Z., Ruiying, A.I., Fengzhen, W., 1989. Solubility of the magnetite+ hematite buffer assemblage and iron speciation in sodium chloride solutions at 300 °C and 500 bars. *Geochim. Cosmochim. Acta* 53 (8), 1875–1882.
- Yoshida, Y., Shibata, M., 2004. Establishment of data base files of thermodynamic data developed by OECD/NEA Part II—Thermodynamic data of Tc, U, Np, Pu and Am with auxiliary species, JNC Technical Report, JNC TN8400 2004–025.
- Zeleznik, F.J., Gordon, S., 1960. An Analytical Investigation of Three General Methods of Calculating Chemical-Equilibrium Compositions. National Aeronautics and Space Administration.
- Zeleznik, F.J., Gordon, S., 1968. Calculation of complex chemical equilibria. *Ind. Eng. Chem.* 60 (6), 27–57.
- Zhang, G., Lu, P., Zhang, Y., Tu, K., Zhu, C., 2020. SupPhreeqc: A program for generating customized Phreeqc thermodynamic datasets from Supcrtbl and extending calculations to elevated pressures and temperatures. *Comput. Geosci.* 143, 104560.
- Zhu, C., Anderson, G., 2002. Environmental Applications of Geochemical Modeling. Cambridge University Press.
- Zimmer, K., Zhang, Y., Lu, P., Chen, Y., Zhang, G., Dalkilic, M., Zhu, C., 2016. SUPCRTBL: a revised and extended thermodynamic dataset and software package of SUPCRT92. *Comput. Geosci.* 90, 97–111.